1966

Flash desorption and isotopic mixing of simple diatomic gases on tungsten, iridium and rhodium

Victor Joseph Mimeault
Iowa State University

66–6993

MIMEAULT, Victor Joseph, 1937–

FLASH DESORPTION AND ISOTOPIC MIXING OF SIMPLE DIATOMIC GASES ON TUNGSTEN, IRIDIUM AND RHODIUM.

Iowa State University of Science and Technology
Ph.D., 1966
Chemistry, physical

University Microfilms, Inc., Ann Arbor, Michigan

FLASH DESORPTION AND ISOTOPIC MIXING OF SIMPLE DIATOMIC GASES ON TUNGSTEN, IRIDIUM AND RHODIUM

by

Victor Joseph Mimeault

A Dissertation Submitted to the
Graduate Faculty in Partial Fulfillment of
The Requirements for the Degree of
DOCTOR OF PHILOSOPHY

Major Subject: Physical Chemistry

Approved:

Signature was redacted for privacy.

In Charge of Major Work

Signature was redacted for privacy.

Head of Major Department

Signature was redacted for privacy.

Dean of Graduate College

Iowa State University
Of Science and Technology
Ames, Iowa
1966

TABLE OF CONTENTS

		Page
I.	INTRODUCTION	1
II.	LITERATURE REVIEW	3
	A. General Background	3
	B. Current Status and Relation to Present Work	12
III.	FLASH DESORPTION SPECTROMETRY	17
IV.	EXPERIMENTAL PROCEDURES	27
	A. Introduction	27
	B. Ultra High Vacuum Techniques	28
	C. Temperature Measurement and Control	39
	D. Flash Desorption Experiments	42
V.	RESULTS	46
	A. Desorption of Hydrogen	46
	B. Hydrogen-Deuterium Exchange	61
	C. Desorption of Nitrogen	64
	D. Desorption of Carbon Monoxide	71
VI.	DISCUSSION	74
	A. Adsorption of Hydrogen	74
	B. Adsorption of Nitrogen	81
	C. Adsorption of Carbon Monoxide	86
VII.	SUMMARY	89
VIII.	SUGGESTIONS FOR FUTURE RESEARCH	94

		Page
IX.	FIGURES	96
X.	TABLES	148
XI.	BIBLIOGRAPHY	155
XII.	ACKNOWLEDGEMENTS	160
XIII.	APPENDICES	161
	A. Relaxation Phenomena Associated with Pumping Speeds and Tube Conductances	161
	B. Response Characteristics of a Linear Recording System	170
	C. Kinetic Analysis of Pressure-Temperature Data, Fortran Program	182
	D. Variation of the Activation Energy of Desorption with Surface Coverage, Fortran Program	186

LIST OF FIGURES

		Page
1.	Schematic diagram of vacuum system and associated electronic equipment	97
2.	Flash filament apparatus	98
3.	Desorption cell used in flash filament experiments	99
4.	Constant current power supply and dc-level detector	100
5.	Resistance-ratio versus temperature for iridium, rhodium and tungsten R_o = resistance at 295°K	101
6.	Desorption spectrum of hydrogen from rhodium. Pressure change monitored with Nottingham ion gauge a. ΔI vs time b. $(\Delta I + \frac{S}{V}\int_o^t \Delta I \, d\tau)$ vs time	102
7.	Analysis of corrected pressure-temperature data for hydrogen on rhodium by first- and second-order kinetics	103
8.	Normalized pressure increase as a function of emission current	104
9.	Effect of emission current of the thoria-coated filament on the pumping term, $\frac{S}{V}$	105

Page

10. Decrease in peak height of pressure burst due to pumping action of ion gauge at higher emission currents 106

11. Flash desorption of hydrogen from tungsten dosed at 300°K 107

12. Analysis of pressure-temperature data for hydrogen on tungsten, dosed at 300°K, by first- and second-order kinetics 108

13. Normalized desorption spectra of hydrogen from tungsten for increasing initial surface coverages 109

14. Desorption of hydrogen from tungsten at different initial coverages, analyzed as a second-order reaction 110

15a. Desorption of hydrogen from tungsten initially at 100°K 111

15b. Desorption of deuterium from tungsten initially at 100°K 112

16. Desorption of hydrogen from iridium dosed at 300°K a. Recorded pressure change b. Curve a corrected for pumping 113

17. Analysis of corrected pressure-temperature data for hydrogen on iridium by first- and second-order kinetics 114

Page

18. Desorption of hydrogen from iridium dosed at 100°K a. Partial pressure of hydrogen b. Total pressure 115

19. Desorption of hydrogen from iridium dosed at 100°K a. Heating rate ~255°/sec b. Heating rate ~75°/sec 116

20. Desorption of hydrogen from iridium for increasing initial doses at 100°K 117

21. Desorption of hydrogen from rhodium dosed at 300°K 118

22. Desorption of hydrogen from rhodium for different initial doses, analyzed as a second-order reaction 119

23a. Desorption of hydrogen from a rhodium filament dosed at 100°K 120

23b. Desorption of hydrogen from an annealed rhodium filament dosed at 100°K 121

24. Equilibrium distribution of the hydrogen isotopes in the ambient 122

25. Effect of an evaporated rhodium film on the distribution of the hydrogen isotopes in the ambient 123

26. Desorption spectra of hydrogen isotopes from iridium dosed at 100°K with a mixture of H_2 and D_2 124

Page

27. Equilibrium distribution of the hydrogen isotopes in the ambient with the rhodium filament at a 300°K and b 100°K 125

28. Desorption spectra of the hydrogen isotopes from tungsten dosed at 100°K with a mixture of H_2 and D_2 126

29. Adsorption-desorption spectrum of nitrogen on tungsten dosed at 300°K 127

30. Flash desorption of nitrogen from tungsten dosed at 300°K 128

31. Kinetic analyses of the pressure-temperature data for α- and β-nitrogen 129

32. Flash desorption of nitrogen isotopes from tungsten dosed at 300°K with a mixture of $^{14}N_2$ and $^{15}N_2$ 130

33. Desorption of nitrogen from iridium as a function of dosing time and temperature of the ion gauge filament 131

34. Temperature dependence of the formation of atomic nitrogen by an incandescent tungsten filament 132

35. Desorption of nitrogen isotopes from rhodium dosed at 300°K with a mixture of $^{14}N_2$ and $^{15}N_2$ 133

Page

36. Equilibrium distribution of nitrogen isotopes as a function of the temperature of the ion gauge filament 134
37. Desorption of carbon monoxide from tungsten for increasing initial doses at 300°K 135
38. Dependence of α_{CO} on the amount of β_{CO} adsorbed 136
39. Desorption of carbon monoxide from tungsten a. Heating rate 320°K/sec b. Heating rate 1380°K/sec 137
40. Desorption of carbon monoxide from rhodium dosed at 300°K 138
41. Desorption of carbon monoxide from iridium dosed at 300°K 139
42. Variation of the heat of adsorption with surface coverage 140
43. Schematic diagram of flash filament apparatus 141
44. Generated desorption spectra as a function of conductance of connecting tubulation a. F = 2.5 liters/sec b. F = 5.0 liters/sec c. F = 10 liters/sec d. F = 20 liters/sec 142
45. Generated desorption spectra as a function of pumping speed a. S_1 = 5 liters/sec b. S_1 = 10 liters/sec c. S_1 = 40 liters/sec d. S_1 = 80 liters/sec 143

Page

46. Block diagram of recording system 144

47. Schematic diagram for measuring the phase lag of the recorder 145

48. Recorder response as a function of frequency 146

49. Effect of recorder response on desorption curve and heating curve a. Recorded curve b. Corrected curve 147

LIST OF TABLES

		Page
1.	Effect of heating rate on pumping term $\frac{S}{V}$	149
2.	Distribution of hydrogen isotopes in the desorbed products from sample filaments dosed at 300°K with a mixture of hydrogen and deuterium	150
3.	Distribution of hydrogen isotopes in the desorbed products from an iridium filament dosed at 100°K with a mixture of hydrogen and deuterium	151
4.	Distribution of hydrogen isotopes in the desorbed products from a rhodium filament dosed at 100°K with a mixture of hydrogen and deuterium	152
5.	Effect of tube conductance and pumping speed on the relaxation parameters β_1, β_2 and β_3	153
6.	Phase lag of the x-y recorder as a function of frequency	154

LIST OF FORTRAN PROGRAMS

		Page
1.	Kinetic analysis of pressure-temperature data	182
2.	Variation of the activation energy of desorption with surface coverage	186

I. INTRODUCTION

The interaction of a gas with a metal surface has been of scientific interest because of its importance in a variety of problems, such as catalysis, corrosion and electron emission. As a result of this interest, much work has been done on the chemical, physical and electrical properties of clean surfaces. Clean surfaces are essential for investigating the interaction of extremely dilute gases with solids.

Flash desorption spectrometry is a sensitive tool for investigating the interaction of dilute gases with macroscopic wire samples. It consists of rapidly heating a metal filament on which adsorption has taken place at a given temperature and pressure. As the filament temperature increases, the rate of gas evolution in the closed system increases, resulting in an increase of the gas density. From the temperature dependence of this increase, one can obtain information concerning the rate processes which control the transfer of molecules from the adsorbed phase to the gas phase. The maximum increase in the gas density is a direct measure of the quantity of gas that was initially present on the metal surface. This technique is also suitable for observing the effect of surface coverage on these rate processes. If the adsorbate is capable of a complex sequence of reactions, as may be the case with hydrocarbons, a sensitive mass spec-

trometer may be used to identify the desorption products. A study of isotopic mixing in the adsorbed layer is useful for better defining the nature of the adsorbed species, and here, a mass spectrometer is essential.

These dynamic measurements of the adsorption of gases on metals are important not only for studying the nature of the adsorbed species, but also for better defining the adsorbing surfaces, and, hopefully, gaining an insight into what characteristics of the adsorbent are important in adsorption. This technique together with other powerful techniques, such as field emission microscopy and low energy electron diffraction, offers a route to a thorough understanding of surface phenomena.

This project is an application of the flash-filament principle to the study of the adsorption-desorption characteristics of simple diatomic molecules (H_2, N_2 and CO) on tungsten and the catalytically active transition metals iridium and rhodium including a study of isotopic exchange in dilute layers of co-adsorbed H_2-D_2 and $^{14}N_2$-$^{15}N_2$ mixtures.

II. LITERATURE REVIEW

A. General Background

The literature covered in this review will deal mainly with the study of adsorption phenomena in ultra high vacuum systems. Techniques for the production of ultra high vacuum ($<10^{-9}$ torr) have only been developed within the last fifteen years and the review will be limited to this period.

Apker (1) was the first to apply the flash filament technique to determine pressures beyond the limit of the ionization gauge. At that time, all his observations were not understood in detail, but he realized the importance of surface phenomena in vacuum technology and vice versa. Becker and Hartman (2) used the ionization gauge developed by Bayard and Alpert (3) to study the adsorption of nitrogen on tungsten. They made use of the sensitivity and speed of this ionization gauge to study the initial stages of adsorption and the variation of sticking probability with surface coverage. Becker (4) summarized in a review article his findings on the variation of sticking probability with surface coverage for a variety of gases and vapors. The character of his results suggested that the uptake of some gases by a metal surface is not a simple monotonically decreasing function of the amount present on the surface. Kisliuk

(5, 6) has derived values for the sticking probability assuming that the rates of migration and desorption for physically adsorbed molecules when they are above sites occupied by chemisorbed molecules are not equal to these rates when they are above unoccupied sites for chemisorption. His results agree with experiment for low surface coverages but do not account for the variation of the sticking probability as the surface coverage approaches a monolayer. Ehrlich (7, 8) also investigated the interaction of nitrogen with tungsten, but extended his investigations to lower temperatures. In addition to the primary chemisorbed state reported by Becker and Hartman (2), he observed two other states of lower binding energy. One of these states is significantly populated at room temperature, the other can only be detected below 200°K. Kisliuk (9) also investigated the chemisorption of nitrogen on tungsten. The aim of his investigation was to obtain a family of curves establishing the amount of nitrogen adsorbed at equilibrium on a tungsten ribbon as a function of temperature and pressure. These data can then be represented as isobars, isotherms or isosteres, from which he was able to obtain the isosteric heat of adsorption, the differential free energy, and hence the differential change in entropy during adsorption. Hickmott and Ehrlich (10), in an extensive article, described the mechanism of desorption of several diatomic molecules from tungsten. From this article, it was

clear that a sensitive mass spectrometer was essential to identify the desorption products, even in the case of simple diatomic gases, such as H_2, N_2, CO and O_2. Apker (1) realized that the mass spectrometer would play a valuable role in investigating surface phenomena, but it was not so used until 1960, when Hickmott (11, 12) used a small ion-resonance mass spectrometer to identify the desorption products and the products of the interaction of these species with the glass envelope of the reaction cell. Becker, Becker and Brandes (13) used a mass spectrometer to investigate the reactions of oxygen with tungsten containing carbon. Eisinger (14, 15) used the flash filament technique to investigate the properties of hydrogen and oxygen chemisorbed on a single crystal tungsten ribbon. He also measured the work function of the tungsten ribbon during adsorption of hydrogen by determining the ribbon's photoelectric threshold when it was illuminated by ultraviolet light.

Redhead (16) and Ehrlich (17) investigated the desorption of carbon monoxide from polycrystalline tungsten filaments. The desorption spectrum they obtained was quite complex, consisting of four binding states with different heats of adsorption. There is a primary chemisorbed state β, with an activation energy of desorption of 80 kcal per mole and a weaker state α, with a desorption energy of 20

kcal per mole, which forms as the rate of growth of β diminishes. Ehrlich (17) found no additional weak binding even at low temperatures. The more tightly bound β state is attributed to carbon monoxide chemisorbed in the bridged

structure (viz, M M), and the α state, to the linear

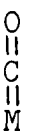

structure ( ). The β peak itself is made up of three subpeaks, which are attributed to surface heterogeneity.

Hickmott (11) found in his study of hydrogen desorption from tungsten that the temperature of the cathode in the detector had to be less than 1100°K to prevent dissociation and hence rapid pumping of molecular hydrogen. Instead of using a common ion gauge with tungsten filaments, he replaced one of the filaments with a lanthanum-boride coated tantalum filament. The low work function of this emitter enables the gauge to operate at a temperature below 1100°K, so that the formation of atomic hydrogen by thermal dissociation is sufficiently reduced that both ion gauge pumping and production of contaminants from reaction between atomic hydrogen and glass are reduced to easily manageable levels.

Pasternak and Weisendanger (18) investigated the interaction of hydrogen and nitrogen with a molybdenum ribbon by

means of the flash filament technique, with modifications designed to reduce the problem of contamination and to improve the resolution of overlapping peaks. They used a high steady flow rate and a conventional ion gauge mounted in a half-liter flask to reduce heating and degassing of the glass envelope. One of the main modifications was the use of high heating rates, approximately 10,000°K per second. Adsorption of hydrogen above 320°K yielded single pressure peaks in the desorption spectra, whereas adsorption at 225°K yielded two pressure peaks one at 350°K and the other at 550°K. The low temperature peak increased with adsorption time, whereas the height of the high temperature peak remained essentially constant. Moore and Unterwald (19) studied the interaction of hydrogen with tungsten and molybdenum ribbons, with the sample mounted adjacent to the ionization cage of a mass spectrometer. They estimated the heat of adsorption of hydrogen on tungsten to be 7 kcal at $\theta = 0.6$, by comparing desorption peaks at various temperatures for a given amount of adsorbed hydrogen.

Arthur (20) was the first to apply the flash-filament principle in conjunction with field emission microscopy (21) to investigate the surface reactions of hydrocarbons and hydrogen on iridium. He studied the adsorption and subsequent dehydrogenation of ethylene, acetylene and ethane

on iridium. Harvey (22) used this technique to study the decomposition of a sterically hindered acetylenic hydrocarbon on rhodium.

Weisendanger (23) studied the chemisorption of hydrogen and nitrogen on a polycrystalline platinum wire by analyzing the desorption spectra obtained on flash-heating the filament after adsorption from a gas stream of constant flow rate. He identified the desorbed gases by comparing these desorption curves with equivalent ones obtained with a tungsten filament in the same ultra high vacuum system under identical conditions.

Madey, Yates and Stern (24) used an omegatron mass spectrometer to study the kinetics of isotope mixing in carbon monoxide adsorbed on tungsten. They found that rapid isotopic mixing occurred at temperatures above 850°K. No evidence was found for dissociation of CO into mobile adsorbed carbon and oxygen atoms. A four-center bimolecular exchange intermediate on the surface was postulated which is consistent with a model for molecular CO adsorption, involving surface bonding through both the carbon and oxygen. They (25) also investigated the isotopic mixing in nitrogen chemisorbed on tungsten. The molecular identity of the low temperature state was confirmed by the absence of $^{14}N^{15}N$ in the desorption spectrum. The strongly held β-nitrogen was completely isotopically mixed on desorption. A study of the

β-peak revealed two overlapping binding states associated with surface heterogeneity in the tungsten substrate.

Moore and Unterwald (26) studied H_2-D_2 exchange and $^{14}N_2$-$^{15}N_2$ exchanged on molybdenum with a mass spectrometer. They found that the H_2-D_2 exchange reaction equilibrates on the surface during a single adsorption, throughout the temperature range 350°-1900°K for covers from 0.05 to 1.0 monolayer, and regardless of contamination by carbon monoxide or by nitrogen. They found that the nitrogen was completely isotopically mixed within experimental error. Evidence was given that nitrogen enters the bulk of the substrate either as a compound or solute or both.

Rigby (27) made a thorough study of the adsorption of nitrogen on polycrystalline tungsten wires. He found that two β-phases were desorbed, β_1 with first-order kinetics and an activation energy of 73 kcal per mole and β_2 with second-order kinetics and an activation energy of 75 kcal per mole. Surface impurities reduced the size of the β_1 phase. Mass spectrometric evidence showed that the small α-phase was adsorbed as molecules and the β-phase as atoms. Recently, Rigby (28) has reported on the adsorption and replacement of hydrogen on polycrystalline tungsten wires. The desorption spectra obtained showed that there are three β-phases of hydrogen as indicated by the three partially resolved peaks desorbing over the temperature range 300-600°K. Ricca,

Medana and Saini (29) also investigated the adsorption-desorption characteristics of hydrogen on polycrystalline tungsten. To observe the contributions of different crystal faces, they desorbed the gas from the adsorbent by slow heating (~2-3 deg/sec). The adsorbent was a cylindrically shaped tungsten sheet with a geometric surface area of 30 cm^2. The sample was heated by means of induced eddy currents which makes it difficult to determine accurately the range of temperatures for the desorption of different chemisorbed species and does not permit the corresponding desorption energies to be calculated. They observe six different peaks all attributed to hydrogen which desorb in groupings of two in the three temperature regions 77-190°K, 190-300°K and 300-600°K.

Delchar and Ehrlich (30) studied the effects of surface structure on the adsorption of nitrogen by contact-potential measurements on macroscopic planes cut from single crystal tungsten. On the (100) face room temperature desorption reveals only one state, β, in which nitrogen is bound as atoms. On the less reactive (111) face, they found two states, α and β and at higher concentrations, a second β state is isolated by flash desorption. No adsorption on the (110) face was observed at 300°K and P = 10^{-7} torr.

Methods of analyzing desorption spectra for the kinetic parameters have been described by many investigators.

Smith's (31) treatment of the thermodesorption of gases from solids is analogous to thermoluminescence, where the energy to free electrons from traps is determined. He treats the case of desorption into a constant volume and the case where there is a large leak into a vacuum. The most extensive treatment has been that of Ehrlich (32), in which he treats both the kinetic and experimental problems associated with the flash filament technique. He describes the procedure for deriving both qualitative and quantitative information on the kinetics of gas desorption. He also analyzes the effect of the ionization gauge on desorption measurements. In a recent review article, Ehrlich (33) has surveyed the modern methods used in studying surface kinetics, namely flash desorption, field emission microscopy and the role played by vacuum technology in these investigations. Redhead's (34) method of analysis deals mainly with the determination of the kinetic parameters from the shape of the desorption spectrum. The activation energy of desorption is estimated from the temperature at which the desorption rate is a maximum for first-order reactions and from the change of this temperature with surface coverage for second-order reactions. The order of the reaction is determined from the shape of the desorption rate versus time curve. This treatment is also applicable to the desorption of ionically trapped gases. Carter's (35) treatment of desorption energy spectra is similar to

Redhead's (34), but in addition, he treats desorption from heterogeneous sites of different discrete desorption energies. He also describes the generality of the numerical technique for the analysis of continuous energy spectra. In a later article, Carter (36) considered the effect of the heating schedule on the resolution of desorption spectra from two types of adsorption sites of slightly different adsorption energy. He concluded that in order to achieve adequate resolution of a given region of an energy spectrum, it is necessary to suitably control the heating rate.

B. Current Status and Relation to Present Work

At the time this work was begun, the flash filament technique had been used principally to investigate the adsorption-desorption characteristics of nitrogen, hydrogen and carbon monoxide from a single adsorbent, namely tungsten. Only the work of Ehrlich, Hickmott and Redhead combined the features of impurity partial pressures less than 5×10^{-10} torr, ultraclean surface preparation and gauge operation precautions with kinetic analysis of reasonable versatility necessary for reliable investigation of surface reactions and these workers limited their studies to the systems just named. None had combined these methods with mass spectrometry to permit supplementary exchange studies, detailed product

analysis and impurity partial pressure monitoring. The methods of kinetic analysis used were insufficiently precise to permit quantitative estimates of good precision of the variation in activation energies with surface coverage.

From the work of Ehrlich, Hickmott and Redhead it was known that each of the three gases hydrogen, nitrogen and carbon monoxide exhibited at least two binding states when adsorbed on tungsten as indicated by the multiple peaks in the desorption spectrum. These were designated as α, desorbing at low temperature, and β, desorbing at high temperature. In the case of carbon monoxide it was further known that the β-peak was split into at least three components and it was suggested, by comparison with infrared spectra of chemisorbed carbon monoxide, that the β-group of peaks resulted from the desorption of bridged-bonded molecules from the various crystal faces exposed on the surface of the adsorbent. It was also known that the desorption of β-hydrogen and β-nitrogen from tungsten was kinetically second order and kinetic parameters (frequency factor and activation energies) of apparently good quality were available for these systems at low coverage. The desorption of α-nitrogen was kinetically first order, but the kinetic data in this case were of much poorer quality. The desorption of α-hydrogen appeared to be kinetically first order, but the data in this case permitted little more than a subjective judgement.

The excellent β-hydrogen and β-nitrogen desorption data on tungsten provides an excellent basis for calibration of experimental and theoretical techniques with a system of known characteristics. No exchange experiments had been done on these systems, and it was therefore considered desirable to check the atomic nature of the adsorbed species in these states, as indicated by the second-order desorption kinetics, by H_2-D_2 and $^{14}N_2$-$^{15}N_2$ exchange experiments. Because the kinetic evidence concerning the α-states was only moderately good in the case of nitrogen and fair, at best, in the case of hydrogen, similar exchange investigations of these states were strongly suggested.

Hydrogen is the simplest chemisorbing element, and a fundamental study of its chemisorption is therefore of great theoretical interest. The chemisorption of hydrogen on transition metals is also of great technical interest because of its relation to catalytic hydrogenation, catalytic ammonia synthesis, and fuel cell operation. Hydrogen chemisorption also exhibits a wide variety of phenomena, including multiple binding states, marked variation in adsorption enthalpy with surface coverage and marked variation in surface mobility with temperature. The dissociation of hydrogen by hot filaments (as in conventional ion gauges) with corresponding pumping and contaminant production, is much more pronounced in the case of hydrogen than in other simple diatomic gases,

such as nitrogen and carbon monoxide, so that an experimental procedure developed for the study of these less reactive gases must be modified for investigating hydrogen. This modified procedure is then suitable for studying many other systems.

The Group VIII transition metals include the metals that are most active in catalytic hydrogenation and ammonia synthesis. Two of these metals, iridium (m.p. = 2443°C, a_o = 3.84 Å, f.c.c.) and rhodium (m.p. = 1966°C, a_o = 3.80 Å, f.c.c.) were selected for the present study, because both are active in a number of catalytic reactions and their surface oxide decomposes at relatively low temperatures. Nickel would have been more desirable to use, since it is active in a wider variety of catalytic reactions and hence a large amount of experimental data is available on its catalytic behavior. Unfortunately its melting point is too low (m.p. = 1455°C) for use in flash desorption.

As a result of this past work, the present study was carried out to gain a thorough understanding of the flash filament technique by supplementing the work of previous investigators and extending this investigation to more catalytically active metals.

The system nitrogen-tungsten was used as a calibration of the flash filament technique. Also, since it exhibits two binding states, it was investigated to gain further informa-

tion on the kinetics and energetics of desorption from these binding states. The behavior of a co-adsorbed mixture of $^{14}N_2$ and $^{15}N_2$ on desorption was investigated to gain additional information on the nature of the adsorbed species.

Carbon monoxide does not dissociate on adsorption, but it does exhibit multiple binding modes on tungsten. Since iridium and rhodium have a different crystal structure than tungsten and since there exists some infrared data for carbon monoxide adsorbed on rhodium, the desorption characteristics of carbon monoxide from tungsten, iridium, and rhodium were investigated to observe the effect of crystal structure (interatomic spacing) on these binding modes.

The most extensive work was carried out with hydrogen. The experimental techniques, particularly those concerned with ion gauge operation, were investigated to determine their effect on the desorption spectrum of hydrogen. A general method of analysis, accounting for the variation of the activation energy of desorption with surface coverage was developed and applied to hydrogen desorption data. Hydrogen-deuterium exchange was investigated to complement the results obtained from kinetic analysis of the desorption of each component.

III. FLASH DESORPTION SPECTROMETRY

Flash desorption spectrometry is in principle a simple technique for gaining information about the rate processes which govern the transfer of molecules from the adsorbed phase to the gas phase. If a metal sample, in the form of a wire or ribbon, is rapidly heated in a closed system at a low background pressure, then the pressure increase in the system is a direct measure of the total number of molecules which have desorbed from the sample. The temperature dependence of this gas evolution yields information on various adsorption parameters, namely, the number of desorbing phases, the activation energy of desorption and the kinetic order of the rate controlling step in the desorption process.

In a closed system, the number of molecules desorbed from the filament on heating can be obtained from the ideal gas law,

$$n_o = \frac{V\Delta P}{kTA} \qquad (1)$$

where n_o is the number of adsorbed molecules per cm^2, V is the volume of the system in liters and A is the surface area of the filament in cm^2. In practice, no system is completely closed, since some molecules are removed from the system by the pressure measuring devices.

The rate at which the number of molecules in the gas phase changes on heating the sample depends on the rate law followed by the desorbing gases, the heating schedule, the rate of removal of gases from the system and the rate of supply of gas from the reservoir. In a flash desorption experiment, the rate of change of the number of molecules in the gas phase is

$$\frac{dN}{dt} = -A\frac{dn}{dt} - \frac{S}{V}N + L \qquad (2)$$

where N is the number of molecules in the ambient, $-A\frac{dn}{dt}$ is the number of molecules released into the system per second from a filament of surface area A, S is the pumping speed of all gas sinks in liters per second and L is the leak rate of the test gas from the reservoir in molecules per second. We have assumed that, during the interval in which desorption occurs, gas flow from the walls and readsorption by the sample is negligible.

Since the mean free path of the molecules at this pressure is much larger than the dimensions of the cell and tubulation, the desorbing molecules must undergo many collisions with the glass envelope before they reach the detector. Hence, we will assume that the molecules have equilibrated with the glass walls.

In an actual experiment the gas density is measured by a detector at some distance from the reaction cell. This

separation of sample and detector is due to the size of the detector and the necessity to minimize electrical interference. The detector and cell are mounted in two separate flasks connected by large bore tubulation. As a result of this tubulation, density gradients may exist during adsorption and desorption. This problem is treated in detail in Section XIII.

If we let $T = T_o$, where T_o is the temperature of the glass envelope, then from the ideal gas law we obtain

$$N = \frac{PV}{kT_o} \tag{3}$$

Substituting this result into Equation 2 and rearranging, we find

$$-\frac{dn}{dt} = \frac{V}{AkT_o}\left[\frac{dP}{dt} + \frac{S}{V}P - \frac{LkT_o}{V}\right] \tag{4}$$

At steady state prior to the flash, $\frac{dP}{dt} = 0$, $\frac{dn}{dt} = 0$ and $P = P_o$. This implies that

$$P_o = \frac{LkT_o}{S} \tag{5}$$

Substituting this value of P_o into Equation 4 and letting $\Delta P = P - P_o$, we obtain

$$-\frac{dn}{dt} = \frac{V}{AkT_o}\left[\frac{dP}{dt} + \frac{S}{V}\Delta P\right] \tag{6}$$

Integrating Equation 6 yields

$$-\Delta n = \frac{V}{AkT_o}\left[\Delta P + \frac{S}{V}\int_{t_o}^{t} \Delta P dt\right] \tag{7}$$

where $-\Delta n = n_o - n$.

Equation 7 gives the amount of material desorbing from the surface as a function of time, corrected for the amount lost by pumping. To obtain the kinetic parameters of interest from the dependence of Δn on time, obtained from Equation 7, we assume that the isothermal rate of gas evolution is given by the Polanyi-Wigner equation,

$$-\frac{dn}{dt} = \nu_k n^k \exp\left[\frac{-\Delta H}{RT}\right] \tag{8}$$

where n is the number of molecules adsorbed per cm^2, ν_k is the frequency factor and k is the kinetic order of the reaction. Let $x = \frac{1}{T}$ and suppose that $t = f(x)$. Presumably t can be made nearly linear in x, but for completeness, we will assume that it is an arbitrary function of x.

Then

$$-\frac{dn}{dt} = -\frac{dn}{dx}\frac{dx}{dt} = -\left[f'(x)\right]^{-1}\frac{dn}{dx} \tag{9}$$

Substituting this in Equation 8 and rearranging, we obtain

$$-\frac{dn}{dx} = \nu_k n^k f'(x) \exp\left[\frac{-\Delta H}{R} x\right] \tag{10}$$

Let $n = \theta n_m$, where n_m is the number of molecules per cm^2 in a monolayer.

Then

$$-\frac{dn}{n^k} = -\frac{1}{n_m^{k-1}}\frac{d\theta}{\theta^k} \tag{11}$$

Substituting this in Equation 10 and rearranging, we obtain

$$-\frac{d\theta}{\theta^k} = \nu_k\, n_m^{k-1} f'(x)\, \exp\left[-\frac{\Delta H}{R}\, x\right] dx \tag{12}$$

We suppose that $\frac{\Delta H}{R}$ is a function of θ, presumably nearly linear in θ. Let $\frac{\Delta H}{R} = g(\theta)$, and $\nu_k\, n_m^{k-1} = \mu$.

Then

$$-\frac{d\theta}{\theta^k} = \mu f'(x)\, \exp\left[-g(\theta)x\right] dx \tag{13}$$

$$-\int_{\theta_o}^{\theta} \frac{d\varphi}{\varphi^k} = \mu \int_{x_o}^{x} f'(y)\, \exp\left[-g(\theta)y\right] dy \tag{14}$$

Integration of the left hand side yields

$$-\int_{\theta_o}^{\theta} \frac{d\varphi}{\varphi^k} = \begin{cases} \ln \frac{\theta_o}{\theta} & k=1 \qquad (15a) \\ \frac{1}{k-1}\left\{\frac{1}{\theta^{k-1}} - \frac{1}{\theta_o^{k-1}}\right\} & k\neq 1 \qquad (15b) \end{cases}$$

Evaluation of the right hand side of Equation 14 is somewhat more complicated. Let $y = x + u$; then $u = 0$ when $y = x$ and $u = x_o - x$, when $y = x_o$.

Then

$$\mu \int_{x_o}^{x} f'(y)\, \exp\left[-g(\theta)y\right] dy = -\mu \int_{o}^{x_o - x} f'(x+u)\, \exp\left[-g(\theta)(x+u)\right] du \tag{16}$$

Most of the value of this integral will come from values of u near zero, and we can therefore use Taylor series terminated after two terms advantageously. We set

$$f'(x+u) = f'(x) + u\,f''(x) \tag{17a}$$

$$g(\theta)(x+u) = xg(\theta) + u(xg)' \tag{17b}$$

and substituting this into Equation 16, obtain,

$$-\mu\int_0^{x_o-x} f'(y)\exp\left[-g(\theta)y\right]dy = -\mu\exp(-xg)\int_o^{x_o-x}\left[f'(x) + uf''(x)\right]\exp\left[-u(xg)'\right]du \tag{18}$$

$$= -\mu\exp(-xg)\left[f'(x)\,\frac{1-\exp\left[-(xg)'(x_o-x)\right]}{(xg)'} + f''\int_o^{x_o-x} u\exp\left[-u(xg)'\right]du\right] \tag{19}$$

$$= -\frac{\mu f'(x)\exp(-xg)}{(xg)'}\left[1 - \exp\left[-(xg)'(x_o-x)\right] + \frac{f''(x)(xg)'}{f'}\left\{\frac{-(x_o-x)\exp\left[-(xg)'(x_o-x)\right]}{(xg)'} - \frac{\exp\left[-(xg)'(x_o-x)\right]}{\left[(xg)'\right]^2} + \frac{1}{\left[(xg)'\right]^2}\right\}\right] \tag{20}$$

$$= -\frac{\mu f'(x)\exp(-xg)}{(xg)'}\left[1 + \frac{f''(x)}{f'(x)(xg)'} - \left\{1 + \frac{(x_o-x)f''(x)}{f'(x)} + \frac{f''(x)}{f'(x)(xg)'}\right\}\exp\left[-(xg)'(x_o-x)\right]\right] \quad (21)$$

Now

$$\frac{d\ln\left[-\int_{\theta_o}^{\theta}\frac{d\varphi}{\varphi^k}\right]}{dx} = \frac{-\frac{1}{\theta^k}\frac{d\theta}{dx}}{-\int_{\theta_o}^{\theta}\frac{d\varphi}{\varphi^k}} \quad (22)$$

But $-\frac{1}{\theta^k}\frac{d\theta}{dx}$ is given by Equation 13 and $-\int_{\theta_o}^{\theta}\frac{d\varphi}{\varphi^k}$ by Equation 21.

Hence

$$\frac{d\ln\left[-\int_{\theta_o}^{\theta}\frac{d\varphi}{\varphi^k}\right]}{dx} = -\frac{(xg)'}{1+\frac{f''(x)}{f'(x)(xg)'} - \left\{1+\frac{(x_o-x)f''(x)}{f'(x)} + \frac{f''(x)}{f'(x)(xg)'}\right\}\exp\left[-(xg)'(x_o-x)\right]} \quad (23)$$

If we neglect all terms other than 1 in the denominator, although they can be determined, then Equation 23 reduces to

$$\frac{d\ln\left[-\int_{\theta_o}^{\theta}\frac{d\varphi}{\varphi^k}\right]}{dx} \approx -(xg)' \quad (24)$$

Now $x = 1/T$, $g = \frac{\Delta H}{R}$ and ΔH depends on θ

Hence,

$$(xg)' = g + xg' = \frac{\Delta H}{R} + \frac{1}{RT}\left(\frac{d\Delta H}{d\theta}\right)\frac{d\theta}{dx} \qquad (25)$$

In an actual experiment, $\ln\left[-\int_{\theta_o}^{\theta} \frac{d\theta}{\phi^k}\right]$ is experimentally available once a value of k is assumed, and can be plotted against $x = \frac{1}{T}$. For small values of θ, where ΔH is essentially constant, and if $\frac{1}{T} = a + bt$, (where, $b = \frac{d\,\frac{1}{T}}{dt}$), then Equation 21 can be integrated to yield, if we neglect all terms other than 1 inside the brackets,

$$\ln \ln \frac{n_o}{n} = \frac{-\Delta H}{RT} + \ln\left\{\frac{R\nu}{\Delta H - \frac{d\ 1/T}{dt}}\right\} \quad \text{if } k = 1 \qquad (26a)$$

$$\ln \frac{n_o - n}{nn_o} = \frac{-\Delta H}{RT} + \ln\left\{\frac{R\nu}{\Delta H - \frac{d\ 1/T}{dt}}\right\} \quad \text{if } k = 2 \qquad (26b)$$

If either the left side of Equation 26a or 26b varies linearly with $\frac{1}{T}$, then the reaction is correspondingly first or second order, and the slope of the linear plot is $\frac{-\Delta H}{R}$. Equations 26a and 26b are obtained assuming that ΔH and ν are independent of surface coverage. Experimentally it is found that both ΔH and ν are essentially constant at low

coverages. For nitrogen on tungsten (8), ΔH is constant for all coverages while for hydrogen on tungsten (11), ΔH is constant up to a surface coverage of 30×10^{12} molecules/cm^2, but decreases at higher coverages. Hence, the results given by Equations 26a and 26b are no longer valid for large values of n, when the heat of desorption is a function of surface coverage. The deviation from linearity of plots derived from Equations 26a or 26b is a measure of the variation of the activation energy of desorption with increasing surface coverage. If we assume a linear variation in the heat of desorption, i.e. $\Delta H = \Delta H_o - \alpha n$, then α can be obtained from Equation 24 and 25. When determined this way, α is somewhat inaccurate due to the difficulty in obtaining $\frac{dn}{dt}$. There are at least two other ways to determine α. Substituting $\Delta H = \Delta H_o - \alpha n$ into Equation 8, yields,

$$-\frac{dn}{dt} = \nu n^2 \exp\left[-\frac{\Delta H_o - \alpha n}{RT}\right] \qquad (27)$$

for a second order reaction. This expression cannot be integrated analytically. But α can be determined by solving Equation 27 at the point of inflection, i.e. $\frac{d^2n}{dt^2} = 0$, of the desorption curve for large initial coverages and using ΔH_o and ν obtained, for low coverages, from Equation 26b. This method is also inaccurate for the reason mentioned above. In the second method, the parameters ΔH_o and ν are again

established from low coverage experiments and a minimum search routine (Section XIII) is carried out with respect to α, using a computer to integrate numerically Equation 27. This latter method gives good agreement between the experimental and the generated values.

Continuous recording of the pressure rise during a flash desorption experiment has revealed that the adsorption process is complex as indicated by the presence of multiple peaks in the desorption spectrum. In most cases only one of the binding states can be treated by the above analysis: the others are usually present in small amounts and/or are not adequately resolved. The activation energy of these other states can be estimated from the temperature range over which desorption occurs.

Hence, flash filament desorption spectrometry can be used to determine the kinetics and energetics of the rate controlling step in the desorption process, the variation of the activation energy of desorption with surface coverage and the quantity of material which is adsorbed.

IV. EXPERIMENTAL PROCEDURES

A. Introduction

Recent developments in the field of vacuum technology have made the generation and preservation of clean surfaces a routine procedure. It can be shown from kinetic theory that extremely low pressures are required to maintain a clean surface; at 10^{-6} torr, enough molecules strike the surface in three seconds to form a complete monolayer, whereas, at 10^{-10} torr, clean surfaces can be generated and maintained for a period of several hours. Since the number of atoms on the surface is about 10^{15} per cm^2, impurity concentrations of 1% either in the test gas or sample surface may markedly alter the adsorption characteristics of the system under investigation. Surface impurities can generally be removed by high temperature heating and since the impurity level of the test gas is determined by the quantity of residual gases, the advantages of investigating adsorption phenomena in ultra high vacuum systems are evident.

B. Ultra High Vacuum Techniques

Pressures in the ultra high vacuum range (below 10^{-9} torr[1]) are essential for the measurement of the properties of clean surfaces and for investigating the interaction of extremely pure gases with these surfaces. These investigations of surface phenomena can be most conveniently carried out in glass systems of small volume (about 2 liters).

Such ultra high vacuum techniques have only become known within the past twelve years. In 1953, Alpert (37) described in detail the methods used for obtaining ultra-high vacuum. His chief contribution was the introduction of an ionization gauge which could measure pressures as low as 10^{-11} torr. This lower limit is determined by the photoelectron current from the collector caused by soft x-rays emanating from the electron bombarded grid and is referred to as the x-ray limit of the gauge. Venema (38) was able to obtain a pressure of 10^{-12} torr by means of a specially designed mercury diffusion pump. The omegatron, originally developed by Sommer, Thomas and Hipple (39) for measuring atomic constants, was used by Alpert and Buritz (40) as a mass spectrometer for measuring the partial pres-

---

[1] 1 torr = 1 mm of Hg.

sures of the residual gases in an ultra high vacuum system. The omegatron paved the way for the development of more sophisticated partial pressure analyzers (higher sensitivity and better resolution) that could be used with ultra high vacuum systems.

The ultimate pressure in any vacuum system is established when the rate of removal of gas by the pumps and the rate of production of gas from all sources are equal. The rates of processes controlling gas production all increase greatly as the temperature is increased. It is therefore possible, by baking out the apparatus for a suitable period, to markedly reduce the amount of gas absorbed on walls, gauge parts, etc. so that, at experimental temperatures, the rates of supply of gas from these sources is markedly reduced and much lower limiting pressures can therefore be achieved. Evolution of water from the glass is the dominant source of gas during bake-out. This water, which is chemically bonded to the glass (41, 42) is adequately removed by normal baking ($350^{\circ}C$-$400^{\circ}C$) although the depletion process is not a simple desorption.

The various components of the vacuum system and the associated electronic equipment are shown schematically in Figure 1 and the actual physical arrangement of the components is shown in Figure 2.

The vacuum system was constructed of borosilicate glass (Corning 7740). It consisted of two, two-stage mercury diffusion pumps in series backed by a rotary forepump. Following the diffusion pumps were two cold traps, separated from the working area by a magnetically operated ground glass valve. The entire system beyond the first trap can be enclosed in a portable oven and baked to 350°C to drive off the adsorbed gas. Gases to be used in adsorption studies were kept in glass ampoules provided with a break-tip and separated from the working area by Granville-Phillips variable leak values. The working area contained a desorption cell, two ion gauges and a mass spectrometer.

The desorption cell shown in Figure 3, was a flask with five outlets connected to a mass spectrometer, two ion gauges, gas supply and diffusion pumps. It was constructed with a reservoir just above the filament assembly which could be filled with the proper coolant to maintain the filament at a fixed temperature during adsorption. Liquids used for this purpose were liquid nitrogen (~100°K) and water (300°K). Two types of reservoirs were used in this work. One was the conventional cold-finger design (Figure 3), similar to the one used by Arthur (20) and it was used to study the desorption of hydrogen, nitrogen and carbon monoxide. The other consisted of a specially designed dewar, containing the tungsten leads, which could be sealed to the reaction cell.

This design minimized the cold surface exposed to the reacting gases and the area of the cold surface was further independent of the level of coolant in the dewar. This type of reservoir is better suited for studying the decomposition of hydrocarbons and other condensable gases.

Three types of total pressure gauges were used with this system, the cold-cathode magnetron gauge developed by Redhead (43), a Nottingham gauge (44), which is a modified form of the hot-cathode Bayard-Alpert (3) gauge, and a modulated ion gauge developed by Redhead (45, 47). The magnetron gauge is a cold-cathode ionization gauge with axial magnetic field and radial electric field which is capable of measuring pressures in the range 10^{-5} to 10^{-12} torr. The gauge is operated with an anode voltage of 6000 volts and a magnetic field of 1000 gauss. It has been shown (43, 46) that the relationship between ion current and pressure, at the normal operating point, is linear in the pressure range 10^{-5} to 5×10^{-10} torr. At lower pressures, the relationship is $I_+ = CP^n$, where the exponent n is approximately 1.5. The magnetron gauge has a sensitivity about 45 times greater than that of a standard ionization gauge. Since it contains no hot filaments, it is capable of measuring pressures of hydrogen and other active gases, which would be decomposed by the hot filament of a thermionic ionization gauge. All of these advantages appear to make the magnetron gauge ideally

suited for investigating the interaction of active gases, such as ethylene, acetylene and hydrogen with metal surfaces by the flash filament technique. There are, however, yet more important limitations. Redhead (47) claims that cold-cathode gauges are not suitable for accurate pressure measurements because of their high pumping speed which cannot be easily reduced. Ehrlich (32) has shown that a high pumping speed is advantageous in resolving overlapping peaks but is not conducive to a quantitative analysis of the desorption spectrum. We have observed a variable pumping speed for the magnetron gauge which is dependent on the state of contamination of the gauge. Immediately after bakeout, the gauge has a high pumping speed, but after extended use the net pumping speed of the gauge is reduced to about 0.2 liters per second for hydrogen. Oscillations of the ion current were observed in the magnetron gauge under almost all conditions. These oscillations varied both in frequency and amplitude. The discontinuities observed in the pressure-current characteristics (Section XIII). may be due to a jump in frequency from one mode of oscillation to another as reported by Peakes and Torney (48). The magnetron gauge was investigated as a possible detector in flash filament experiments, but it was observed that the gauge instability and oscillatory behavior of the ion current made it unsuitable for this purpose.

The Nottingham ionization gauge differs from the conventional Bayard-Alpert (B. A.) type gauge in that the cylindrical grid is closed at top and bottom and a second grid, acting as a screen grid, is installed around all the electrodes. The purpose of closing the cylindrical grid is to prevent the ions, with a component of velocity parallel to the collector, from escaping to the negatively charged glass wall. This increases the collection efficiency of the ions. The screen grid shields the gauge from the wall potential. In the present case, the screen grid was a platinum film deposited on the inner wall of the gauge and connected to an external lead. The screen grid was operated at a given potential (ground) relative to the filament, which increased the average path length of the electrons, thereby increasing the probability of a collision with the ambient gas molecules. The ion gauge was connected to the reaction cell by 25 mm tubulation to increase the conductance between the reaction cell and detector. These modifications increase the sensitivity of this gauge by a factor of two or three over the conventional B. A. gauge.

The Nottingham ionization gauge was normally operated with a grid-to-filament voltage of +150 volts and a filament-to-collector voltage of +45 volts. Under these conditions the ion current from this gauge was a linear function of the ion current from the magnetron gauge (Section XIII).

If we assume the sensitivity of the magnetron gauge to be 4.5 amps/torr for nitrogen (49, p. 377) then the sensitivity of the Nottingham gauge is 25 $torr^{-1}$ for nitrogen, in good agreement with Redhead's (47) value of 22 $torr^{-1}$ for the modulated B. A. gauge.

An additional feature of the ionization gauge is its ability to act as a pump. If the gauge is connected to the system through small tubulation, then this pumping action may result in misleading pressure indications in both steady state and transient measurements. The removal of gases by an ionization gauge may proceed by several mechanisms. Initially the clean surfaces of the electrodes and/or the glass envelope may adsorb certain gases. The gauge may act as an ion-pump, in which the ions formed outside the grid are trapped at the negatively charged electrodes or walls. The hot filament of the gauge may cause thermal dissociation of some gases, with dissociation products removed by attachment or recombination at the walls of the gauge.

In flash desorption experiments it is necessary to reduce the pumping speed of the ion gauge to a minimum. The ionic pumping speed of the gauge can be reduced by decreasing the electron emission current. Reducing the electron current not only decreases the pumping but also reduces the temperature of the filament, thereby reducing the thermal decomposition of chemically active gases. But reducing the electron

current also decreases the ion current proportionately for a given pressure, and associated with this small ion current is a longer response time of the electrometer when measuring pressure bursts. Ideally, one would like an ion gauge that has a low temperature of operation for a relatively high emission current and/or an electrometer that has a fast response for small ion currents ($\sim 10^{-9}$ amps).

The other ion gauge that was used in this work appeared to meet all the ideal requirements mentioned above. The electrode structure of the modulated B. A. gauge is mounted in a half-liter flask coated with stannous oxide. The larger dimensions of this gauge minimized heating of the glass envelope, thereby reducing the outgassing of the gauge. This gauge differed from the Nottingham gauge in the emitting temperature of the filament for a given electron current. Two low work-function filaments were used in this gauge. One was a tungsten filament coated with thorium oxide which delivered 40μa electron current at $\sim 1050^{\circ}$K and 4 ma at $\sim 1400^{\circ}$K. The other filament was a platinum ribbon coated with a mixture of lanthanum oxide and barium oxide, which when properly activated, delivered 40μa at $\sim 900^{\circ}$K and 4 ma at $\sim 1200^{\circ}$K. This gauge was normally operated with a grid-to-filament voltage of +135 volts and a filament-to-collector voltage of +45 volts. Under these conditions the

ion current from this gauge was a linear function of the ion current from the Nottingham gauge. The gauge factor for nitrogen was taken to be 20 $torr^{-1}$ (Section XIII).

A more complete understanding of the vacuum conditions can be obtained by incorporating a sensitive mass spectrometer into the vacuum system. There are several advantages to using a mass spectrometer rather than a total pressure gauge; first, composition of both residual and desorbing gases can be obtained, second, mass spectrometers do not usually have an x-ray limit, and third, the ionic pumping speed is usually much lower than that of an ion gauge.

The mass spectrometer used in this work was a deflection type developed by Davis and Vanderslice (50). This instrument consists of an electron-bombardment ion source, a 90^{o} sector type magnetic analyzer and a 10-stage electron multiplier ion detector. It is capable of measuring pressures as low as 10^{-14} torr, resolving adjacent masses up to mass 100 and detecting masses up to mass 200. For quantitative analysis of the desorption spectra using the mass spectrometer as the detector, focussed on a given species, the output of the electron multiplier was connected to a high speed picoameter (Keithley 415). With this arrangement, one was not only able to identify the products formed on flashing but also the temperature at which desorption occurs and hence, some

information about the kinetics and energetics of the rate-determining step. It was also possible to obtain the relative quantities of the desorption products and their dependence upon surface coverage, since the ion current is directly proportional to the molecular density.

The system was evacuated in the following way. The vacuum system was initially pumped down to about 10^{-7} torr with the diffusion pumps. The oven was then placed in position and the temperature raised to 300°C slowly enough so that the pressure in the system did not increase above 10^{-5} torr. When the pressure had decreased to about 1 x 10^{-7} torr, the oven was removed and the pressure further decreased by an order of magnitude. All the metal parts in the system were then extensively outgassed. Following this outgassing the oven was put in place and the whole system, including the second trap, was heated to 350°C. During this baking cycle, the filaments in the ion gauge were operated at 1 ma emission current. This current was high enough to prevent adsorption on the filament and low enough to prevent overheating of the glass envelope. After the pressure in the system decreased to less than 10^{-7} torr, the oven was shut off, and the ion gauges were carefully outgassed. In this way, most of the gas given off by the gauge was removed by the diffusion pumps, since the system was too hot for adsorption to take place on the walls. The oxide coated fila-

ments produce large quantities of carbon monoxide during activation, so that activation during bakeout drastically reduces the time required to activate them. In the case of the oxide-coated platinum filament, the lower the pressure of activation, the lower is the final temperature of operation. After outgassing the gauges, the second trap was then cooled with liquid nitrogen and the ovens were removed. The sample filament was then outgassed. The pressure in the system as indicated by the magnetron gauge was usually 2 x 10^{-10} torr and it decreased to 5 x 10^{-11} torr after a few hours, where it could be maintained for a period of weeks. Over such a period of time, the total pressure may not vary by more than 10-20%, but the ordering of the residual components may be completely altered. Hence, it is evident that a mass spectrometer is extremely useful in analyzing the varying composition of residual gases and the effect they have on the adsorption of the test gas.

Pressures in the ultra high vacuum range have become a routine procedure in investigating surface phenomena. The above discussion in no way exhausts the fascinating subject of ultra high vacuum, but it does illustrate the basic principle of vacuum work, namely, the ultimate pressure in the vacuum system is dictated by a balance between rate of removal and rate of evolution of gas. A more detailed discussion of vacuum technique and of the various components used in vacuum systems is given in references 49, 33, 51.

C. Temperature Measurement and Control

For kinetic studies of surface reactions, it is essential to know the filament temperature as a function of time during adsorption and desorption. The temperature of the filament can be determined by using the filament as a resistance thermometer. It is also desirable to be able to vary the rate at which the filament is heated and to terminate the heating at a predetermined temperature.

The filament was heated by constant current obtained from the power supply shown in Figure 4. With this circuit, it is possible to vary the heating rate from ~40°/sec to ~400°/sec. The voltage drop across the filament is monitored on a recorder during an experiment. The voltage drop across the filament, for a given current, is a direct measure of the resistance and hence, the temperature of the filament. The final temperature reached by the filament in a given experiment was determined as follows. The voltage drop across the filament was monitored by a dc-level detector (trigger circuit) shown in Figure 4. When the voltage drop reached a predetermined value, the relay in the trigger circuit closed, switching the current from the filament to a dummy load. The final temperature is determined by the current applied to the filament and the voltage level of the trigger circuit. The voltage level is adjustable from 0.5

volts to 9.5 volts, which corresponds to a range of final temperatures from ~150°K to 1701°K.

The temperature dependence of resistance of the metal filaments was determined as follows. A twenty centimeter length of 5 mil wire, from the same lot as the sample filament, was annealed with direct current for three hours. The middle ten centimeters was then spot-welded to the calibrating assembly. The resistance of the filament was determined by passing a small current (1 to 10 ma) through the filament, while it was immersed in various constant temperature baths, and measuring the voltage drop with a high input impedance recorder. The baths used for this purpose were: liquid nitrogen, 77°K; dry ice-acetone, 189°K; water, 295°K; boiling acetone, 325°K; boiling water, 373°K; boiling decalin, 464°K and boiling narcoil-10, 640°K. The temperature of the low-temperature baths was measured with a calibrated copper-constantin thermocouple and a Leeds and Northrup potentiometer. A plot of resistance-ratio versus temperature for the three metals used in this investigation is shown in Figure 5. The resistivity was not calculated, since the dimensions of the wire filaments were not accurately known. But the temperature coefficient of resistivity α is independent of filament dimensions, and for these filaments, a least squares analysis of the data points yielded, 4.19×10^{-3}, 3.72×10^{-3}

and 3.19×10^{-3} reciprocal degrees, for tungsten, rhodium and iridium respectively.

In flash desorption spectrometry, it is assumed that the temperature of the filament during an experiment is uniform over the whole length except for small portions near the ends of the filament which are welded to the tungsten leads. If the temperature were not uniform, then multiple peaks may arise from a single species on the surface, because different sections of the filament are heated at different rates. Ehrlich (32) has actually measured the temperature distribution during a flash and in steady state by measuring the voltage drop across potential probes attached to the filament. He found that throughout the temperature range $200^{\circ}K$-$1480^{\circ}K$, the filament temperature is considerably more uniform during the flash than in steady state. More precisely, the further away the filament is from steady state, the more uniform is the temperature distribution and this can be accomplished by using current densities of 6×10^{3} to 1×10^{4} amps per cm^{2}.

Prior to an experiment the filament was cleaned by resistive heating and then allowed to cool to the temperature of the bath. At the end of the adsorption period, the filament was heated, resulting in a desorption spectrum. The temperature of the filament only slowly approaches that of the bath when the cleaning sequence is terminated. For a tungsten filament, 1.27×10^{-2} cm in diameter and approxi-

mately 18 cm. long, an interval of two minutes is required for the temperature of the filament to come within thirty degrees of a room temperature bath and about four minutes for a liquid nitrogen bath. Hence, quantitative measurements can only be made at the end of this cooling period.

D. Flash Desorption Experiments

The tungsten, iridium and rhodium used in this work were obtained from Engelhard Industries. The iridium and rhodium were specified to be >99.9% pure. A spectrographic analysis of the bulk metal from which the wire was drawn indicated that the major impurities in the case of iridium were: Pt <.02%, Pd = .046%, Rh <.016%, and Fe <.01% and in the case of rhodium were: Pt <100 ppm, Ir <90 ppm, Si <70 ppm, Ca <56 ppm, Mg <36 ppm and Pd <20 ppm.

The hydrogen used was Reagent Research Grade obtained from the Baker Chemical Company in one liter flasks with break-off tips. The deuterium was obtained from Volk Radiochemicals in 100 ml. flasks with break-off tips and was specified to be 99.8% pure. $^{15}N_2$ was prepared by hypobromite oxidation of enriched ammonium sulfate in which the nitrogen was specified to be 99.78% ^{15}N. The nitrogen was collected in ampoules with break-off tips. The carbon monoxide was

Assayed Reagent Grade obtained from the Matheson Company in one liter flasks with break-off tips.

The system was pumped down in the usual manner. Particular care was taken in outgassing the ion gauges and in activating the low work-function filaments. When the system pressure was 3×10^{-10} torr or less, the Granville-Phillips valve was closed and the gas ampoule was opened. The filament was flashed to a high temperature and then held at some lower temperature at which no adsorption occurred. The ground glass valve, which isolated the cell from the pumps, was adjusted so that the pumping speed was extremely small. The valve to the gas supply was then carefully opened until the pressure in the tube increased to about 1×10^{-8} torr. When the pressure in the cell had stabilized, the filament was then cooled and held either at $100^{\circ}K$ or $300^{\circ}K$ for varying periods of time to allow adsorption to occur. The rate of adsorption and cooling of the filament could be followed on a recorder. Following the adsorption period, the filament was flashed at the desired heating rate, and the total ion current, partial ion current and voltage drop across filament were recorded as functions of time using a linear time sweep of either one or two inches per second depending on the heating rate. In a given experiment only two of these variables were recorded on a Moseley 136A two pen recorder. At the end of the desorption cycle, the filament

was cleaned and then maintained at a temperature at which no adsorption occurred (~800°K for H_2, and ~2000°K for N_2 and CO) and the desorbed gases were pumped away with the valve partially closed, so as not to alter the valve setting. The next adsorption interval began only after the pressure had decreased to its previous value.

The above procedure was followed to obtain quantitative results from the kinetic analysis of the desorption spectra, i.e. at most, a small correction had to be made for the amount lost by pumping during the desorption interval. This procedure was modified when investigating desorption spectra with multiple peaks and hydrogen-deutrium exchange at room temperature. In these cases, the valve to the gas supply was opened until the pressure in the tube increased to about 5×10^{-8} torr with the valve to the pumps open. Desorption experiments were carried out in the same manner as above. The higher pumping speed and hence higher flow rate permitted better resolution of overlapping peaks but the desorption spectra were not subject to accurate kinetic analyses.

In early experiments, when hydrogen was adsorbed at room temperature for extended periods of time, a second peak appeared in the total pressure desorption spectra. The peak occurring at the lower temperature was small if the adsorption period was relatively short, but it increased markedly

in size as the adsorption period was prolonged. This other peak has been identified with a mass spectrometer as carbon monoxide, which agrees with the findings of Hickmott and Ehrlich (10). Becker, Becker and Brandes (13) and Hickmott (11) have independently shown that the carbon monoxide results from a complex sequence of reactions involving carbon dissolved in the tungsten filaments of the ion gauge, hydrogen and oxygen from the glass walls. They also showed that the carbon could be completely removed from a tungsten filament by heating it to 2500^{o}C for 24 hours in an ambient of oxygen at 10^{-6} torr. This technique was applied to the ion gauge filaments, and eliminated the peak due to carbon monoxide.

V. RESULTS

A. Desorption of Hydrogen

The first flash desorption experiments of hydrogen from a rhodium filament were carried out in a flow system using the Nottingham ion gauge to monitor the pressure burst. It was not immediately obvious why this experimental technique should not work, but it will be shown to give reproducible but erroneous results. The problems associated with measuring hydrogen pressures with an ion gauge were apparently minimized by operating the Nottingham gauge at a reduced emission current. Also, the effect of contamination by residual gases was minimized by establishing a pressure of hydrogen in the system 100 to 1000 times greater than the background pressure, which was about 5×10^{-11} torr. A typical desorption curve obtained under these conditions is shown in Figure 6. It is obvious that the pumping speed is not trivial from the rapid decay of the pressure burst. The pumping speed is determined as follows. Rearranging Equation 6, we obtain

$$\frac{d\Delta P}{dt} = - \frac{AkT_o}{V} \frac{dn}{dt} - \frac{S}{V} \Delta P \qquad (6a)$$

At some point in the desorption process, the amount of material desorbing from the surface will be negligible and hence

we can set $\frac{dn}{dt} = 0$ in Equation 6a. This implies that

$$\frac{d(\log \Delta P)}{dt} = - \frac{1}{2.303} \frac{S}{V} \qquad (28)$$

The pumping speed is obtained from the slope of the plot of log ΔP versus time for the backside of the desorption curve. For the curve in Figure 6, $\frac{S}{V} = 1.83 \text{ sec}^{-1}$, which corresponds to an apparent pumping speed of 3.66 liters per second in a two liter system. The amount of material desorbing from the filament as a function of time, corrected for the amount lost by pumping can then be calculated by Equation 7. The corrected curve is also shown in Figure 6 . This corrected curve is than analyzed by Equations 26a and 26b and the results are shown in Figure 7. The heat of desorption obtained from the 2nd order plot is 9.6 kcal per mole, and this value was reproducible to 0.5 kcal per mole as indicated by the analyses of several desorption curves and was independent of surface coverage.

Results obtained under these conditions were not consistent with theoretical expectations. The pumping term, $\frac{S}{V}$, was a function of the heating rate and surface coverage as shown by the results in Table 1. A plot of peak height versus adsorption time approached a limit, although the amount of material desorbed corresponded to only 0.06 of a monolayer at saturation. The activation energy of desorption

9.6 kcal per mole was considerably less than 31 kcal per mole obtained by Hickmott (11) for hydrogen on tungsten. The behavior of desorption spectra similar to Figure 6, which were obtained as a function of increasing initial coverages, indicated first-order desorption kinetics (32), although the kinetic analysis of the corrected desorption curves indicated a second-order process.

These observations can be interpreted by a model which takes into account the effect of a large pumping speed on the desorption spectra.

Rearranging Equation 4, we obtain

$$V \frac{dP}{dt} = - AkT_o \frac{dn}{dt} + LkT_o - SP \tag{4a}$$

At steady-state prior to the flash

$$P = P_o \quad , \quad n = n_o$$

$$\frac{dP}{dt} = 0 \text{ and } \frac{dn}{dt} = 0 \tag{29}$$

Then,

$$LkT_o = S P_o \tag{30}$$

Letting $\Delta P = P - P_o$, Equation 4a becomes

$$\frac{d\Delta P}{dt} + \frac{S}{V} \Delta P = - \frac{AkT_o}{V} \frac{dn}{dt} \tag{31}$$

Case I.

$$\text{When } \frac{S}{V} \Delta P << \frac{d\Delta P}{dt} \ , \tag{32}$$

Then,

$$\frac{dn}{dt} = - \frac{V}{AkT_o} \left(\frac{d\Delta P}{dt}\right) \tag{33}$$

Integrating Equation 33, yields

$$n_o - n = \frac{V}{AkT_o} \Delta P \tag{34}$$

This will always be true for sufficiently small ΔP, that is, sufficiently small t.

Case II.

If

$$\frac{S}{V} \Delta P >> \frac{d\Delta P}{dt} \tag{35}$$

Then,

$$-\frac{dn}{dt} = \frac{V}{AkT_o} \left(\frac{S}{V} \Delta P\right) \tag{36}$$

Hence, ΔP is then proportional to $\frac{dn}{dt}$ rather than to $n_o - n$ as in Case I. The larger $\frac{S}{V}$, the lower ΔP and the lower the t at which this condition is reached. Hence the backside of the desorption curve will also be proportional to $\frac{dn}{dt}$ and since $\frac{dn}{dt}$ is a function of the heating rate and surface coverage, it will exhibit the behavior obtained by treating the decay of the pressure burst as due to pumping.

Further consideration of the experimental technique reveals that even though the Nottingham ion gauge is operating at a reduced emission current, 20 microamps, the temperature

of the filament, 1900°K, is considerably above the temperature for dissociation of molecular hydrogen, which is about 1100°K. Hickmott (12) and Langmuir (52, 53) have shown that atomic hydrogen is efficiently trapped by glass. Hence, the large pumping speed observed for hydrogen in the present system is due to the dissociation of molecular hydrogen on the ion gauge filament and subsequent removal of the atomic hydrogen by the glass envelope. This mechanism was substantiated by observing the decrease in the partial pressure of hydrogen when the sample temperature was greater than 1100°K.

As a result of these findings, an ion gauge with two low work-function filaments was sealed to the system, Figure 2, and the rhodium filament was replaced with a tungsten filament. With these two low work-function filaments and the Nottingham ion gauge on the system, it was then possible to systematically investigate the effect of ion gauge operation, particularly filament temperature and emission current, on the desorption spectrum of hydrogen. The effect of emission current was determined by using the oxide-coated platinum filament to monitor the pressure burst for a given adsorption interval at various emission currents. The results are shown in Figure 8. It is evident from the linear plot with slope unity, that the flux of energetic electrons, emission current, confined in a small volume in the ion gauge exhibits no

detectable pumping of molecular hydrogen. The range of emission currents covered by these results is 10 microamps to 100 microamps. At higher emission currents, and hence higher temperatures, it is difficult to separate ionic pumping from pumping due to thermal dissociation of molecular hydrogen and subsequent trapping of the atomic hydrogen.

The effect of heating rate on the pumping term $\frac{S}{V}$, was investigated using the thoria-coated filament to monitor the pressure burst. As can be seen from the results in Table 1, the pumping term determined under these conditions is considerably less and essentially constant, compared to the apparent pumping term obtained when the Nottingham ion gauge is on.

The temperature of operation of the thoria-coated tungsten filament is slightly above the temperature of operation of the oxide-coated platinum filament but considerably below that of the tungsten filaments in the Nottingham ion gauge. It was impossible to determine accurately the temperature of the filament using a pyrometer, due to a stannous oxide conductive coating on the inside of the ion gauge. The effect of operation of this filament at various emission currents (temperature) on the desorption spectrum of hydrogen is summarized in Figures 9 and 10. It is evident from Figure 10, that the pumping action of the ion gauge at higher emission currents reduces the peak height considerably. This reduction

in peak height becomes appreciable for emission currents greater than 0.5 milliamps. Also shown in Figure 10 is the value of Δn obtained from Equation 7, for four desorption curves at various emission currents. The amount lost by pumping was about 7% for the curve obtained using 10 microamps and about 40% for 10 milliamps emission. Even for these large corrections required for desorption curves obtained at high emission currents, the corrected amount of material desorbed from the surface agrees quite well (~5%) with data obtained at reduced emission currents.

Thus, conventional hot filament ion gauges are not suitable for quantitative analysis of the desorption of hydrogen from metals. We have found that two types of oxide coated cathodes operate at a low enough temperature, less than 1000°K, if properly activated, to permit a quantitative analysis of the desorption of hydrogen.

A typical desorption spectrum of hydrogen from tungsten at low surface coverage is shown in Figure 11. The curve is the normalized surface coverage obtained from the change in the ion current as the filament is flashed. The pressure burst was recorded by the ion gauge with the oxide-coated platinum filament operating at 20 microamps emission, hence, no correction for pumping was required. This curve was then analyzed for both first and second order kinetics by Equations 26a and 26b and the results are shown in Figure 12.

From the linearity of the second order plot, it was concluded that the rate-controlling step in the desorption of hydrogen from tungsten is a second order process which suggests that the hydrogen is on the surface as independent mobile hydrogen atoms. The activation energy for desorption was determined from the slope of the second order plot to be 35 kcal per mole. From Equation 26b, the frequency factor ν, was found to be 2×10^{-3} cm^2 $molecule^{-1}sec^{-1}$. As a check on the consistency of the method, Equation 8 was numerically integrated using a computer and the values obtained for n_o, ΔH and ν. The calculated points (open circles) are shown on the measured desorption curve of Figure 11.

For surface coverages less than 50×10^{12} molecules per cm^2, the second order plots were linear with constant slope indicating that for low surface coverages, the activation energy for desorption changes negligibly during desorption. Figure 13 shows typical normalized desorption spectra of hydrogen from tungsten for increasing surface coverages. The temperatures at which evaporation begins and at which desorption is complete, shift to lower values for larger initial coverages. This behavior is characteristic of a second-order desorption process (32). For values of n_o greater than 50×10^{12} molecules per cm^2, deviations from linearity of second-order plots, Figure 14, become apparent and the slopes decrease indicating a lowering of the activa-

tion energy. This deviation from linearity is a measure of the variation of the activation energy of desorption with increasing surface coverage. If we assume a linear variation in the heat of desorption, that is, $\Delta H = \Delta H_o - \alpha n$, then the parameter α can be determined using ΔH_o and ν obtained from the data at low initial coverages, where the quantity αn is negligible compared to ΔH_o, and letting a computer carry out a minimum search routine on α. That is, a computer numerically integrates Equation 27, varying α, until the sum of squares of the differences between the calculated value and the experimental value passes through a minimum. Using this approach we have obtained the following results for hydrogen on tungsten initially at 300°K. Using ΔH_o and ν obtained for an initial coverage of 47 x 10^{12} molecules per cm^2, that is, 35 kcal per mole and 2 x 10^{-3} cm^2 $molecules^{-1}sec^{-1}$, a value of $\alpha = 28 \pm 2$ cal per mole per 10^{12} molecules per cm^2 was obtained for initial surface coverages ranging from 47 x 10^{12} to 400 x 10^{12} molecules per cm^2.

The maximum value of n_o at a given temperature and pressure was obtained by increasing the adsorption interval until n_o was constant. With the filament at 300°K and a hydrogen pressure of 5 x 10^{-8} torr, the maximum amount adsorbed was 480 x 10^{12} molecules per cm^2.

The desorption spectrum of both hydrogen and deuterium from tungsten initially at 100°K contained two peaks as shown in Figure 15. These spectra were obtained by recording the output of the mass spectrometer, tuned to either hydrogen or deuterium; this eliminated the possibility that one of the peaks might be due to some contaminant species present in the residual gases. No attempt was made to obtain low temperature desorption data at reduced pumping, since reduced pumping is not conducive to resolving partially overlapping peaks (32, 36). As is evident from Figure 15, even at relatively high pumping the two peaks are not well resolved.

These results indicate that hydrogen adsorbed on tungsten at low temperature exists in two distinct forms with different binding energies. Neither of these peaks can be analyzed in the manner described previously. It is believed that the high temperature peak, which we shall designate as the β form, is due to the same species which desorbs from tungsten dosed at 300°K, and is therefore present on the surface as atoms. The low temperature α-peak becomes appreciable when the β-peak is approximately 80% saturated. From the relative peak heights of α and β in Figure 15, it appears that both species are present on the surface in equal amounts. Hickmott (11) also observed two forms of adsorbed hydrogen on tungsten, but the low temperature α form was never present in amounts comparable

to the β form. He felt that the low temperature peak was due to molecular hydrogen on the surface.

A typical flash desorption curve for hydrogen adsorbed on iridium is shown in Figure 16, in which change in cell pressure, due to hydrogen desorption, is recorded as a function of filament temperature. The change in cell pressure was measured by the ion gauge with the thoria-coated tungsten filament operating at 20 microamps emission. It is evident from the decay of the pressure burst that the pumping is not negligible. The pumping term was determined from Equation 2[3]. The desorption curve corrected for the amount of material lost by pumping is also shown in Figure 16. Figure 17 is the analysis of the corrected pressure-temperature data by both first-and second-order kinetics, and shows that the data at low surface coverage, less than 40 x 10^{12} molecules per cm^2, are well represented by second-order desorption kinetics with an activation energy for desorption of $\Delta H = 24$ kcal per mole and a frequency factor, $\nu = 2.2 \times 10^{-2} cm^2$ molecules^{-1}sec^{-1}. At higher surface coverages, deviations from linearity in plots analogous to Figure 17 indicate that the activation energy for desorption is a function of surface coverage. The variation in the activation energy with surface coverage was obtained in the manner previously described for hydrogen and tungsten. ΔH_o and ν

were established for an initial surface coverage of 38 x 10^{12} molecules per cm^2 as 24 kcal per mole and 2.2 x 10^{-2} molecules per cm^2 $molecules^{-1}$ sec^{-1}. A value of $\alpha = 14 \pm 1$ cal per mole per 10^{12} molecules per cm^2 was then obtained for initial surface coverages ranging from 38 x 10^{12} to 230 x 10^{12} molecules per cm^2. Taking 1400 x 10^{12} atoms per cm^2 as the mean surface density of iridium, the decrease in activation energy of desorption becomes noticeable, that is, plots analogous to Figure 18 begin to deviate noticeably from linearity, when the number of hydrogen atoms adsorbed exceeds one per seven surface iridium atoms, and the maximum adsorption observed at 300°K corresponds to one hydrogen atom per three surface iridium atoms.

When hydrogen was adsorbed on iridium at 100°K, two peaks were observed in the flash desorption spectrum; typical results are shown in Figures 18, 19 and 20. In Figure 18, both the output of the mass spectrometer tuned to mass two and the output of the ion gauge were recorded simultaneously during an experiment. From the excellent agreement of the two curves, it is evident that the two peaks recorded by the ion gauge are due to hydrogen and not to some contaminant species. The low temperature α-peak becomes appreciable after the β-peak has reached 70-80% of saturation as shown in Figure 20, which is similar to the behavior of hydrogen on tungsten at low temperatures. Hence, hydrogen is adsorbed

on iridium at low temperature in two forms. The high temperature, 280°K, at which the α-peak occurs, as contrasted to 180°K in the case of tungsten, makes it unlikely that the peak from iridium is due to molecularly adsorbed hydrogen, that is, to hydrogen molecules held to the surface by van der Waals forces, and would suggest rather that it is due to atomic hydrogen adsorbed with a binding energy less than in the case of β-hydrogen. The atomic nature of the β-phase has already been shown.

Flash desorption curves of hydrogen from rhodium initially at 300°K are shown in Figure 21. The change in the ion current was measured by the ion gauge with the thoria-coated filament operating at 100 microamps. Also shown in Figure 21 is the voltage drop across the filament, at a fixed current, during the experiment. The rhodium sample used to obtain these results was the middle section of a 50 centimeter length of 5 mil rhodium that was annealed at 1525°K for 24 hours.

Analysis of the pressure-temperature data by Equation 26a and 26b indicates that the data at low surface coverage are well represented by second-order desorption kinetics with an activation energy of desorption of 18 kcal per mole and a frequency factor of 1.3×10^{-3} cm^2 $molecules^{-1}sec^{-1}$. The analysis of the data at higher coverages by second-order kinetics, Figure 22, does not exhibit the pronounced devia-

tions from linearity observed for iridium and tungsten. The maximum initial dose of hydrogen was approximately 100 x 10^{12} molecules per cm^2. The variation of the activation energy of desorption with surface coverage, was obtained as previously described. The best agreement between calculated and experimental points was obtained using ΔH_o = 18.5 kcal per mole, $\nu = 1.3 \pm 0.2 \times 10^{-3}$ cm^2 molecules^{-1}sec^{-1} and α = 24 ± 2 cal per mole per 10^{12} molecules per cm^2 for initial surface coverages ranging from 20 x 10^{12} to approximately 100 x 10^{12} molecules per cm^2. This value of α corresponds to a decrease of only 2.5 kcal/mole from the initial value for the amount of gas adsorbed at saturation namely 100 x 10^{12} molecules per cm^2.

The heat treatment given the filament prior to its use in flash filament experiments apparently has an effect on the adsorption-desorption characteristics of hydrogen and this can best be illustrated by comparison of some results obtained from filaments that have different thermal histories. Figure 23 shows desorption spectra of hydrogen from rhodium dosed at 100°K for two different filaments. One of the filaments was annealed with direct current, whereas the other filament was used as it was received from the manufacturer. In the case of the untreated filament, the α and β state are approximately equally populated, whereas in the case of the dc-annealed filament, the α state is only 50% of the β state.

Ehrlich (30) has shown that the adsorption of nitrogen on tungsten is very dependent on surface structure. It is not unlikely that the adsorption of hydrogen would be similarly dependent. Thus, the differences in surface coverage for hydrogen on rhodium, 100×10^{12} molecules per cm^2 and hydrogen on iridium, 230×10^{12} molecules per cm^2, and the differences in the activation energy of desorption, namely 18 kcal per mole for rhodium and 24 kcal per mole for iridium are attributed to the effect of surface structure resulting from the dc-annealing of the rhodium filament. Unfortunately these conclusions can only be inferred since the flash-filament technique is not amenable to observing specifically the effect of surface structure on adsorption. A field emission study of the adsorption of hydrogen on rhodium would be desirable, since this technique is better suited for observing the areas where adsorption predominates.

B. Hydrogen-Deuterium Exchange

The desorption of hydrogen from tungsten, iridium and rhodium initially at room temperature proceeds by a second-order process which strongly suggests that the hydrogen is on the surface as independent mobile hydrogen atoms. The distribution of H_2, HD and D_2 in the desorbed phase resulting from the co-adsorption of a mixture of H_2 and D_2 on the metals at room temperature should further clarify the nature of the adsorbed species.

If hydrogen and deuterium are adsorbed as atoms and combine randomly on desorption, the expected distribution of H_2, HD and D_2 in the desorption products can be readily obtained. Let P_H and P_D be the surface fractions of hydrogen atoms and deuterium atoms, respectively. Let n_{H_2}, n_{HD} and n_{D_2} be the number of moles of H_2, HD and D_2 in the desorbed product respectively. Then

$$n_{H_2} : n_{HD} : n_{D_2} = P_H^2 : 2P_HP_D : P_D^2 \tag{37}$$

$$1 : \frac{n_{HD}}{n_{H_2}} : \frac{n_{D_2}}{n_{H_2}} = 1 : \frac{2\,P_HP_D}{P_H^2} : \frac{P_D^2}{P_H^2} \tag{38}$$

The mass spectrometer ion currents will reflect the differences in mean velocities of H_2, HD and D_2; where $I^+_{H_2}$, I^+_{HD} and $I^+_{D_2}$ are the corresponding ion currents, we obtain finally

$$1 : \frac{I^+_{HD}}{I^+_{H_2}} : \frac{I^+_{D_2}}{I^+_{H_2}} = 1 : 1.63 \frac{P_H P_D}{P_H^2} : \left(\frac{1}{2}\right)^{\frac{1}{2}} \frac{P_D^2}{P_H^2} \qquad (39)$$

The results of the hydrogen-deuterium experiments on the three metals are summarized in Table 2. It was observed that even the low temperature of operation of the oxide-coated filament in the ion gauge, resulted in an increase in the amount of HD present in the ambient. As a result of this, all desorption spectra of H_2, HD and D_2 were obtained using only the mass spectrometer to record the pressure change and the small amount of HD present in the ambient under these conditions is due to exchange occurring on the mass spectrometer filament (Figure 25).

It is evident from Table 2 that the isotopes in the desorbed phase are statistically distributed within experimental error, while the ambient distribution is clearly non-statistical. This result is also consistent with a mobile adatom model for hydrogen adsorbed on these metals. The almost statistical distribution, Figure 25, of hydrogen isotopes in the ambient in a previous investigation of hydrogen-deuterium exchange on rhodium was due to the presence of rhodium film on the inside walls of the reaction cell formed by filament cleaning.

Hydrogen-deuterium exchange on these metals is somewhat different at low temperature, 100°K. For iridium, Figure 26,

two peaks are observed for H_2, HD and D_2 and the ratio of the high temperature β-peak to the low temperature α-peak is the same for all three species. If we assume that the peak height is a measure of the amount of each species present, then we can calculate the distribution of the isotopes in each peak. The results are summarized in Table 3. The results for rhodium, Table 4, are similar to those for iridium except that the ratio of the β-peak to the α-peak is not the same for all three species. The temperature at which evaporation occurs is also lower for rhodium than for iridium.

Figure 27 shows the equilibrium distribution of the hydrogen isotopes in the ambient with the rhodium filament at 300°K and 100°K respectively. The reduction in the relative amount of HD present as the filament is cooled indicates that adsorption and desorption are occurring simultaneously with the former predominating.

Hydrogen-deuterium exchange on tungsten at low temperature, 100°K, differs considerably from the results obtained for iridium and rhodium. Typical desorption curves are shown in Figure 28. The α-peak occurs at a much lower temperature, 150°K for D_2, 190°K for H_2, compared to 280°K for iridium and it is almost devoid of HD if the filament has been dosed with a mixture of H_2 and D_2. Isotopic mixing is hence negligible in the α-peak, indicating that the low temperature α-peak in the case of tungsten is due to molecularly adsorbed hydrogen.

C. Desorption of Nitrogen

The desorption of nitrogen from tungsten has been the subject of many investigations (2, 7, 8, 54). There has been general agreement on the gross desorption characteristics, but recently, there has been some controversy (25, 27, 54) on the fine structure of some of the binding states. As a result of this extensive work, the system nitrogen on tungsten provides an excellent basis for calibration of the flash-filament technique. Also contributing to this basis of calibration is the ease of generating a clean tungsten surface and the apparent inertness of nitrogen in the presence of hot-filament ionization gauges.

The flash filament technique, besides yielding information on the energetics of the desorption process, provides a simple means for evaluating the sticking coefficient, that is, the probability that a molecule colliding with a surface will adsorb. This was done by recording the pressure in a closed system as a function of time after cleaning the filament. The number of molecules colliding with unit are of surface per second is given by kinetic theory as

$$N = \frac{P'}{(2\pi mkT)^{1/2}} = \frac{3.5 \times 10^{22}}{(MT)^{1/2}} P \qquad (40)$$

where P is the pressure in torr and M is the molecular weight.

The surface concentration increases at the following rate.

$$\frac{dn_o}{dt} = \frac{3.5 \times 10^{22}}{(MT)^{1/2}} \; Ps \tag{41}$$

where s is the sticking coefficient. The amount of material on the surface is determined by measuring the pressure increase after various adsorption intervals

$$\frac{dn_o}{dt} = \frac{V}{AkT} \; \frac{d\Delta P}{dt} \tag{42}$$

Therefore s can be evaluated from

$$s = \frac{(MT)^{1/2}}{3.5 \times 10^{22}} \; \frac{V}{AkT} \; \frac{1}{P} \; \frac{d\Delta P}{dt} \tag{43a}$$

For nitrogen on tungsten in the present system Equation 43a reduces to

$$s = 0.22 \; \frac{1}{P} \; \frac{d\Delta P}{dt} \tag{43b}$$

It is evident from Equation 43a that the sticking coefficient s is independent of the gauge constant. The results for nitrogen on tungsten are shown in Figure 29. The maximum amount of nitrogen adsorbed is about 400×10^{12} molecules per cm^2.

Typical flash desorption curves of nitrogen from tungsten initially at $300^{\circ}K$ are shown in Figure 30. These results were obtained by measuring the change in ion current on flashing with the ion gauge containing the oxide-coated platinum filament operating at 15 microamps. It is evident

from Figure 30 that two binding states exist. The low temperature α-peak desorbs over the temperature range 400 to 500°K and the high temperature β-peak, from 1350 to 1950°K. Both of these peaks can be analyzed by Equations 26a and 26b, due to the large temperature range, approximately 900°K, separating the desorption peaks and the absence of pumping due to the reduced emission, 15 microamps, of the ion gauge. Kinetic analyses of the pressure-temperature data for both α- and β-nitrogen on tungsten are shown in Figure 31. The linearity of the first order plot for α-nitrogen indicates that this species is due to molecularly bound nitrogen, that is, chemisorbed nitrogen molecules, whereas the linearity of the second-order plot for β-nitrogen, indicates that nitrogen is dissociatively adsorbed in this state.

The distribution of nitrogen isotopes in the desorbed products formed on adsorbing a mixture of $^{14}N_2$ and $^{15}N_2$ on tungsten at 300°K, indicates that the low temperature α state is indeed molecular by the absence of $^{14}N\ ^{15}N$ in the desorption spectrum (Figure 32). The tightly bound β state is completely isotopically mixed on desorption, indicating that the nitrogen in this state is adsorbed atomically, as had also been indicated by its second-order desorption kinetics. Since the presence of any carbon monoxide in the desorption products would also be detected at mass 28, the contribution of nitrogen to the mass 28 peak on flashing

was determined from the ratio of the species present in the cracking pattern of $^{14}N_2$ and $^{15}N_2$. Hence, for a given adsorption period, five desorption curves were obtained, one each for masses 14, 15, 28, 29 and 30.

In addition to investigating the adsorption of nitrogen on tungsten, we have found some evidence that nitrogen adsorption occurs on iridium and rhodium if the nitrogen is thermally activated. Nitrogen was leaked into the vacuum system until the pressure was 4×10^{-7} torr. The pressure increase on flashing the filament, either iridium or rhodium, was measured with the ion gauge containing the thoriated tungsten filament operating at 0.4 ma. The residual gases present in the background were less than 0.5% of the total nitrogen pressure. It was observed that under these conditions, no adsorption of nitrogen occurred as indicated by the absence of a pressure increase on flashing the filament after an adsorption interval of approximately fifteen minutes. But adsorption of nitrogen can be made to occur if the tungsten filament in the Nottingham ion gauge is operated at a temperature, T_f, greater than 2000°K (Figure 33). The amount of nitrogen desorbed varied linearly with the adsorption interval for a fixed filament temperature, T_f. But the amount of nitrogen desorbed increased with the temperature of the filament, T_f, for a fixed adsorption interval. Figure 34 shows a plot of the log of the amount of nitrogen

desorbed versus the reciprocal temperature of the filament. The slope of this plot corresponds to an activation energy of 58 kcal per mole which is approximately one-fourth the dissociation energy of molecular nitrogen, 226 kcal per mole. The statistical distribution of the nitrogen isotopes in the desorption products (Figure 35) formed from adsorbing a mixture of $^{14}N_2$ and $^{15}N_2$ indicates that the adsorbed phase is atomic rather than molecular; this is also indicated by the high temperature, approximately 1000°K, at which the nitrogen desorbs.

The adsorption of nitrogen on iridium and rhodium can be explained by a model based on the dissociation of molecular nitrogen on the hot tungsten filament and steady-state adsorption and re-emission of nitrogen atoms from the glass walls, together with catalytic recombination on the glass.

Let N_W, N_G and N be the concentration of nitrogen atoms on tungsten, glass surfaces and in the gas respectively. On the tungsten ion gauge filament, we assume

$$\frac{1}{2} N_2(\text{gas}) \xrightleftharpoons{K} N_W$$

$$K = e^{\frac{-\Delta G^\circ}{RT}} = e^{\frac{+\Delta S^\circ}{R}} e^{\frac{-\Delta H^\circ}{RT}}$$

$$= \frac{N_W}{P_{N_2}^{1/2}}$$

and

$$N_W \xrightarrow{k'} N$$

where,

$$k' = A' e^{-\Delta H^{\ddagger}/RT}$$

Now the production of gas phase nitrogen atoms due to the filament is given by

$$\frac{dN}{dt} = k' N_w = k' K P_{N_2}^{1/2} = k P_{N_2}^{1/2}$$

where, $k = Ae^{-\Delta H_1/RT}$, $A = A' e^{+\Delta S^{o}/R}$

$$\Delta H_1 = \frac{1}{2} \Delta H^{o}(N_2(gas) \longrightarrow 2N_w) + \Delta H^{\ddagger}(N_w \longrightarrow N)$$

$$= \frac{1}{2} (2 E_{NW} - E_{NN}) + (-E_{NW})$$

$$= - \frac{1}{2} E_{NN}$$

$-E_{NN}$ = dissociation energy of N_2.

Therefore ΔH_1 = + 113 kcal per mole

On the glass surfaces, we suppose

$$N \underset{k_r}{\overset{k_f}{\rightleftharpoons}} N_G$$

and

$$2 N_G \xrightarrow{k''} N_2$$

Hence, at steady state

$$\frac{d N_G}{dt} = k_f N - k_r N_G - k'' N_G^2 = 0$$

Suppose that both $k_f N$ and $k_r N_G$ are large compared to $k'' N_G^2$,

then it follows that

$$k_f N - k_r N_G \lesssim 0$$

or

$$N_G \lesssim \frac{k_f}{k_r} N$$

Also at steady state

$$\frac{dN}{dt} = k\, P_{N_2}^{1/2} - k_f N + k_r N_G = 0$$

Substituting, $k_f N - k_r N_G = k'' N_G^2$, we obtain

$$k''\, N_G^2 = k\, P_{N_2}^{1/2}$$

or

$$N_G = \left(\frac{k}{k''}\right)^{1/2} P_{N_2}^{1/4}$$

Hence,

$$N = \frac{k_r}{k_f}\left(\frac{k}{k''}\right)^{1/2} P_{N_2}^{1/4}$$

Now the rate constant k_i is given by

$$k_i = A_i\, e^{-\frac{\Delta H_i}{RT}}$$

Therefore

$$N = \frac{A_r}{A_f}\left(\frac{A}{A''}\right) e^{-\frac{(\Delta H_r - \Delta H_f)}{RT'}}\; e^{-\frac{\Delta H''}{2RT'}}\; e^{-\frac{\Delta H_1}{2RT}}\; P_{N_2}^{1/4}$$

where T' is the temperature of the glass envelope and T is the temperature of the filaments in the ion gauge. Hence,

$$\Delta H_{eff} = \frac{\Delta H_1}{2}$$

$$= 56 \text{ kcal per mole.}$$

Figure 36 shows the equilibrium distribution of the nitrogen isotopes as a function of the temperature of the ion gauge filament. The decrease in masses 28 and 30 indicates that the nitrogen is being dissociated and that the resulting atoms are pumped by the glass envelope; some recombination is indicated by the increase in mass 29.

D. Desorption of Carbon Monoxide

Figure 37 shows the desorption spectra observed for carbon monoxide from tungsten for different surface coverages at an adsorption temperature of 300°K and at an equilibrium pressure of about 6×10^{-8} torr. In these spectra the ion current, pressure, was measured with the ion gauge containing the thoriated filament operating at 4.0 ma emission. It is evident from Figure 37 that the adsorption of carbon monoxide on tungsten is quite complex as indicated by the presence of four partially resolved peaks in the

desorption spectrum. The desorption peaks are divided into two groups: the α peak, appearing at low temperature, about 500°K and the β group of peaks, appearing at higher temperatures, 1200-1900°K. The high temperature β group is made up of three overlapping peaks, $\beta_1 \backsim 1300°K$, $\beta_2 \backsim 1700°K$ and $\beta_3 \backsim 1850°K$; these three peaks are not sufficiently resolved to permit kinetic analysis. At low surface coverage, $<2 \times 10^{14}$ molecules per cm^2, the α and β_1 states are barely detectable, but the α state grows rapidly (Figure 38) when the β_2 and β_3 states are ~60% saturated. At saturation, which is about 8.5×10^{14} molecules per cm^2, the α state makes up 22% of the total surface concentration.

Figure 39 shows the effect of heating rate at constant pumping speed and surface coverage on the resolution of the β states. It was found that at low heating rates, ~350° per sec., the β_1, β_2 and β_3 stats were clearly revealed, but at high heating rates, ~1300° per sec, the β_1 state was barely detectable and the β_2 and β_3 states appeared as one.

The desorption characteristics of carbon monoxide from iridium and rhodium at 300°K are considerably different from those observed for tungsten. Typical desorption curves are shown in Figures 40 and 41. The desorption spectrum in each case is characterized by one main peak occurring at about 600°K for rhodium and 780°K for iridium. In the case of rhodium, a shoulder is clearly detectable and reproducible

at 970°K. It is obvious from Figures 40 and 41 that the pumping is not trivial (note the rapid decay of the pressure burst). The pumping is intentionally large to enhance the resolution of partially overlapping peaks (Figure 40).

VI. DISCUSSION

A. Adsorption of Hydrogen

$$H_2(gas) \rightleftharpoons 2\ H(ads)$$

The desorption of hydrogen from tungsten, iridium and rhodium initially at room temperature proceeds by a second-order process indicating that the hydrogen is adsorbed dissociatively on these metals. Moreover, the hydrogen atoms on the surface must be quite mobile as indicated by the statistical distribution of the hydrogen isotopes in the desorbed phase even for adsorption at 100°K in the case of iridium and rhodium. The pre-exponential factor in the desorption rate constant is 2×10^{-3}, 1.35×10^{-3} and 2.2×10^{-2} cm^2 $molecules^{-1}sec^{-1}$ for tungsten, rhodium and iridium respectively. If the hydrogen atoms behaved as an ideal two-dimensional gas, the pre-exponential factor for evaporation would be given by

$$\nu_2 = \sigma \left[\frac{\pi kT}{m}\right]^{1/2} \tag{49}$$

where σ is the hard sphere collision diameter and m is the mass of the hydrogen atom. For T = 500°K and σ = 1Å, then $\nu_2 = 3.6 \times 10^{-3} cm^2$ $molecules^{-1}sec^{-1}$ which is in reasonably good agreement with the measured values when we consider that the experimental values are based on geometric area which is surely less than the true area and the predicted

value is based on an ideal two-dimensional gas. The calculation also presumes the density of hydrogen atoms to be uniform over the surface, which is probably not the case.

Desorption, unlike adsorption, is always activated since adsorption is in general exothermic. From the temperature coefficient of desorption, the energy of adsorption of hydrogen can be calculated, since adsorption of hydrogen on these metals occurs with negligible activation energy. This is confirmed by the increased work-function observed on adsorption of hydrogen even at $4^{\circ}K$ (20, 55). Hence, the binding energy for a hydrogen atom is then given by

$$E_{M-H} = \frac{1}{2} (E_{H-H} + \Delta H) \qquad (45)$$

where E_{H-H} is the dissociation energy of hydrogen. For tungsten, iridium and rhodium E_{M-H} is 69, 63.5 and 60.5 kcal per mole respectively which is in good agreement with Culver's (56) value of 75 kcal per mole obtained for hydrogen on tungsten films. The energy of the surface metal-hydrogen bond (M-H) may be calculated from Pauling's equation (57).

$$E(M-H) = \frac{1}{2} \left\{ E(M - M) + E(H - H) \right\} + 23.06 \, (X_M - X_H)^2 \qquad (46)$$

Eley (58) calculated E(M - M) from the sublimation energy of the metal and sets

$$E_{M - M} = \frac{1}{6} S \qquad (47)$$

where S is the sublimation energy.

The term involving the difference in electronegativities $X_M - X_H$ may be estimated by Pauling's (57) approximation which assumes that this difference is equal to the dipole moment of the bond expressed in debyes. This dipole moment may be obtained from the change in contact potential caused by the adsorbed layer. Calculation of the terms of Equation 46 leads to values of E_{M-H} of 73.4 and 63.1 kcal per mole for tungsten and rhodium respectively.

Since the samples used are polycrystalline, it is difficult to specify exactly which crystal planes are exposed at the surface. Johnson (59) has shown that in the surface of aged tungsten filaments (110) and (100) planes predominate. The numbers of atoms per cm^2 in these planes are 1.42×10^{15} and 1.01×10^{15} respectively, giving an average of 1.21×10^{15} atoms per cm^2. The maximum amount of hydrogen adsorbed at $300^{\circ}K$ and 5×10^{-8} torr is 480×10^{12} molecules per cm^2 which corresponds roughly to one hydrogen atom per surface tungsten atom. Arthur has shown (20) that for iridium the wire axis has a <100> orientation and from his field emission pictures, he concluded that the surface consisted mainly of 100 and 110 areas, with the former being better developed. These observations were made on a tip that was subjected to both chemical and flame etching and do not necessarily hold for the surface of wires. On the basis of packing in the crystal planes, the areas of the (111), (100) and (110) faces

in the polycrystalline wire satisfy A(111)>A(100)>A(110). Since the numbers of atoms in these planes are 1.6×10^{15}, 1.39×10^{15} and 0.98×10^{15} atoms per cm^2 respectively, we can then assume that 1.4×10^{15} atoms per cm^2 is the approximate surface density and the maximum adsorption observed at $300^{\circ}K$, namely 230×10^{12} molecules per cm^2, corresponds to one hydrogen atom per three surface atoms.

We have assumed a linear dependence of the heat of desorption on surface coverage and find that this model fits the data with reasonably small standard deviation, and the results so obtained are in good agreement with the values reported by other investigators (11, 60, 61, 62) as shown in Figure 42. Brennan and Hayes (60) and Beeck (61), Wahba and Kemball (62) obtained their results on evaporated films, whereas Hickmott (11) obtained his results using the flash filament technique and Gomer (55) obtained his by field emission microscopy. There is in principle a way to determine explicitly the variation of the activation energy of desorption with surface coverage. That is, a family of desorption traces is obtained at different initial concentrations. For each curve, then, it is possible to obtain a value of the slope dn/dt for a fixed surface coverage, but at a different temperature. Hence, a plot of $\ln(\frac{dn}{dt})$ at constant n versus $\frac{1}{T}$ gives the heat of desorption for a given surface coverage and from a series of these plots we obtain

the heat of desorption as a function of n. Unfortunately, the difficulty in obtaining an accurate value for $\frac{dn}{dt}$ either numerically or electronically, makes this method unsuitable at the present time.

The adsorption of hydrogen and deuterium on tungsten at 100°K occurs in two distinct binding states with different binding energies. Neither state lends itself to the usual method of kinetic analysis, so that conclusions about the molecular or atomic nature of these species are not available through this approach. But a study of isotope distribution provides strong evidence for dissociative or associative adsorption. The absence of HD in the low temperature α-peak indicates that this species is molecular, and the statistical distribution of the hydrogen isotopes in the high temperature peak indicates that this species is atomic. This is also indicated by the low temperature approximately 170°K, at which the α-peak occurs. The activation energy for desorption is approximately 5-7 kcal/mole, as determined by using Redhead's (51) "rule of thumb", that is, 20 E_d(kcal/mole) $\simeq$ T°K. This low binding energy would indicate that the α-hydrogen is held by weak van der Waals forces. The temperature range over which the β-peak desorbs is the same range over which desorption occurs when tungsten is dosed with hydrogen at 300°K. This temperature range for desorption agrees with the findings of Gomer, Wortman and Lundy (55), that hydrogen

on a tungsten emitter raises the work function and that hydrogen desorption is complete in a few seconds at 600°K.

The adsorption of hydrogen on iridium and rhodium at 100°K occurs in two distinct binding states, as indicated by the presence of two partially resolved peaks in the desorption spectrum. Adsorption into the β-state at 100°K is quite rapid, whereas adsorption into the α state is much slower and only becomes appreciable when β is ~75% saturated. Pasternak (18) has observed similar behavior for hydrogen on molybdenum. Hydrogen is more strongly adsorbed on molybdenum, so that the temperature of the two states is shifted, that is, α-350°K and β-550°K, whereas for iridium the peaks occur at 280°K and 450°K respectively. The high temperature (280°K) at which the α-peak occurs, together with the fact that it is completely isotopically mixed on desorption, would eliminate the possibility that this α phase is molecular, that is, held by van der Waals forces only, and would indicate rather, that it is atomic, with a lower binding energy, about 14 kcal/mole (51), than the β phase. Arthur (20) found in a field emission study of hydrogen on iridium, that adsorption at 300°K, resulted in an increased work function, that is, the emission decreased; whereas adsorption at 77°K, resulted in an initial work function increase followed by a slight decrease. Since the low temperature α-peak begins to form after the β-peak is ~75%

saturated, we can then associate this β-peak with that species that gives rise to an increased work function and the α-peak, to the species that causes a work function decrease.

Mignolet (63), Suhrmann, Wedler and Gentsch (64) and Sachtler and Dorgelo (65) have observed the effects of adsorbed hydrogen on the work function and the electric resistance of evaporated platinum films. They concluded that there existed two types of adsorption as had also been reported for hydrogen on nickel (66).

Pliskin and Eischens (67) studied the infrared adsorption of hydrogen adsorbed on supported platinum. They observed two bands, one broad and the other sharp, the latter being more intense at lower temperatures. They attributed the band at 4.86μ to strongly bonded hydrogen adatoms and the band at 4.74μ to weakly bonded ones. The deuterium spectra show bands at 6.76μ and 6.60μ which were similarly attributed to strongly and weakly bonded deuterium respectively. They observed no new bands, when hydrogen and deuterium were simultaneously adsorbed, hence they concluded that the weakly bound form is also present as atoms. They suggested that the strongly bound hydrogen atoms were situated between the surface atoms and held by shared bonds, and the weakly bound atoms were located above the surface, each singly bound to a platinum atom. The temperature

dependence of the respective band intensities as well as the half-widths of the bands have been interpreted theoretically by Toya (68).

Flash desorption of hydrogen from tungsten, iridium and rhodium initially at 100°K and 300°K together with a study of isotopic mixing of the hydrogen isotopes at these temperatures has provided fairly conclusive identification of the various adsorbed species.

B. Adsorption of Nitrogen

At 300°K, nitrogen adsorbs on tungsten in two states, the weakly bound α and the primary chemisorbed species, β. These are clearly resolved in the desorption traces. The α-peak passes through a maximum at higher concentrations of β. Our data are not sufficient, however, to characterize explicitly the desorption mechanism of the α state. Ehrlich (69) in a field emission study of nitrogen on tungsten observed a strong structural effect for the weakly bound α state and found this state to be concentrated around the (111) plane. In a later article (30), Ehrlich studied the effects of surface structure on the adsorption of nitrogen by contact-potential measurements on macroscopic planes cut from single-crystal tungsten. On the (100) plane, he found that room temperature adsorption lowers the work function

and flash desorption reveals only one state, β. On the (111) plane, the work function increases and both α and β are present in the desorption spectrum.

On the basis of Ehrlich's findings and the presence of α in the desorption spectra of nitrogen from tungsten, we can conclude that (111) planes exist on the surface. The nature of the adsorbed species which gives rise to the α-peak is elucidated by the distribution of the nitrogen isotopes in the desorption products. Since the α-peak is devoid of $^{14}N^{15}N$ and follows first order desorption kinetics, this would eliminate the possibility that the nitrogen is adsorbed as mobile atoms, but rather, it would indicate that the α phase is chemisorbed molecular nitrogen. The postulated surface complexes of nitrogen on iron (61) are

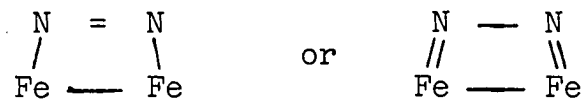

at low temperature and Fe ≡ N at room temperature . But these complexes are not plausible on the (111) plane of tungsten, due to the large separation (4.47Å) of adjacent tungsten atoms in this plane. Further, the binding of nitrogen in the β phase is different on the (100) and the (111) planes as indicated by the opposite effects of adsorbed nitrogen on the work function of these planes. It is conceivable that the binding of β-nitrogen is analogous to the two forms of adsorbed hydrogen, which also have opposite

effects on the work function. In addition, both phases of hydrogen and the β phase of nitrogen are completely isotopically mixed on desorption. We have found no evidence of a splitting of the β phase as reported by Rigby (27) and Madey and Yates (25). This could possibly be attributed to the fact that our experiments were carried out at reduced pumping which is not conducive to resolving overlapping peaks. It would be desirable to obtain desorption spectra of nitrogen from tungsten at reduced heating rates and high pumping speeds to investigate the splitting of the β-peak and the effect of surface structure on this splitting. It would also be desirable to obtain some infrared absorption data for nitrogen adsorbed on tungsten, for it would definitely elucidate the nature of the α species on the surface. Recently, Eischens and Jacknow (70) have observed the infrared spectra of nitrogen chemisorbed on nickel at low temperature. They attributed the observed band to the nitrogen-nitrogen stretching vibration in the structure Ni - $N \equiv N^{+}$. Molecular, rather than atomic adsorption, was confirmed by the behavior of the bands formed from an adsorbed mixture of $^{14}N_2$, $^{14}N^{15}N$ and $^{15}N_2$.

Even though there are some questions still unresolved about the interaction of nitrogen with a tungsten surface, there is general agreement on the gross desorption char-

acteristics of nitrogen from tungsten and, as a result this system provides an excellent starting point for calibration of the flash filament technique.

According to Bond (71), nitrogen is not chemisorbed on Group VIIIB metals. We have found this to be the case for iridium and rhodium by the absence of a pressure burst on heating the dosed sample filament. However, adsorption could be made to occur if the nitrogen is thermally activated. The source of this thermal energy is the hot tungsten filament present in conventional ionization gauges. Since there exists no line of sight between the components of the hot filament ion gauge and the sample filament, the activated species cannot all be trapped by the surrounding glass envelope. From the steady-state distribution of the nitrogen isotopes as a function of the ion gauge filament temperature, it is concluded that the "activated" species are nitrogen atoms. The statistical distribution of the nitrogen isotopes in the desorption spectra from iridium or rhodium indicates that the adsorbed phase is atomic. Unfortunately the nitrogen desorption peak was not subject to kinetic analysis, due to the presence of residual contamination resulting from prolonged adsorption intervals. The atomic nature of the "activated" species is explained by a model based on the dissociation of molecular nitrogen on the hot tungsten filament and steady-state adsorption and re-

emission of nitrogen atoms from the glass walls, together with catalytic recombination on the glass. It would be desirable to determine the kinetic order of the desorption of nitrogen from iridium and rhodium to further elucidate this mechanism.

C. Adsorption of Carbon Monoxide

It has been deduced, from studies in the field emission microscope, that carbon monoxide is bound on the tungsten surface as molecules (72, 73). Non-dissociative adsorption is confirmed by the rate of evolution of carbon monoxide on heating; this occurs as a first-order process (74).

The nature of the chemisorption bond between carbon monoxide and various metals has been studied by infrared absorption spectroscopy (75, 76). For nickel, rhodium and palladium, two main absorption bands occur at 4.85 and 5.3μ. These bands have been attributed to the linear form of bonding 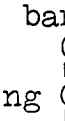 and the bridged form 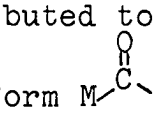 by comparison with the infrared spectra of gaseous metal carbonyls. The other metals examined (copper, iron and platinum) showed only one adsorption band at 4.85μ. It was also shown that the bridged form of bond on nickel is the stronger bond. The existence

of two adsorbed phases of carbon monoxide on tungsten has also been shown in the flash filament measurements of Hickmott and Ehrlich (77) and Becker (4).

Lanyon and Trapnell (78) have shown that the carbon-metal spacing in the bridged type of bond is about 2Å and that the preferred angle between the bonds is 120°. This makes the separation of the metal atoms, to which the carbon monoxide is bridged-bonded, about 3.5Å. They also showed that equal amounts of CO and H_2 were taken up on molybdenum and rhodium films, suggesting a two-site mechanism, while on tungsten films, the CO adsorbed was 1.40 times the hydrogen chemisorption, suggesting mixed one and two site mechanisms.

From a comparison of the infrared and flash filament results, it is suggested that the β-group of peaks observed on tungsten is the result of bridged-bonded molecules on the various crystal faces exposed on the surface, and that the α-peak is the result of linear form of bonding to single surface atoms occurring in gaps in the bridged-bonded layer. Hence in the case of tungsten, the subgroup of peaks in the β-phase is an indication of surface heterogeneity.

Yang and Garland (79) find one and two site adsorption on rhodium, together with a third mechanism in which one rhodium atom adsorbs two molecules of CO.

In the desorption spectrum of carbon monoxide from iridium and rhodium, no fine structure is observed as in the case of tungsten. The temperature range over which desorption occurs is 450°K to 750°K. The shoulder that exists at 970°K in the desorption spectrum of CO from rhodium, may be due to the bridged-bonded structure, that is, higher temperature, stronger bond; the large peak would then be due to the linear form. Since the temperature range for desorption is very nearly the same for both iridium and rhodium, it is possible that the bondings of CO on iridium and rhodium are similar. If this main peak is due to the linear form, then we would expect the adsorption of CO to be approximately twice that of H_2, whereas in fact approximately equal amounts are adsorbed. This indicates that two sites are required per CO molecule, and that the CO is probably in the bridged form. Hence, if the main desorption peak is due to the bridged form, then the shoulder observed at 970°K is analogous to the splitting of the β-peaks on tungsten. If we attribute the appearance of many peaks to the bridged form of CO, then we can conclude that multiple peaks indicate surface heterogeneity and the absence of multiple peaks is indicative of fairly homogeneous surface.

An unexpected phenomenon in CO adsorption is the isotopic exchange between CO molecules on tungsten (24). Madey, Yates and Stern observed rapid isotopic mixing at temperatures

above 850°K, which corresponds to the temperature of desorption of the more strongly adsorbed CO species. They found no evidence for dissociation of CO into mobile adsorbed C and O atoms, hence, they postulated a four-center bimolecular exchange intermediate on the surface, which involves surface bonding through both the carbon and oxygen. Infrared spectra of CO on various metals and of metal carbonyls does not support this type of binding.

SUMMARY

Flash desorption of hydrogen, nitrogen and carbon monoxide from tungsten, iridium and rhodium dosed at 300°K and 100°K was investigated, together with isotopic mixing in co-adsorbed mixtures of H_2-D_2 and $^{14}N_2$ - $^{15}N_2$. The effect of ion gauge pumping on flash desorption spectra and their analysis was also studied.

The desorption apparatus was constructed so that ultimate pressures less than 5×10^{-10} torr were easily attainable. Provisions were made to vary the throughput of gas through the reaction cell. The filament could be thermostated at various temperatures by placing the proper coolant in the re-entrant dewar containing the filament assembly. The filament was heated by direct current which permitted a simultaneous measurement of temperature and pressure during an experiment and the heating could be terminated at any desired temperature by means of a trigger circuit in the power supply. The use of a small, bakeable, sensitive mass spectrometer permitted the unambiguous identification of the desorbing species.

It was found that conventional hot filament ion gauges exhibited a high pumping speed for hydrogen. As a result of this high pumping speed, it was shown that the pressure in-

crease on flashing is a measure of the time derivative of surface coverage, rather than a measure of the variation of surface coverage with time.

The desorption of hydrogen from tungsten, iridium and rhodium initially at room temperature proceeds by a second order process with activation energies of 35, 24 and 18 kcal per mole respectively at low surface coverage. It was also found that the activation energy of desorption was strongly dependent on surface coverage. Assuming a linear variation in the heat of desorption ($\Delta H = \Delta H_o - \alpha n$), the parameter α was determined from desorption curves obtained at different initial surface coverages by programming a computer to carry out a minimum search routine with respects to α. For tungsten, iridium and rhodium, α was found to be 28 ± 2, 14 ± 1, 24 ± 2 cal per mole per 10^{12} molecules per cm^2 respectively. When these metals are dosed at room temperature with a mixture of H_2 and D_2, the isotopes in the desorbed phase are statistically distributed within experimental error, while the ambient distribution is clearly non-statistical.

When hydrogen is adsorbed on these metals at 100^oK a second low temperature peak is observed in the desorption spectrum. The distribution of the isotopes in the desorbed phase formed from the co-adsorption of H_2 and D_2 indicated that this low temperature peak was due to an atomic species

in the case of iridium and rhodium and a molecular species in the case of tungsten.

Flash desorption spectra of nitrogen adsorbed on tungsten at 300°K contains two well resolved pressure peaks, α and β both subject to kinetic analysis; the α-peak was kinetically first order and the β, second order with activation energies of 20 and 75 kcal per mole respectively. The distribution of desorbed products formed on adsorbing a mixture of $^{14}N_2$ and $^{15}N_2$ on tungsten indicated that the low temperature α state is molecular (chemisorbed molecular N_2) by the absence of $^{14}N^{15}N$ in the desorption spectrum, whereas the tightly bound β state is completely isotopically mixed on desorption.

Evidence is presented that nitrogen adsorption does occur on iridium and rhodium if the nitrogen is thermally activated. It was found that the amount of nitrogen adsorbed was a function of the temperature of the filament in the ion gauge. The distribution of the nitrogen isotopes in the desorbed phase indicated that the adsorbed phase is atomic. The results for nitrogen desorption from iridium and rhodium are explained by a model based on the dissociation of molecular nitrogen on the hot tungsten filament and steady-state adsorption and re-emission of nitrogen atoms from the glass walls, together with catalytic recombination on the glass.

Flash desorption of carbon monoxide from tungsten initially at 300°K indicates four separate bound states, α, β_1, β_2 and β_3. From an infrared study of carbon monoxide adsorbed on various metals, it is suggested that the β-group of peaks is the result of bridged-bonded molecules on the various crystal faces exposed on the surface, and that the α-peak is the result of the linear form of bonding to single surface atoms. The α-peak becomes appreciable only when the β-peak is approximately 60% saturated.

The desorption spectrum of carbon monoxide from iridium and rhodium contains only one peak which desorbs over the range 450-750°K. From the equal amounts of CO and H_2 adsorbed, it is inferred that the desorption peak is due to the bridged form of adsorbed CO. Also it is inferred that the lack of fine structure in the desorption spectra is an indication of surface homogeneity, since there are several conceivable crystal planes that have the appropriate metal-to-metal distance (~ 3.5Å) to accomodate the bridge form of carbon monoxide.

The results of these studies indicates that the flash filament technique in conjunction with mass spectrometry is a valuable research tool and provides a powerful approach to the study of the interaction of gases with metal surfaces. By the proper choice of experimental conditions, a large amount of information can be obtained on the adsorption-

desorption characteristics of reactive gases. This technique together with other techniques, such as field electron emission microscopy, low energy electron diffraction and infrared spectroscopy offers a route to a thorough understanding of surface phenomena.

VIII. SUGGESTIONS FOR FUTURE RESEARCH

Flash desorption of hydrogen from tungsten, iridium and rhodium initially at 100°K together with a study of isotopic mixing of the hydrogen isotopes at this temperature has provided fairly conclusive identification of the low temperature peak. But it would be desirable to determine the kinetic order of the desorption of the α-hydrogen. In the present low temperature experiments, the data are not subject to the present methods of analysis, due to the inadequate resolution of the peaks. The resolution of the α and β peaks can be improved by reducing the heating rate and increasing the pumping speed, both of which mitigate against quantitative analysis by the present methods. If the present methods of analysis can be modified to give semi-quantitative information about the kinetics and energetics of the desorption spectra obtained at high pumping speeds and low heating rates, then this would elucidate further the exact nature of this low temperature α-peak.

It would be desirable to obtain desorption spectra of CO from iridium and rhodium using a slow heating rate, approximately 10°/sec, and a high pumping speed to increase the resolution of the flash filament technique and elucidate the existence of any fine structure. It would be informative to investigate the distribution of the isotopes of CO on

desorption and to correlate these findings with the results obtained by infrared spectroscopy of gaseous metal carbonyls.

Since simple compounds containing the isotopes of hydrogen, nitrogen and carbon can be obtained with a known purity, 99%, then a study of the decomposition of these compounds, namely ethylene, acetylene and ammonia, by the flash filament technique will be greatly elucidated by using the isotope enriched compounds.

IX. FIGURES

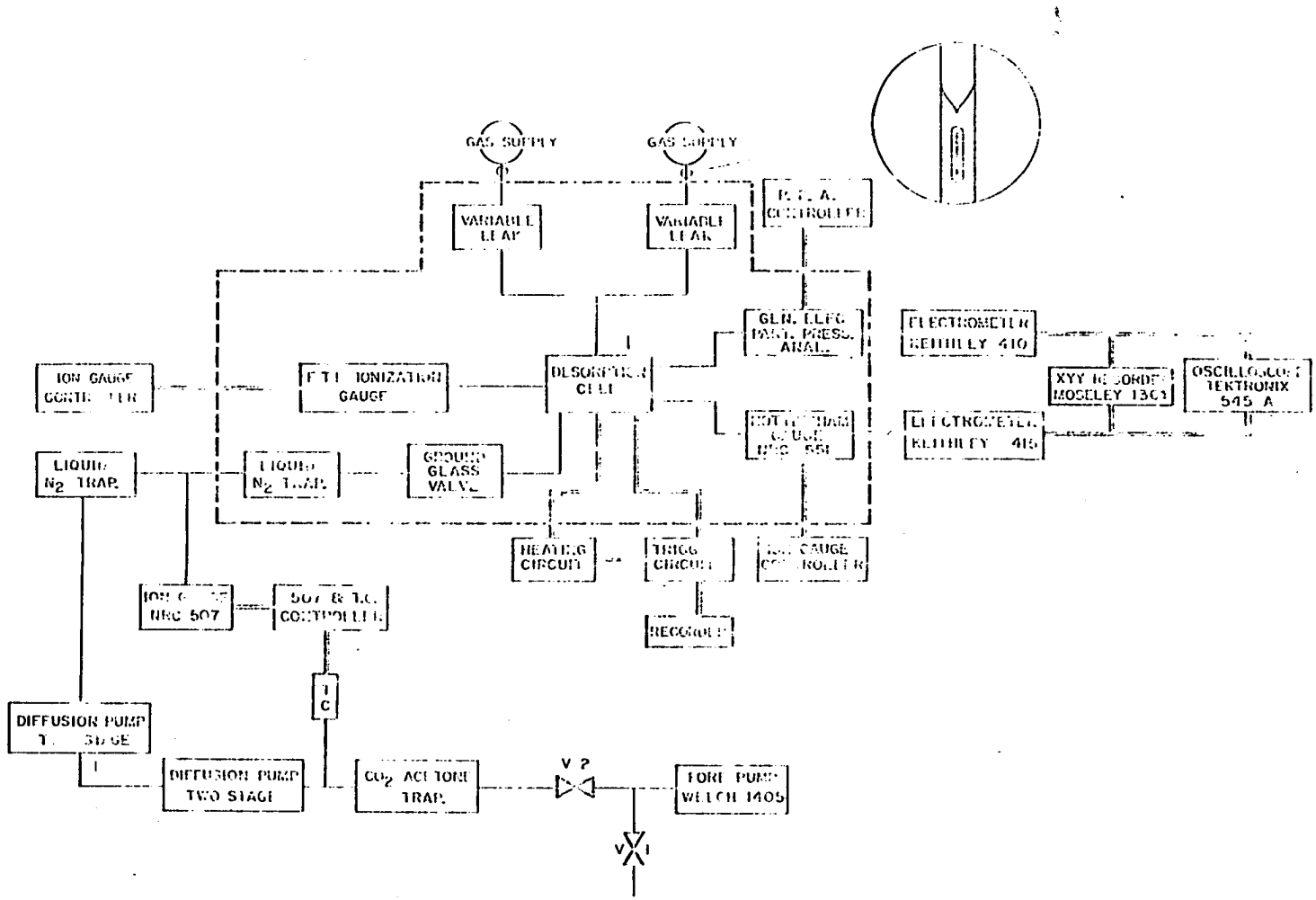

Figure 1. Schematic diagram of vacuum system and associated electronic equipment

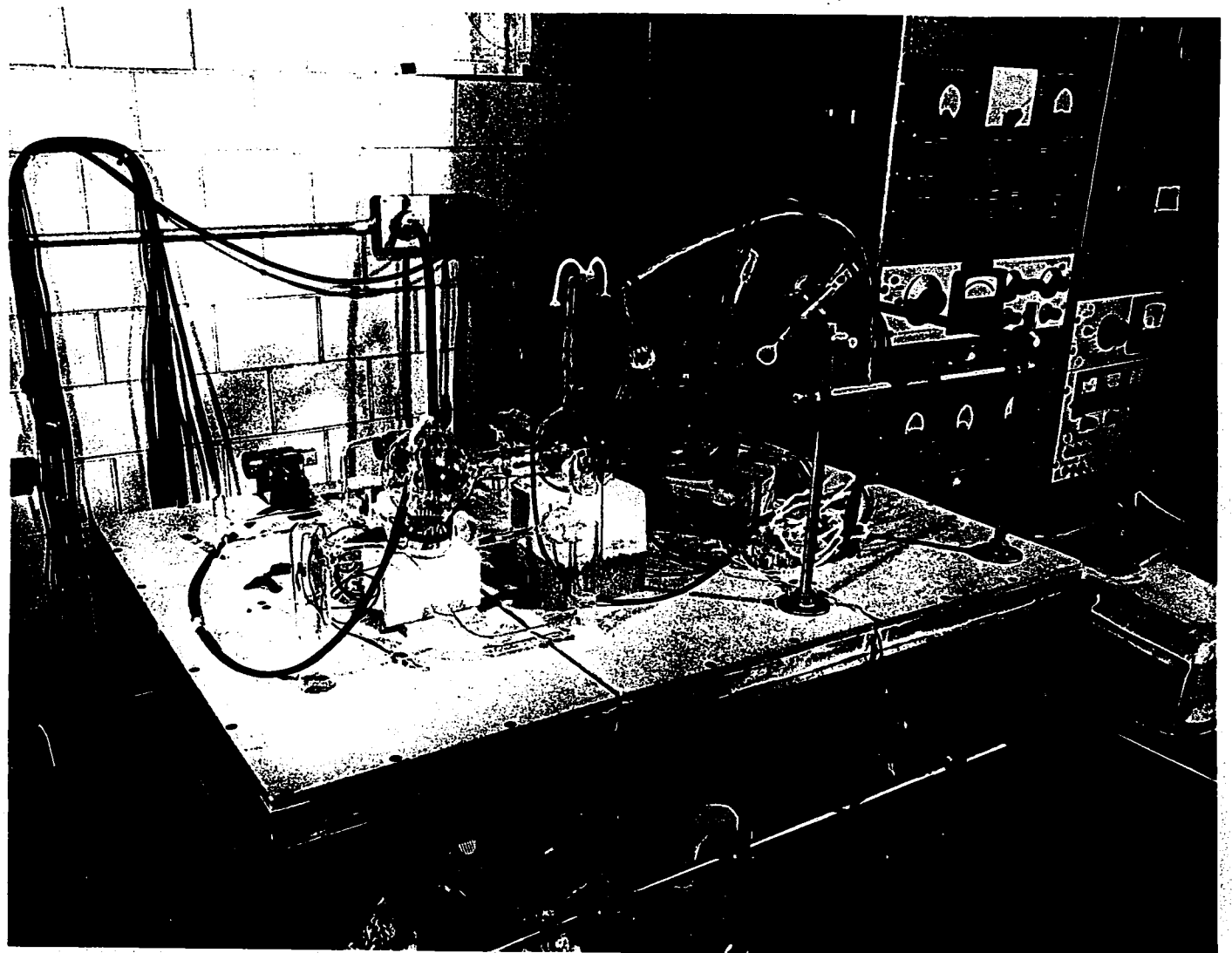

Figure 2. Flash filament apparatus

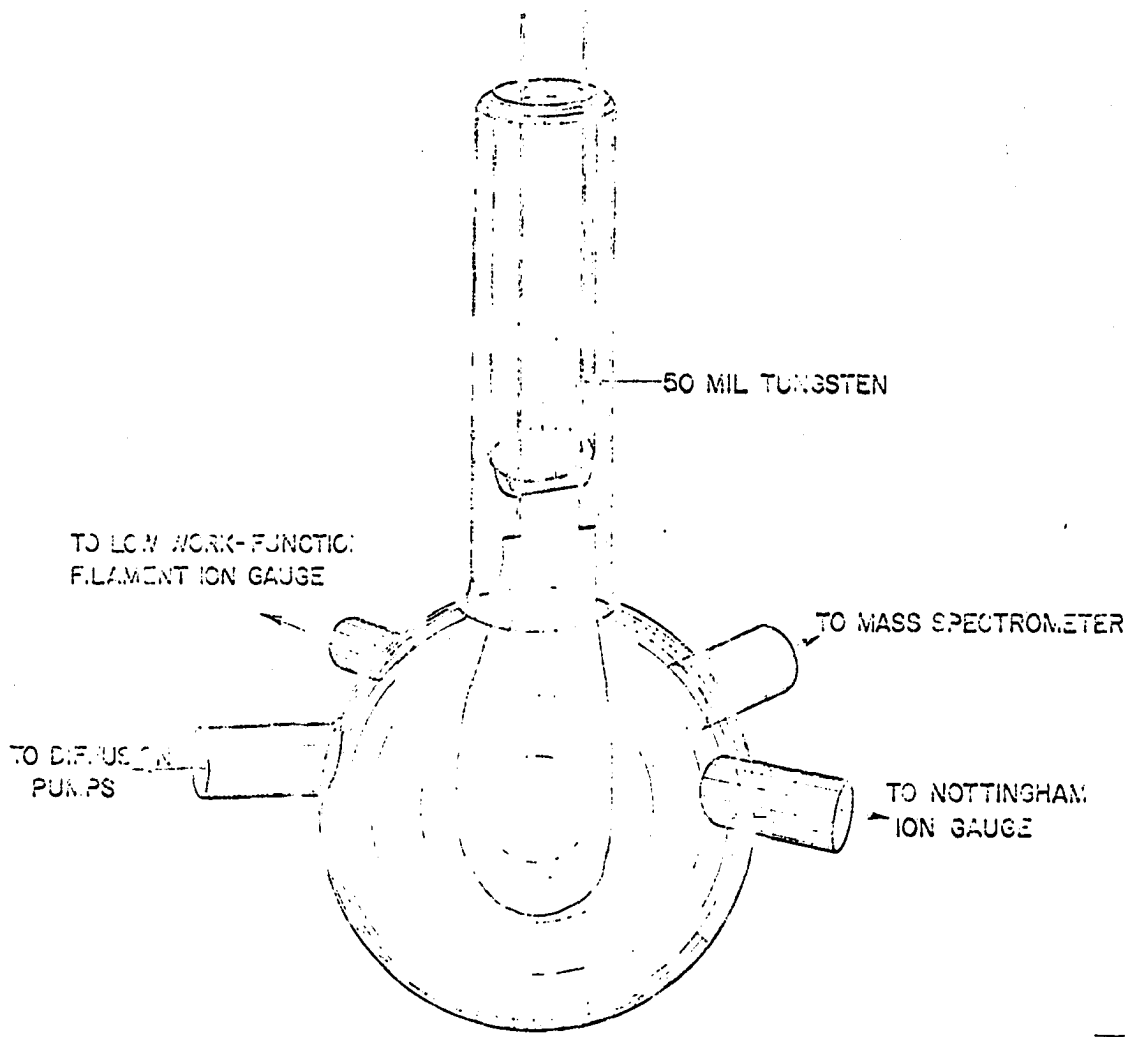

Figure 3. Desorption cell used in flash filament experiments

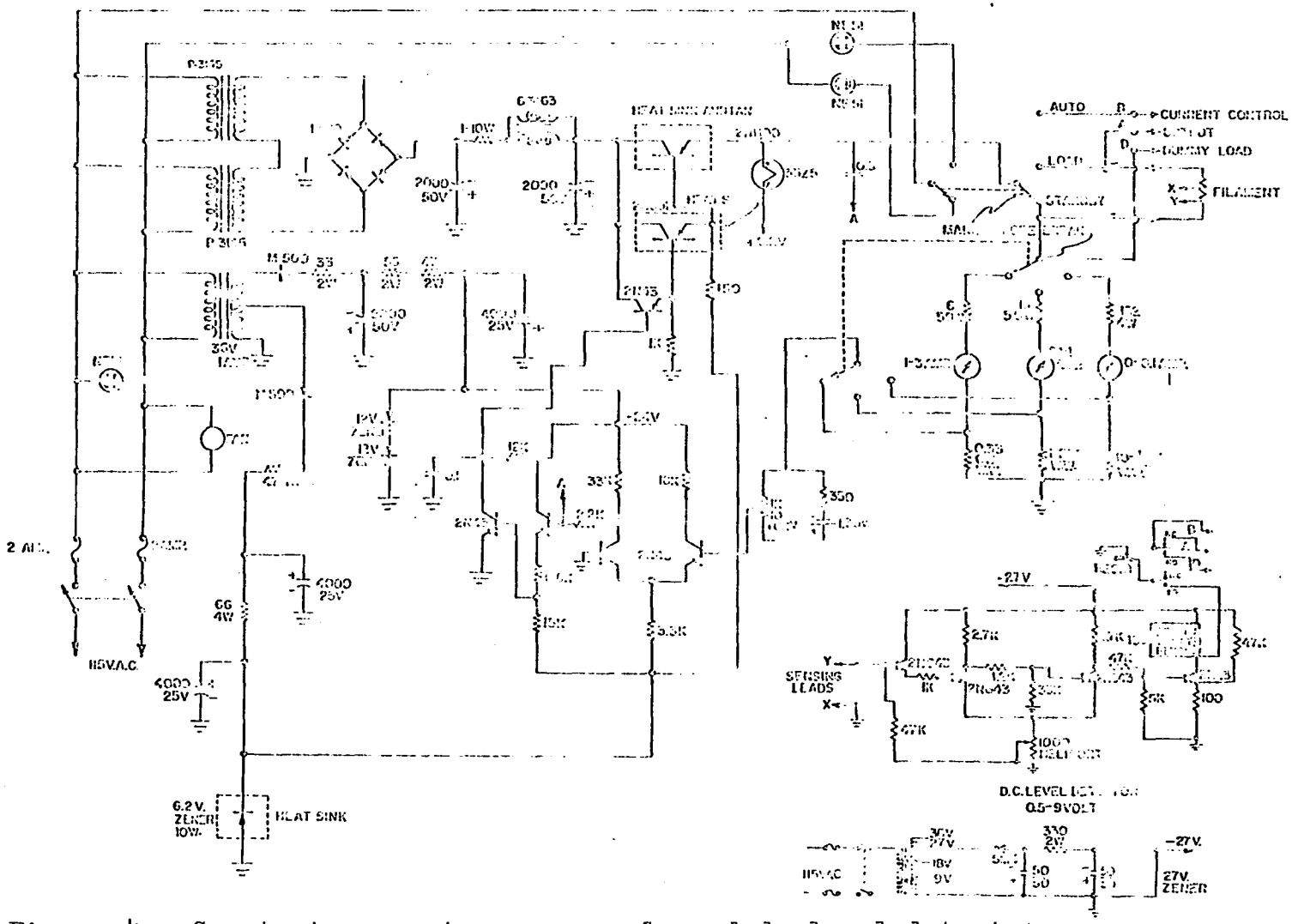

Figure 4. Constant current power supply and dc-level detector

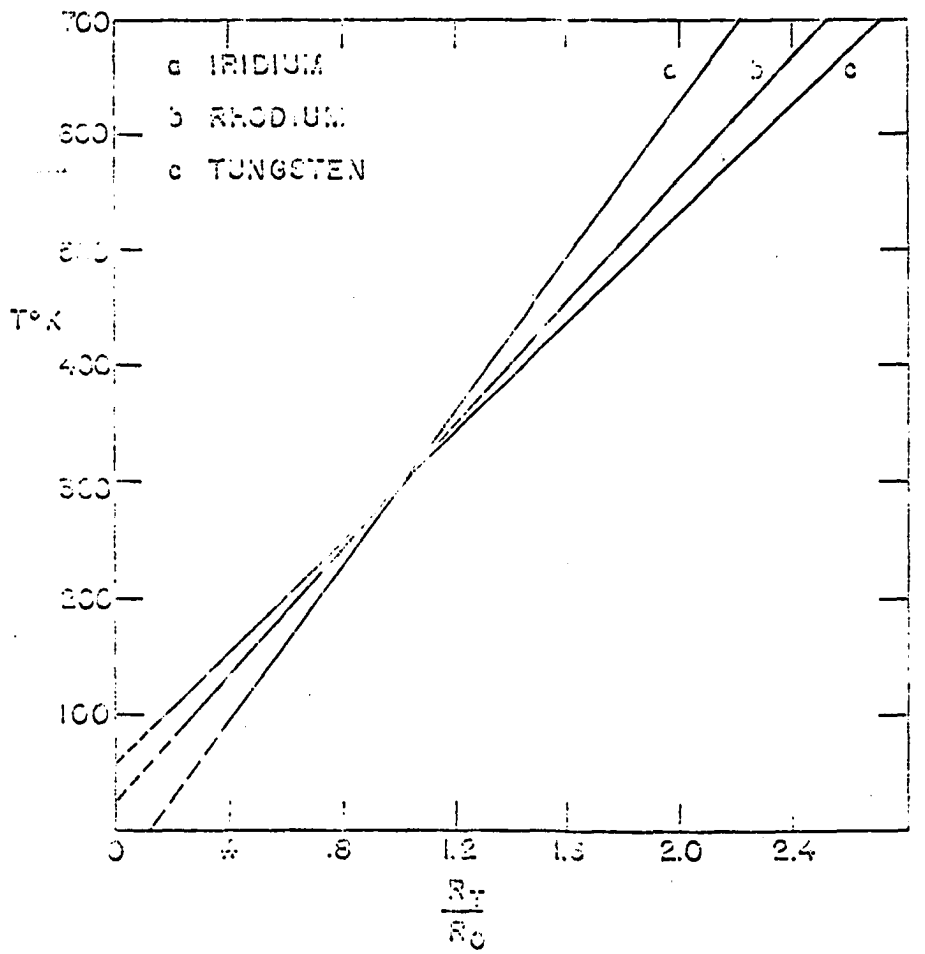

Figure 5. Resistance-ratio versus temperature for iridium, rhodium and tungsten
R_0 = resistance at 295°K

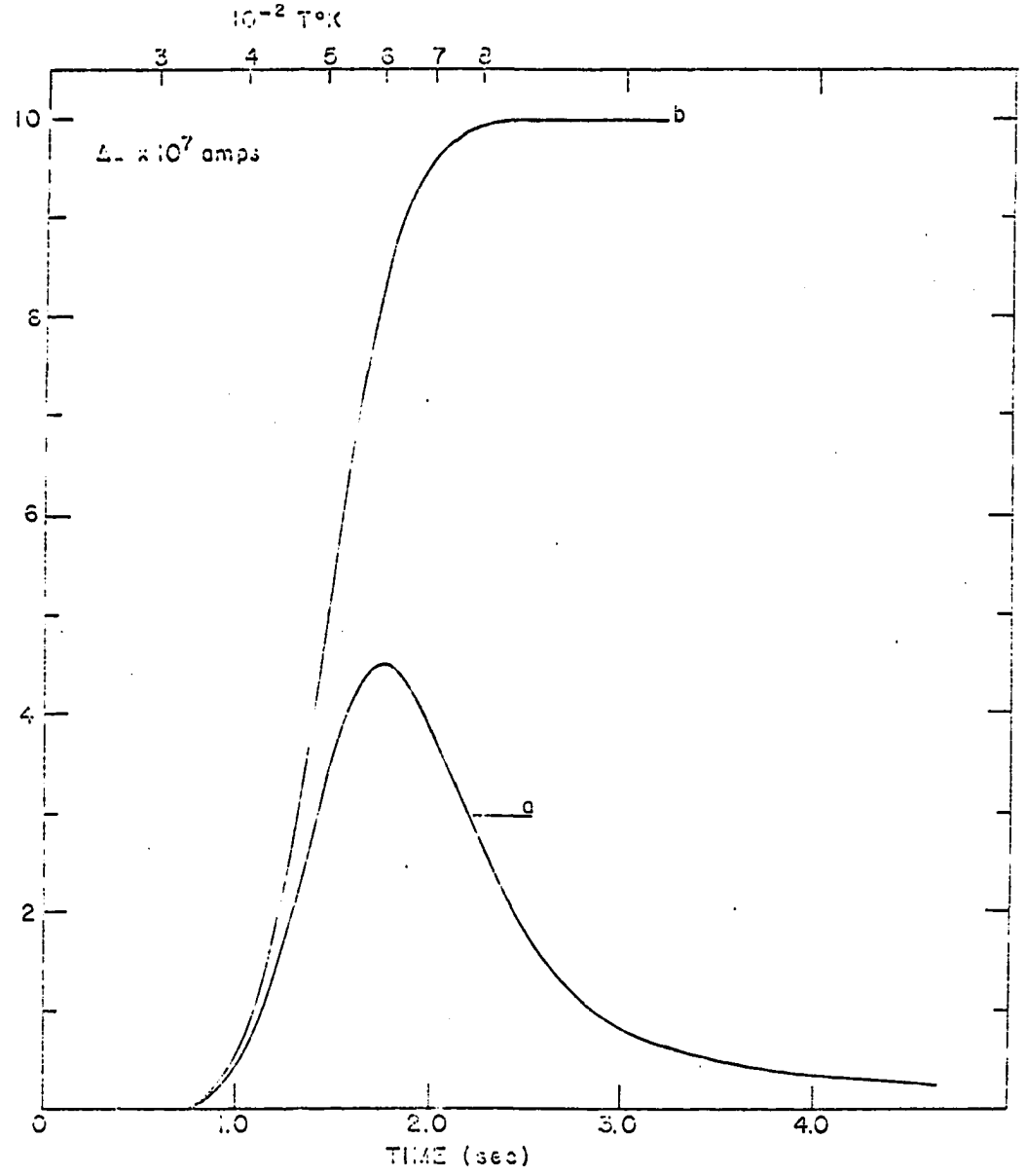

Figure 6. Desorption spectrum of hydrogen from rhodium. Pressure change monitored with Nottingham ion gauge. a. ΔI vs time b. $(\Delta I + \frac{S}{V}\int_0^t \Delta I dt)$ vs time

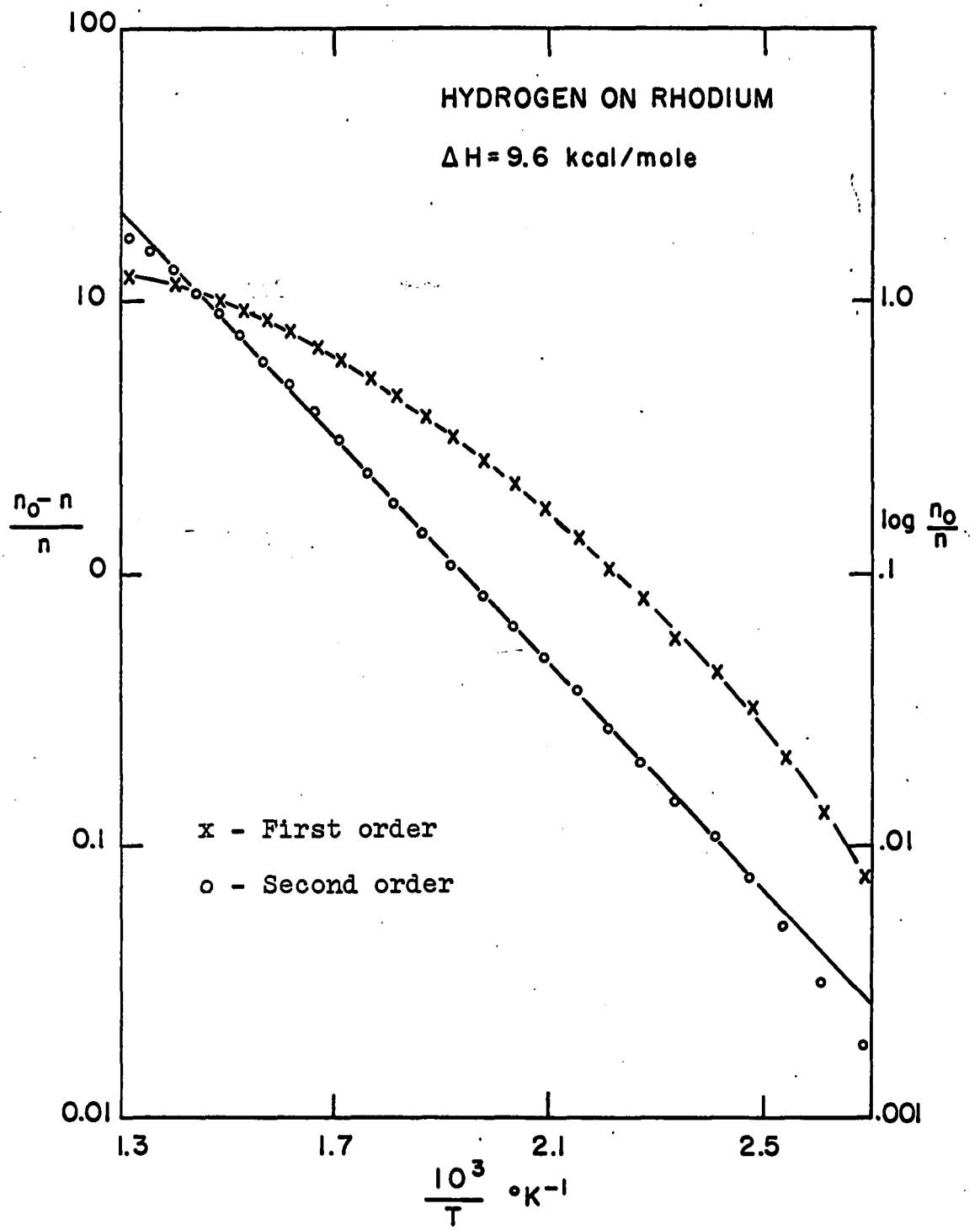

Figure 7. Analysis of desorption curve obtained using hot filament ion gauge to monitor pressure burst (erroneous result as a result of ion gauge pumping, correct ΔH is 18 kcal/mole)

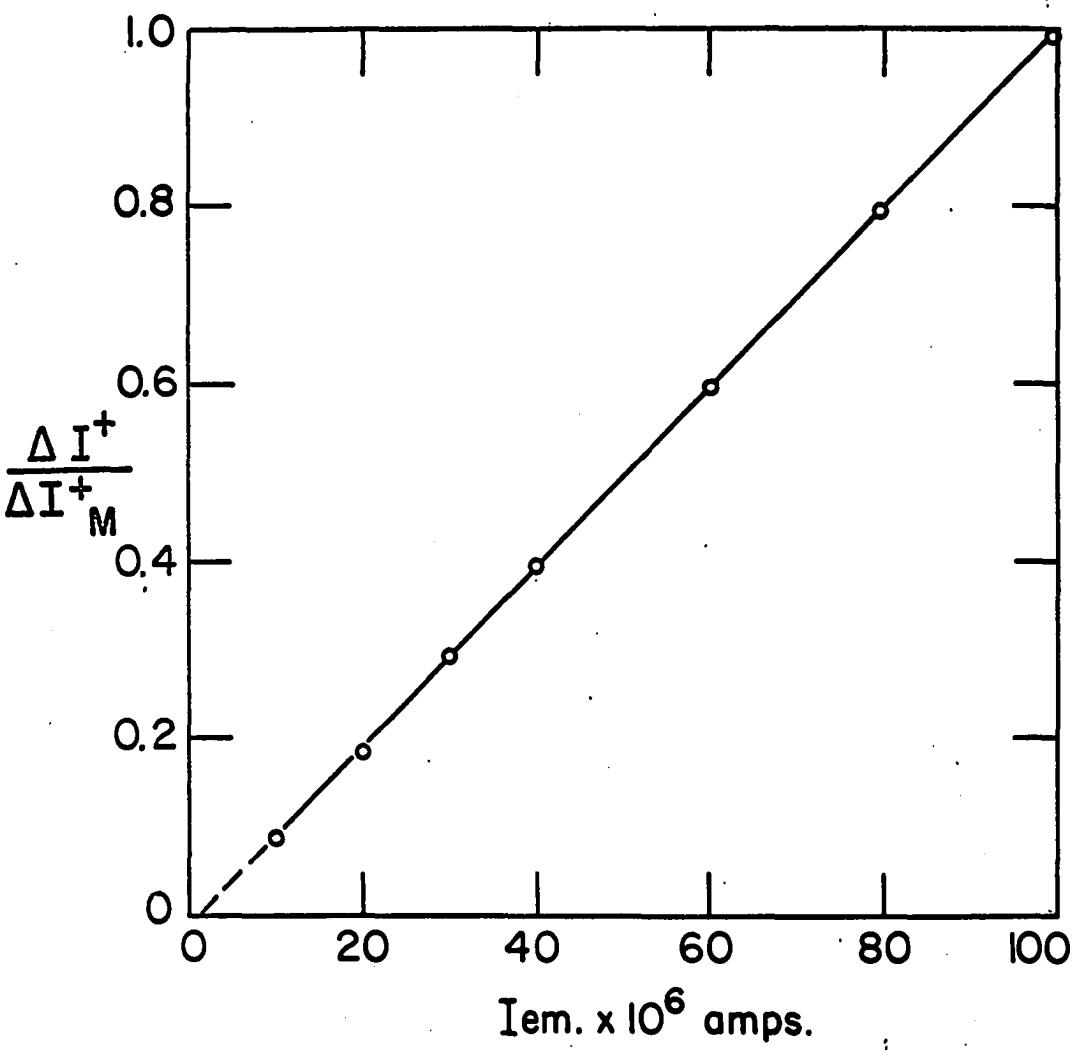

Figure 8. Normalized change in ion current as a function of the emission current of the ion gauge for the same initial dose of the sample filament and same heating rate

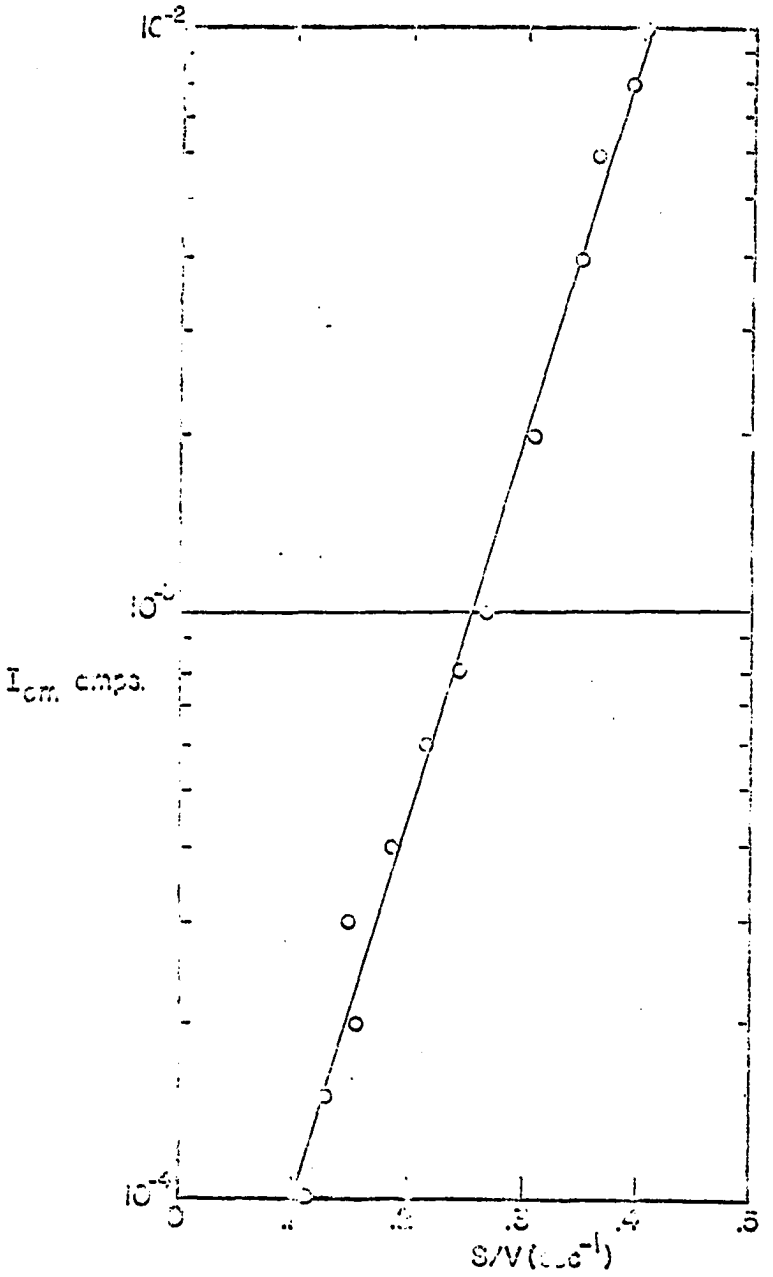

Figure 9. Effect of emission current of the thoria-coated filament on the pumping term, $\frac{S}{V}$

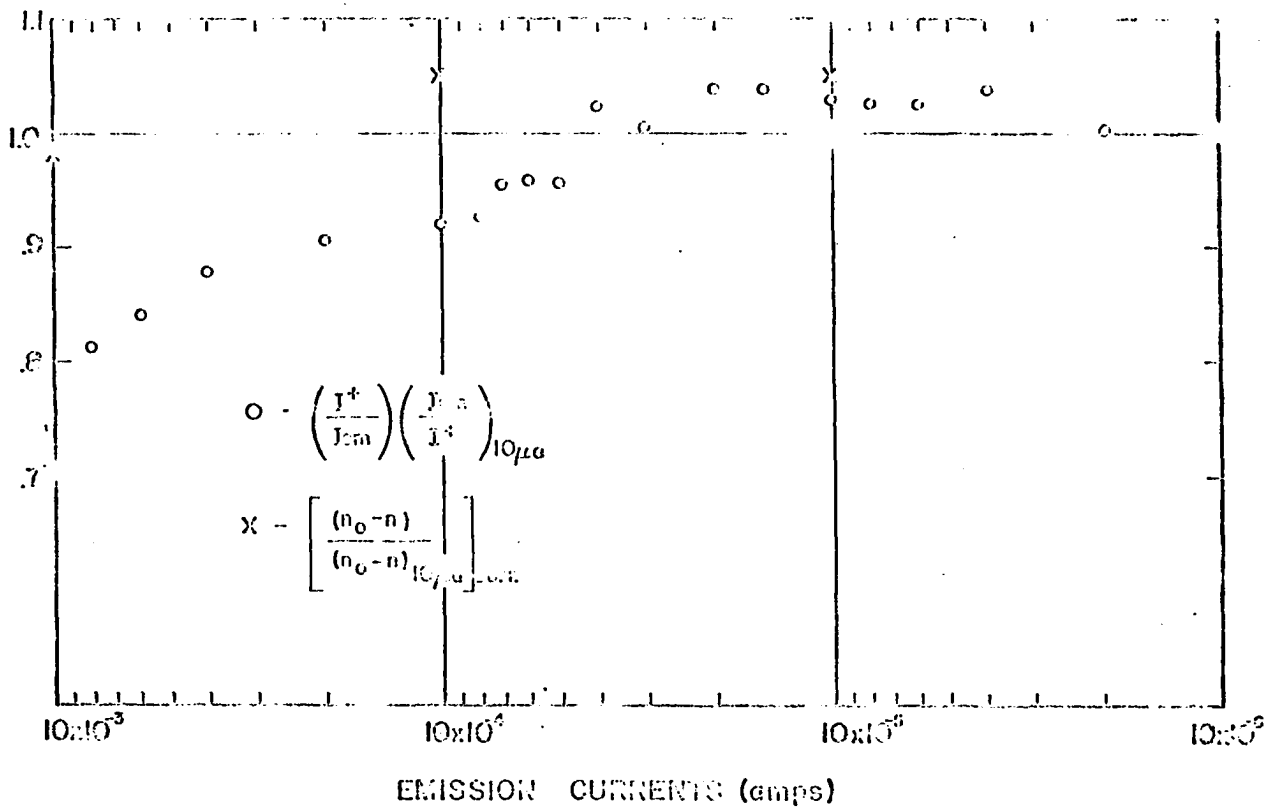

Figure 10. Decrease in peak height of pressure burst due to pumping action of ion gauge at higher emission currents

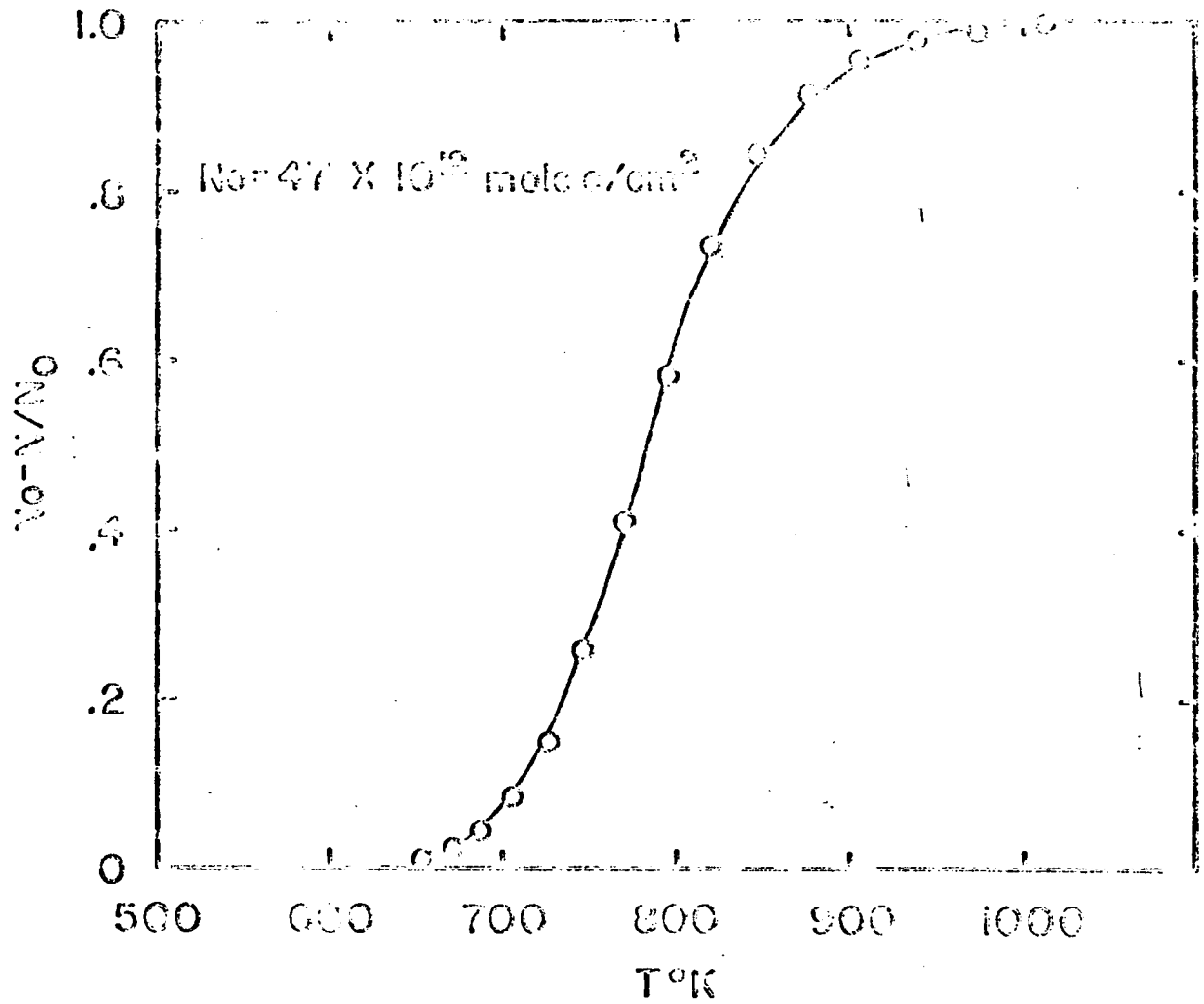

Figure 11. Flash desorption of hydrogen from tungsten dosed at 300°K

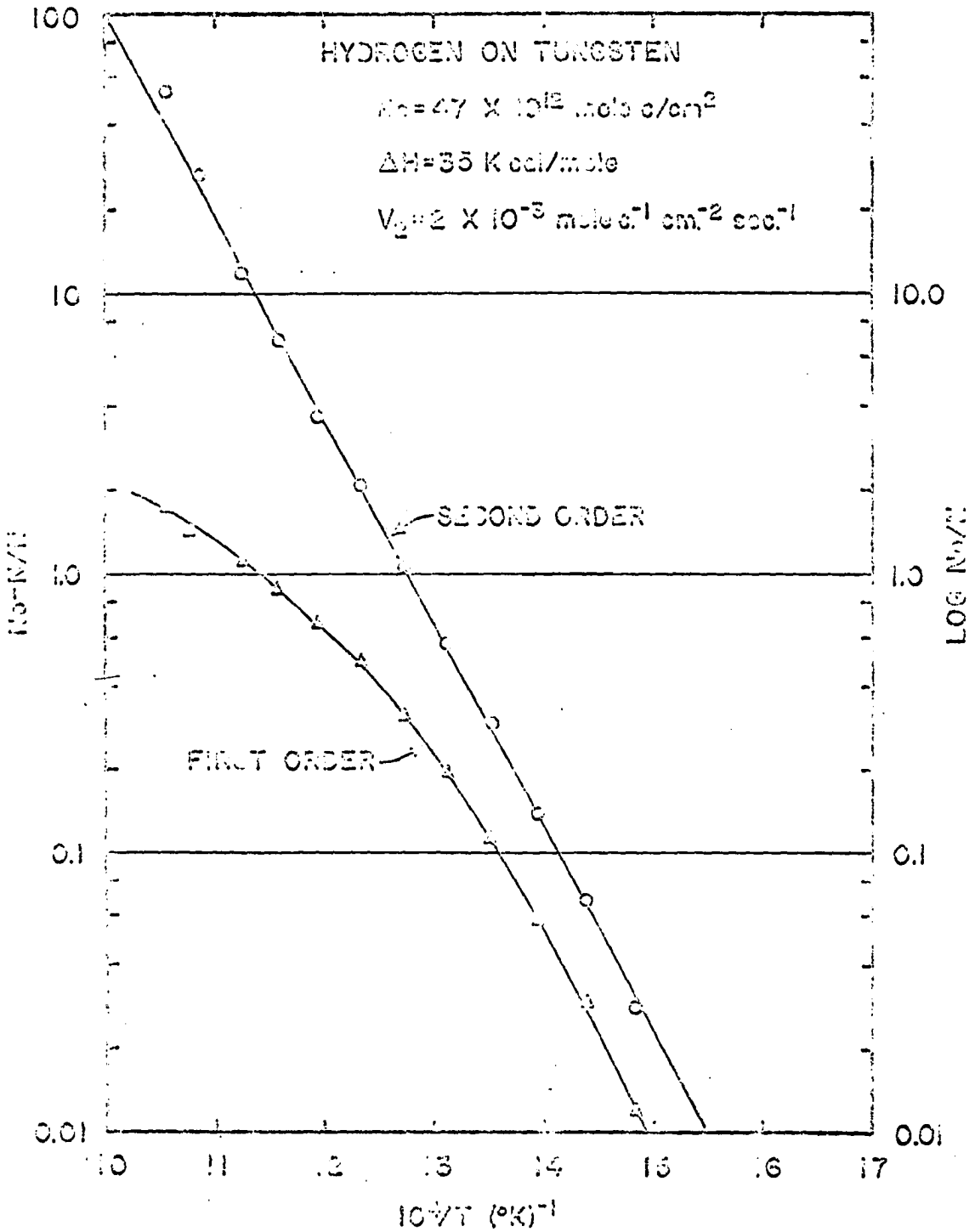

Figure 12. Analysis of pressure-temperature data for hydrogen on tungsten, dosed at 300°K, by first- and second-order kinetics

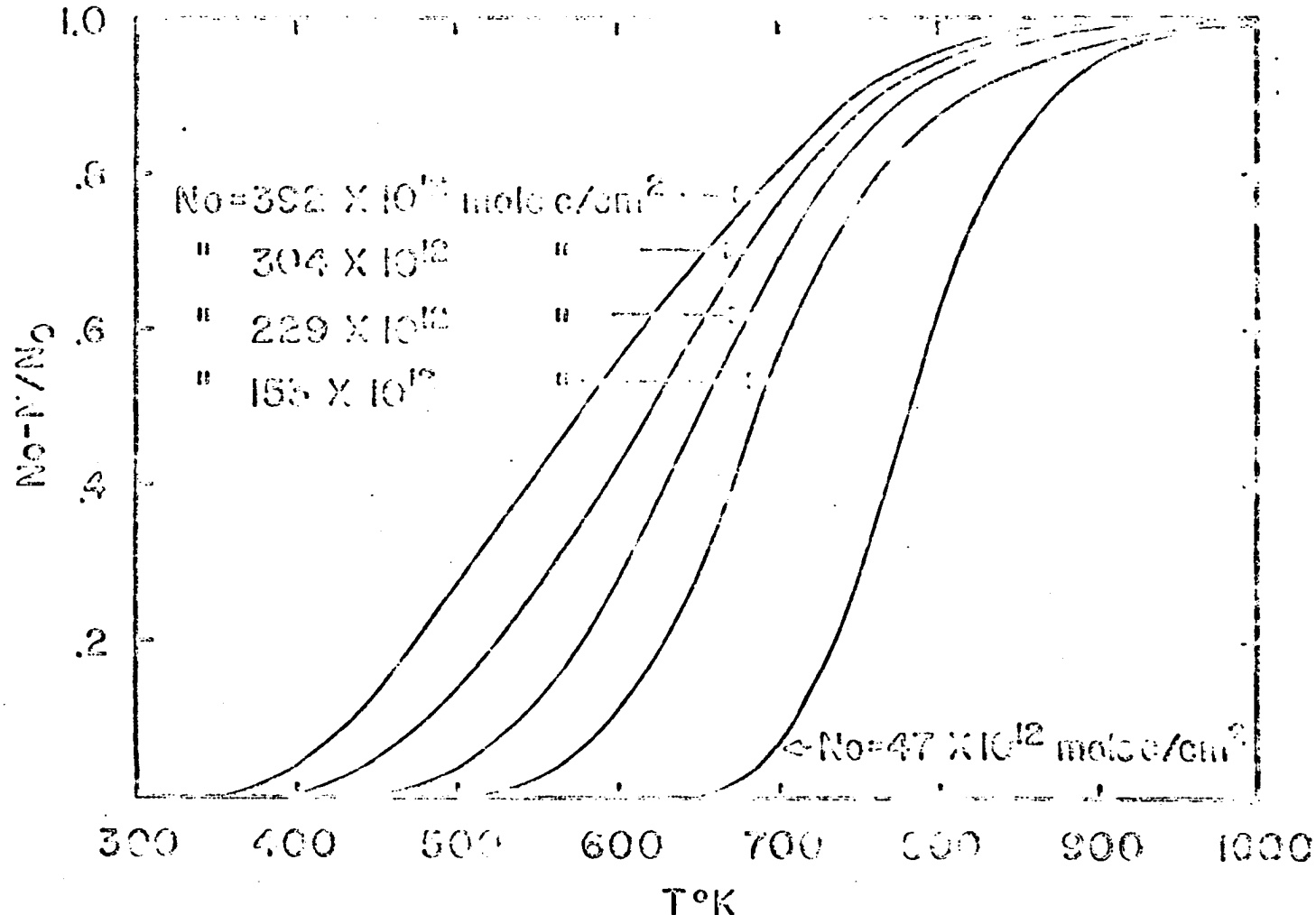

Figure 13. Normalized desorption spectra of hydrogen from tungsten for increasing initial surface coverages

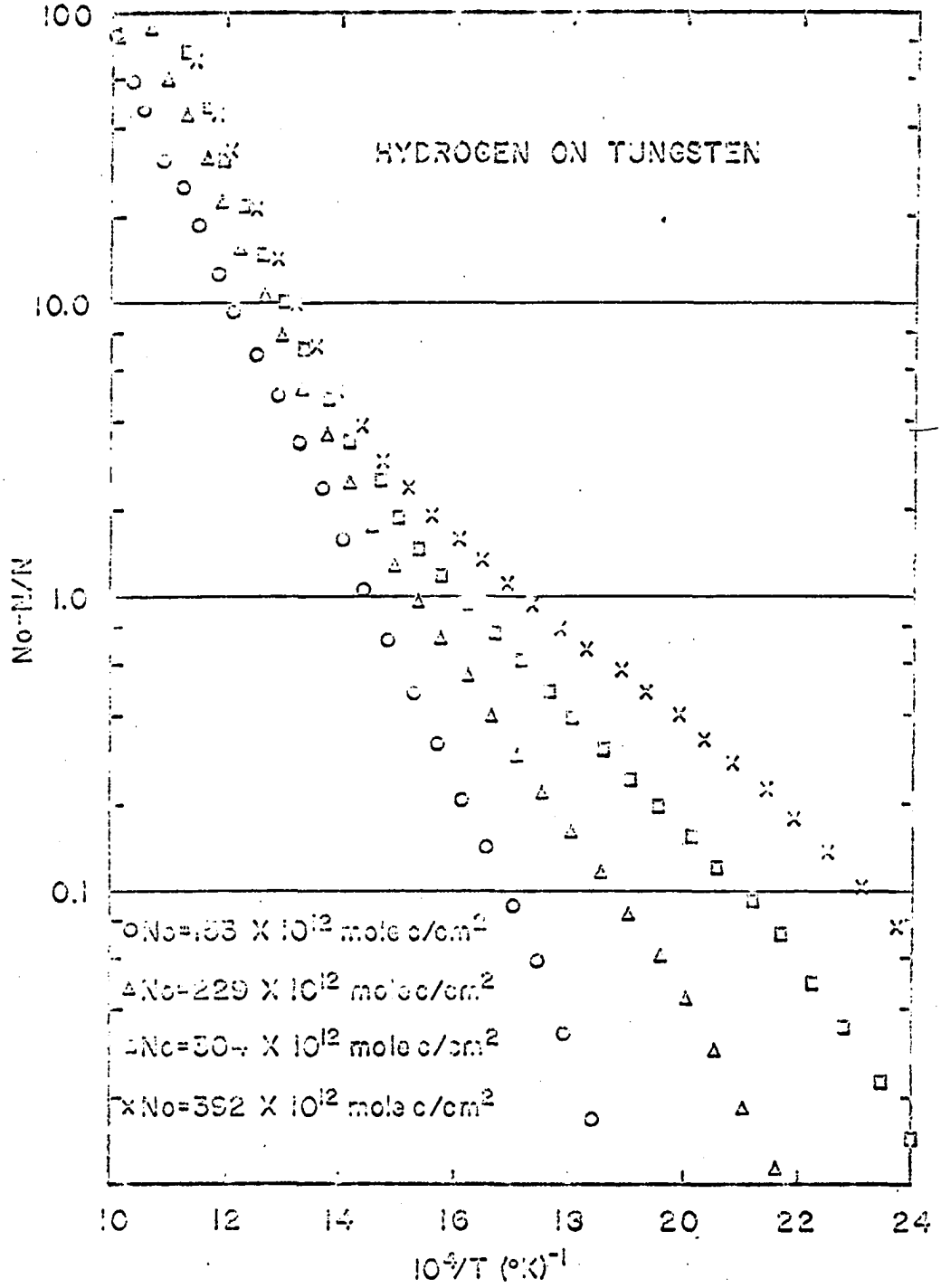

Figure 14. Desorption of hydrogen from tungsten at different initial coverages, analyzed as a second-order reaction

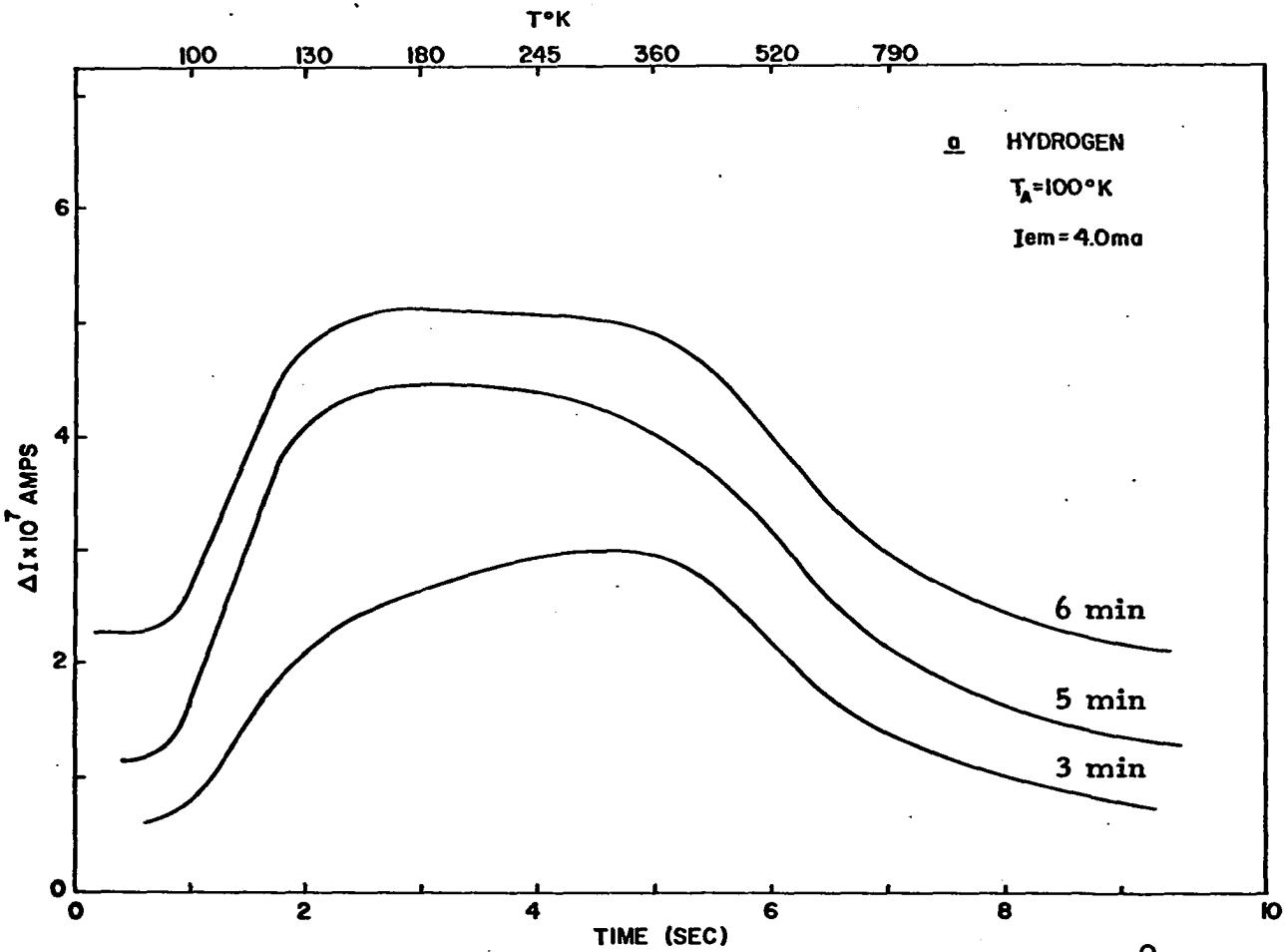

Figure 15a. Desorption of hydrogen from tungsten initially at 100°K

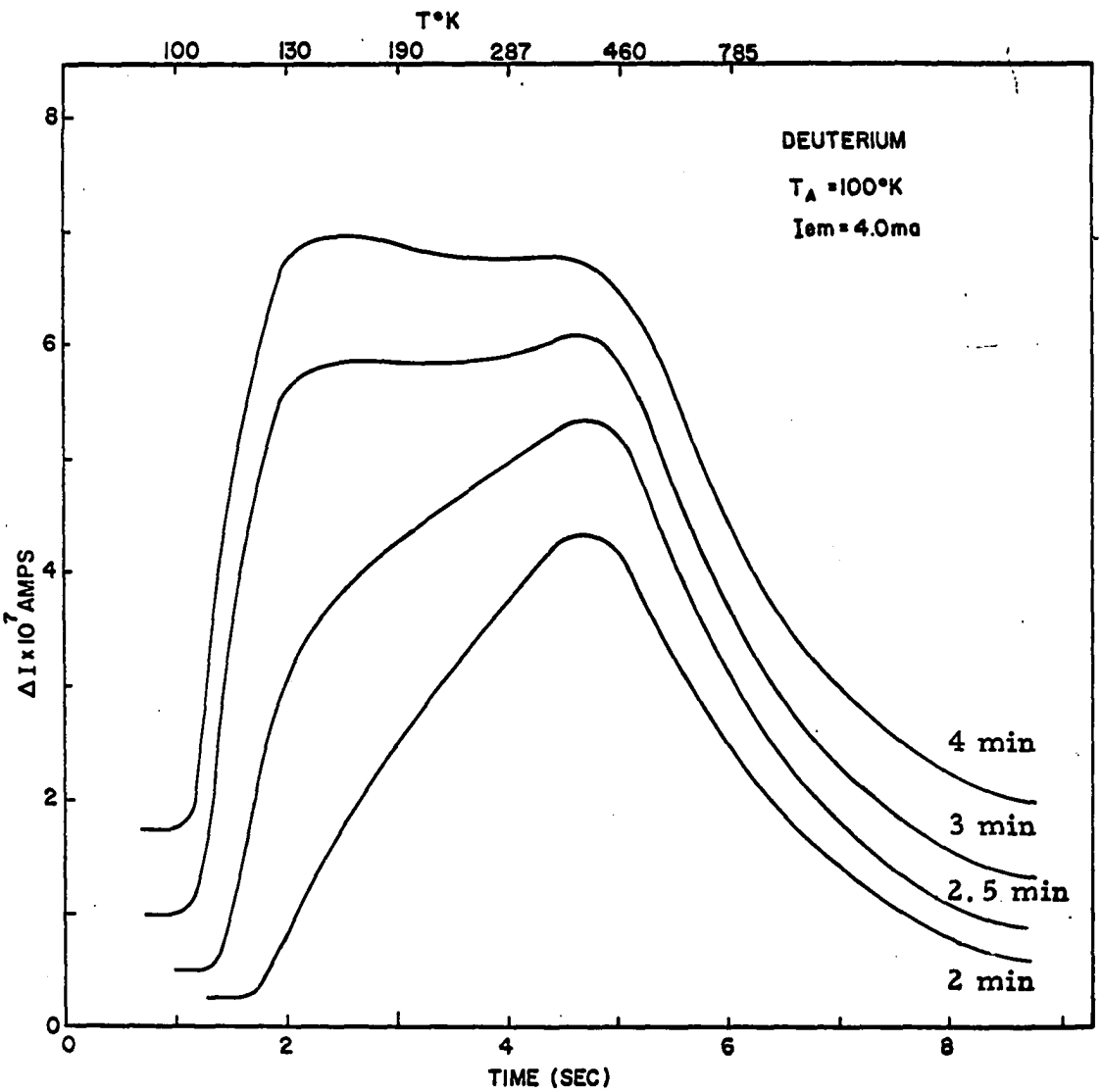

Figure 15b. Desorption of deuterium from tungsten initially at 100°K

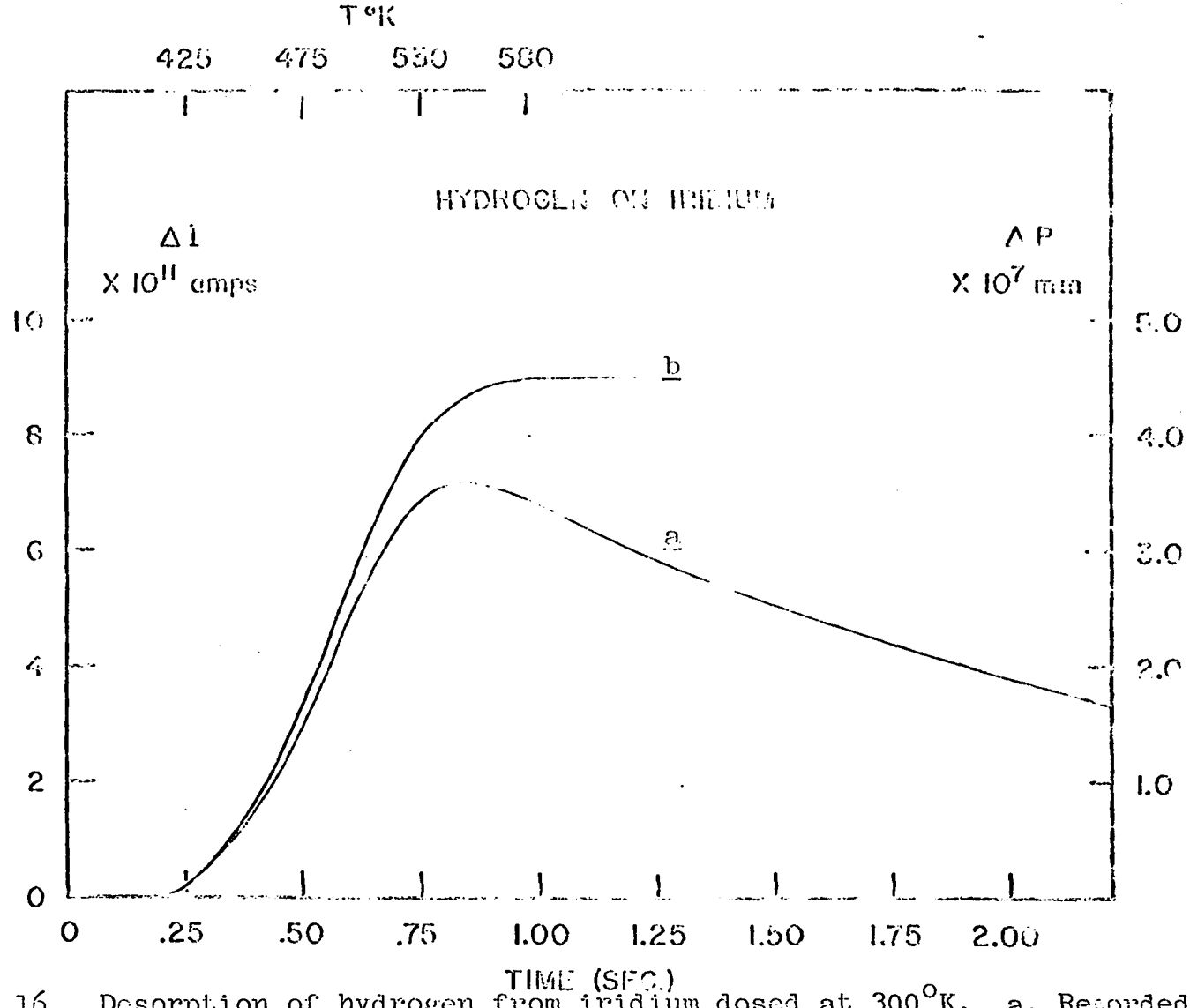

Figure 16. Desorption of hydrogen from iridium dosed at 300°K. a. Recorded pressure change. b. Curve a corrected for pumping

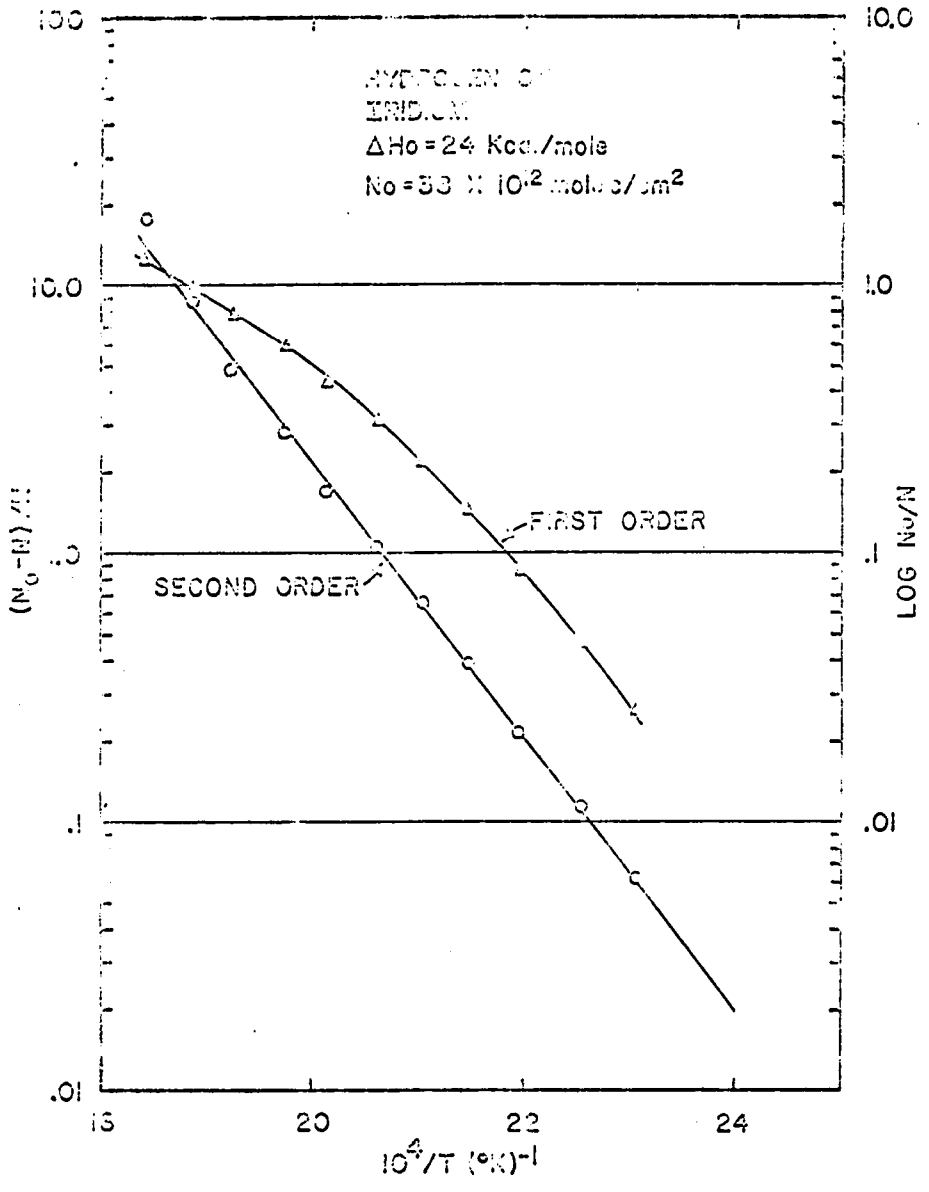

Figure 17. Analysis of corrected pressure-temperature data for hydrogen on iridium by first- and second-order kinetics

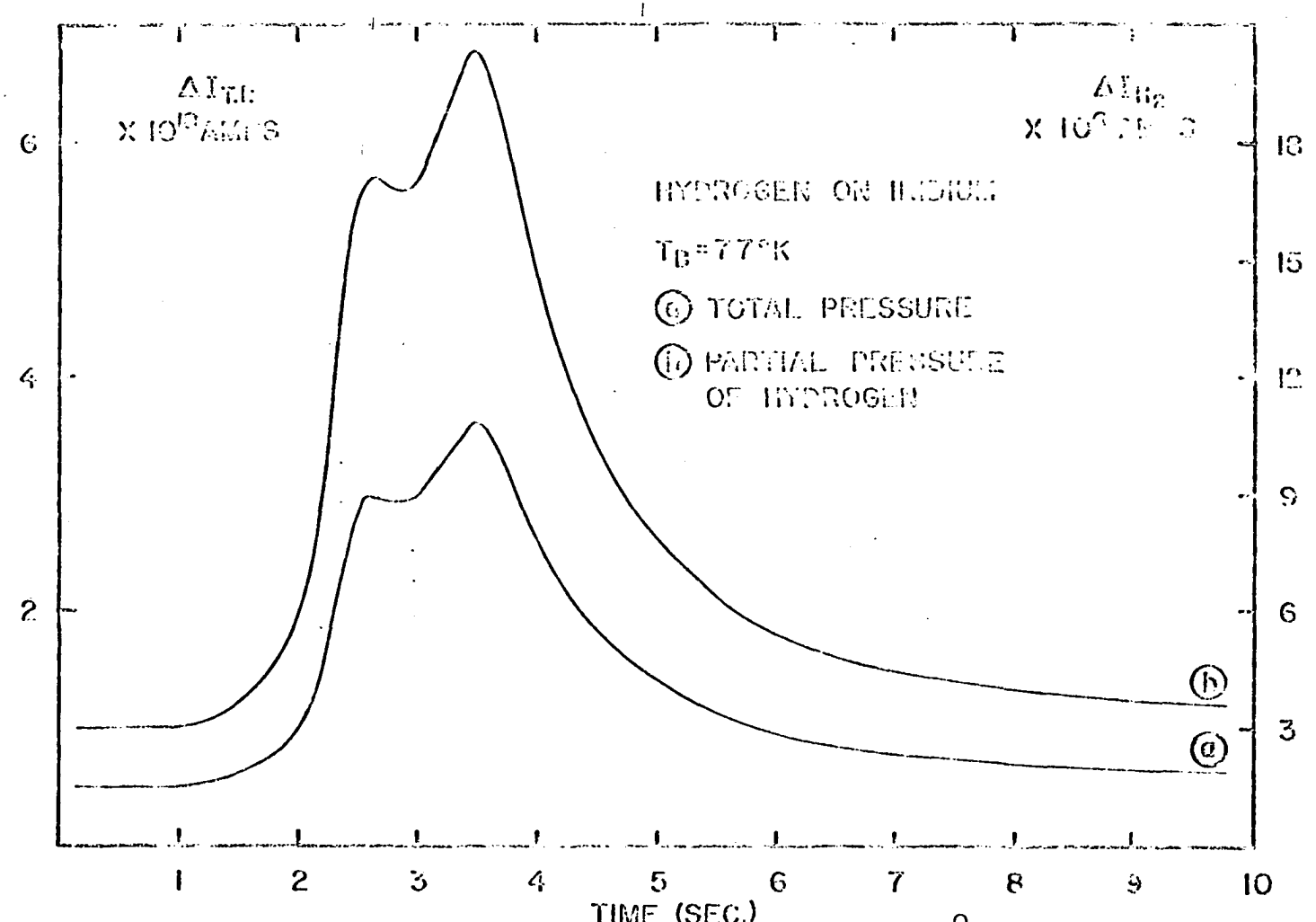

Figure 18. Desorption of hydrogen from iridium dosed at 100°K. a. Partial pressure on hydrogen. b. Total pressure

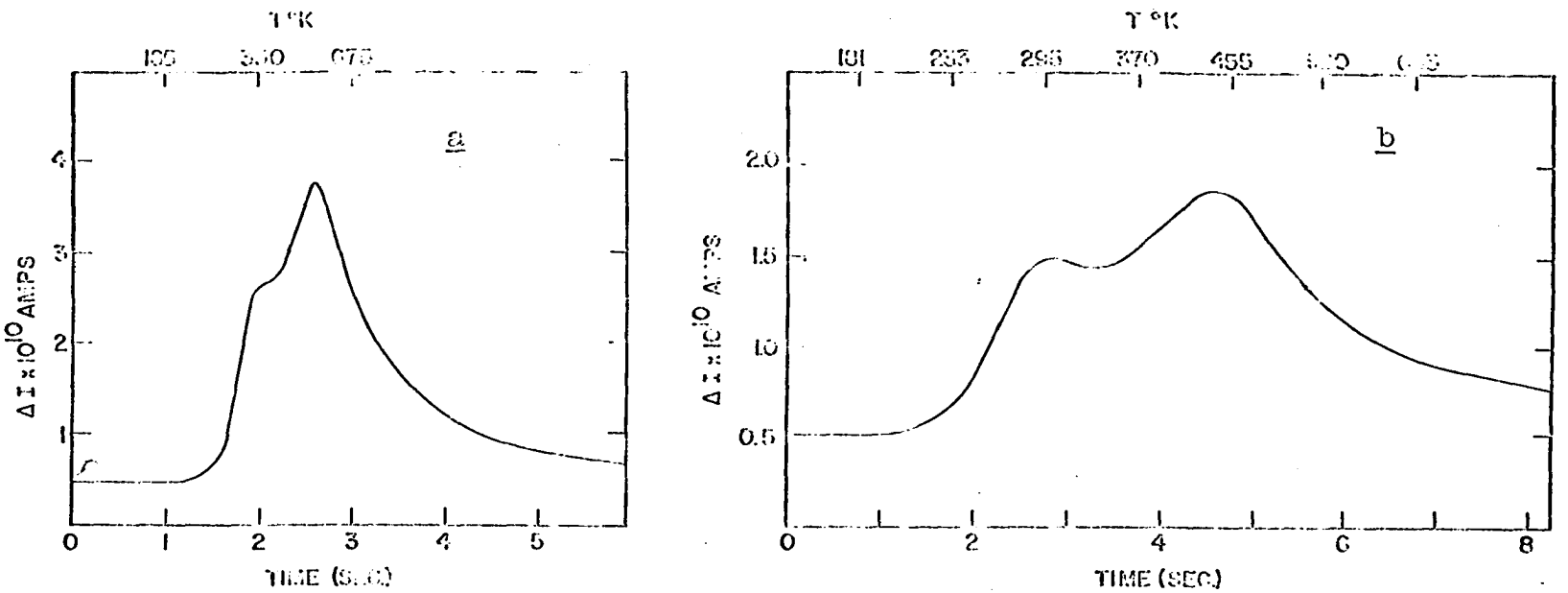

Figure 19. Desorption of hydrogen from iridium dosed at 100°K. a. Heating rate ~255°/sec. b. Heating rate ~75°/sec

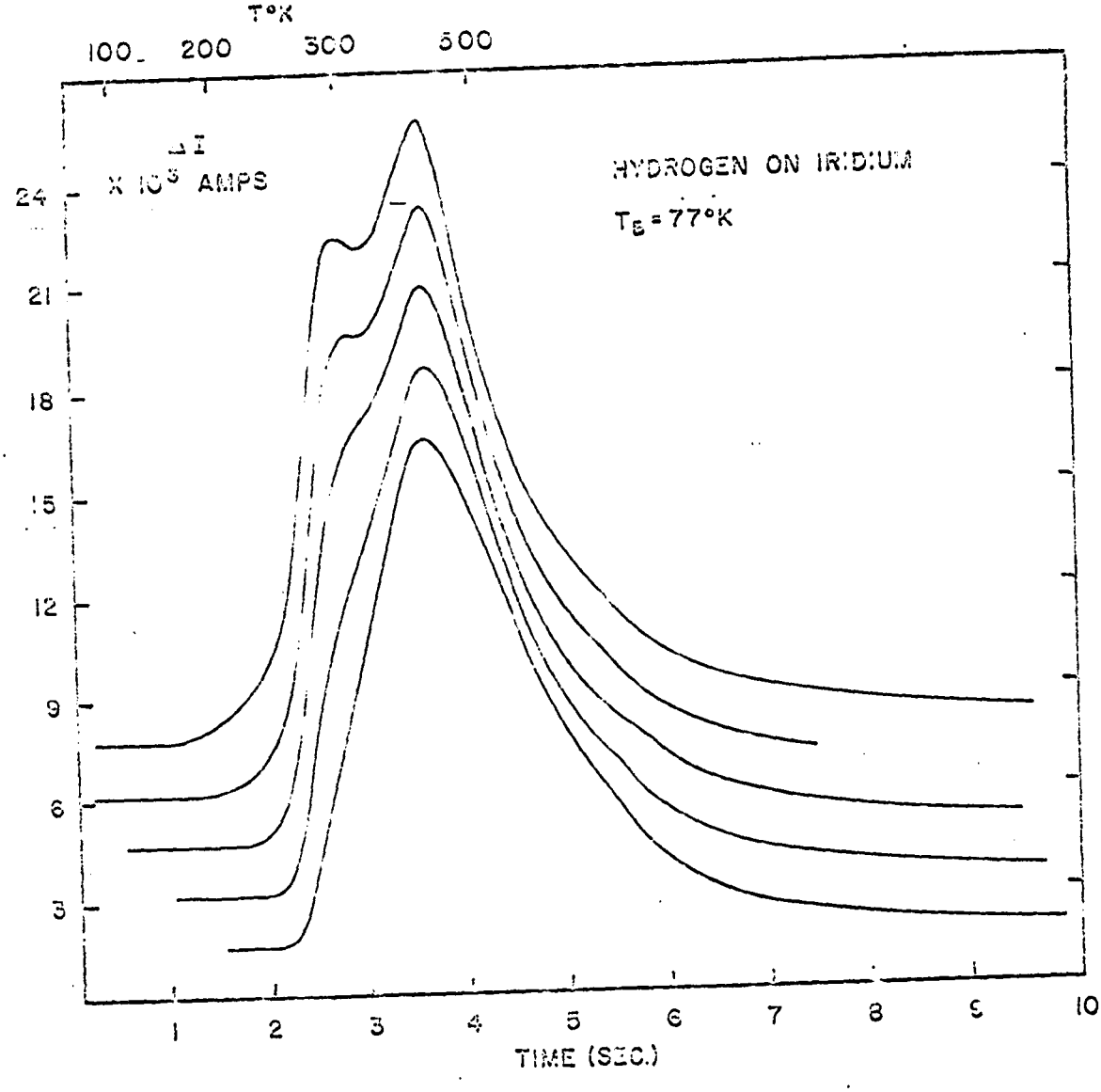

Figure 20. Desorption of hydrogen from iridium for increasing initial doses at 100°K

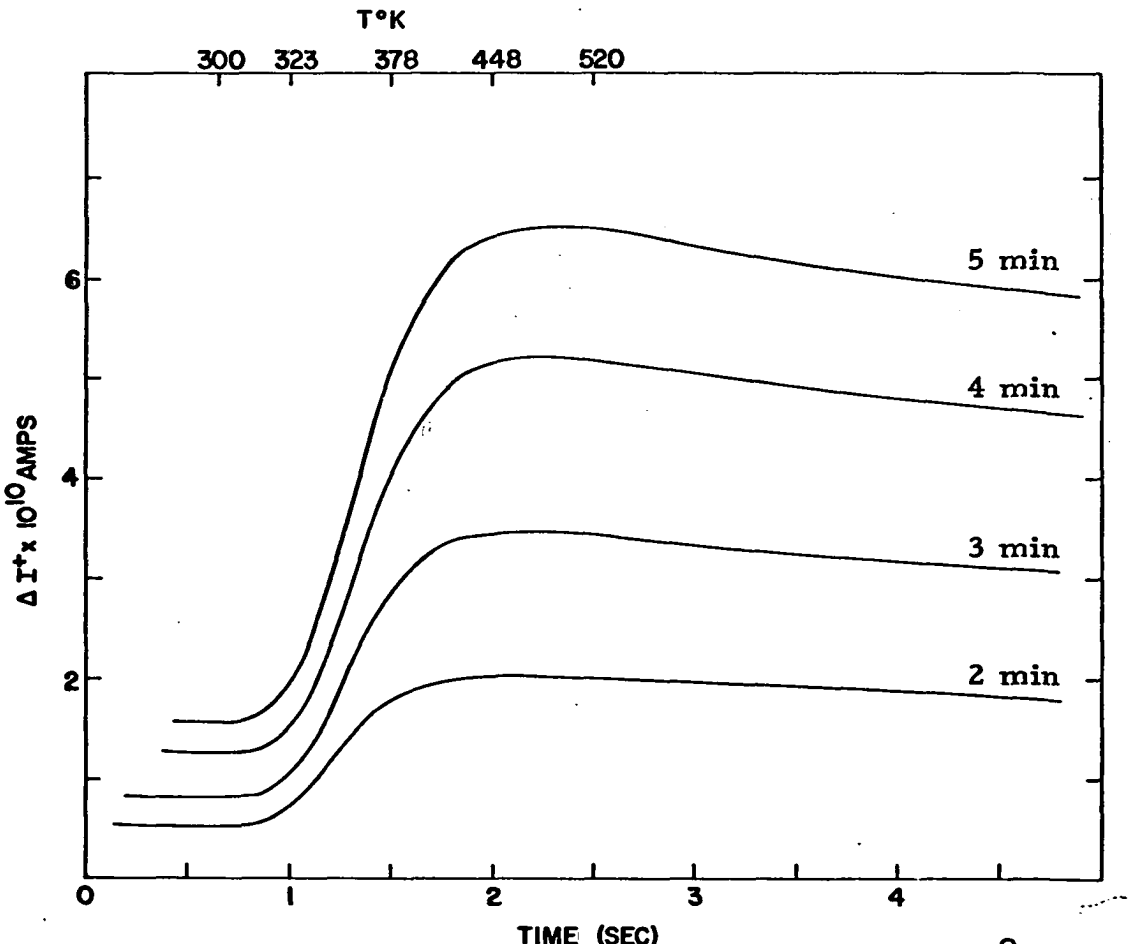

Figure 21. Desorption of hydrogen from rhodium dosed at 300°K

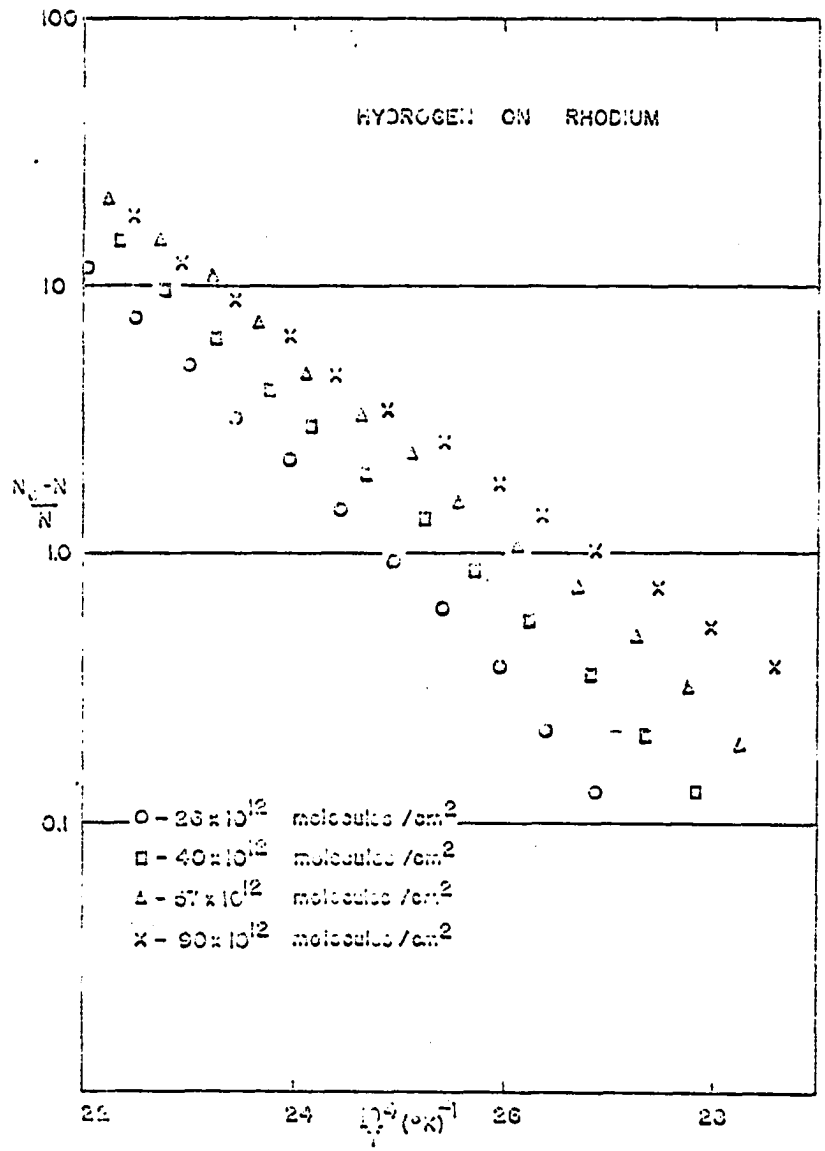

Figure 22. Desorption of hydrogen from rhodium for different initial doses, analyzed as a second-order reaction

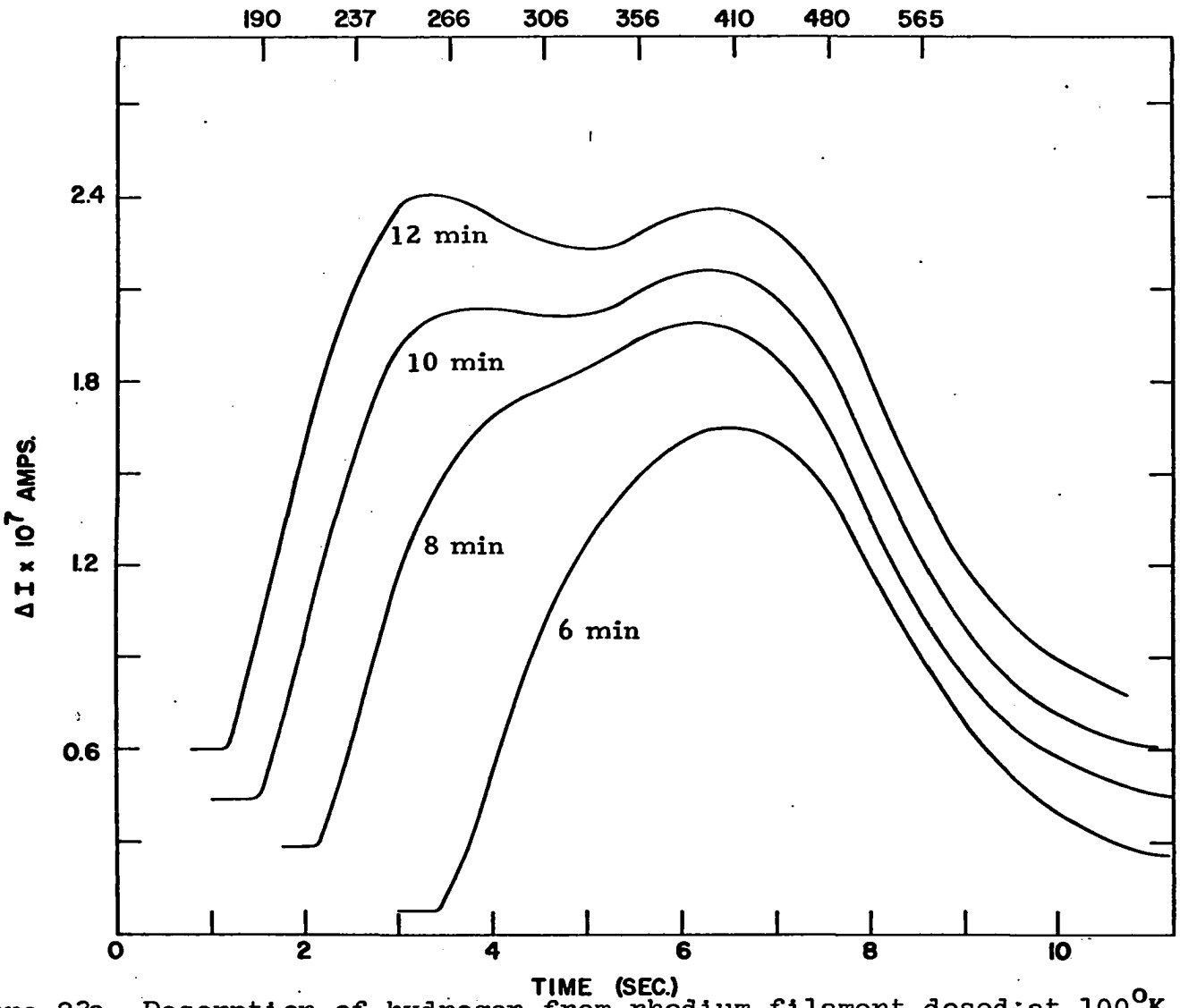

Figure 23a. Desorption of hydrogen from rhodium filament dosed at 100°K

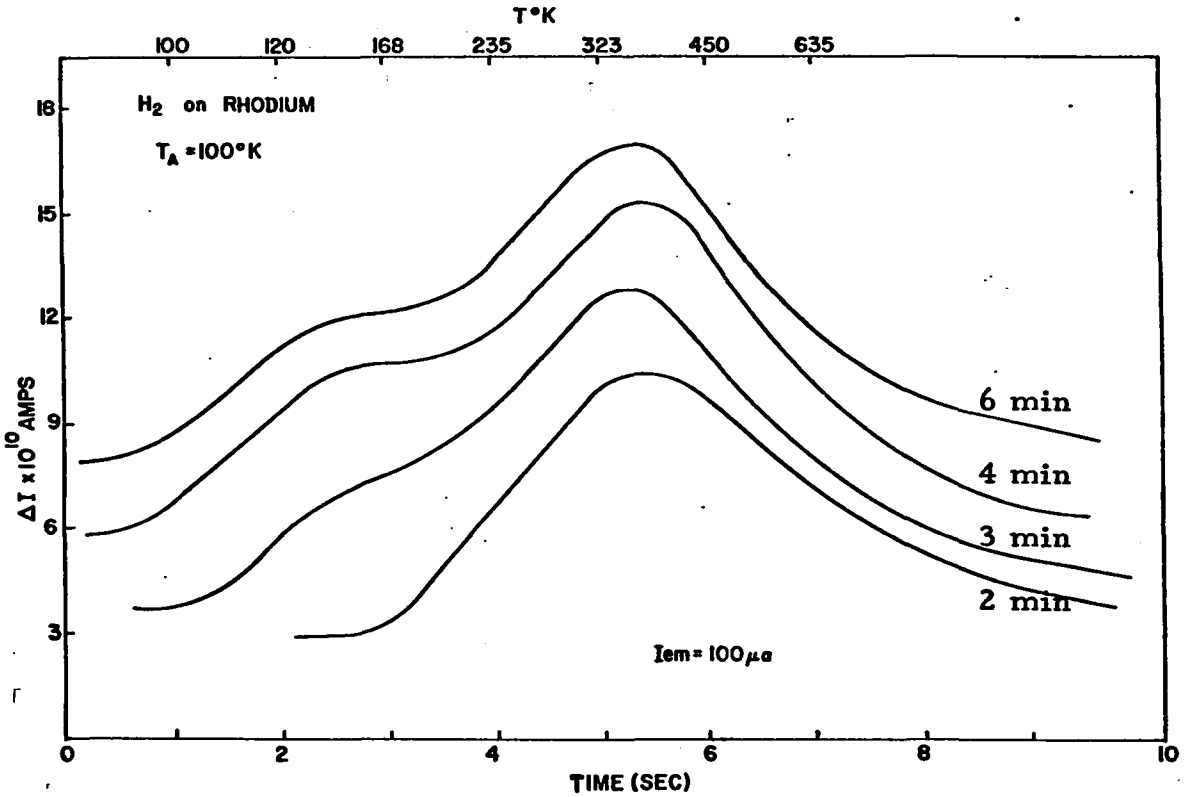

Figure 23b. Desorption of hydrogen from an annealed rhodium filament dosed at 100°k

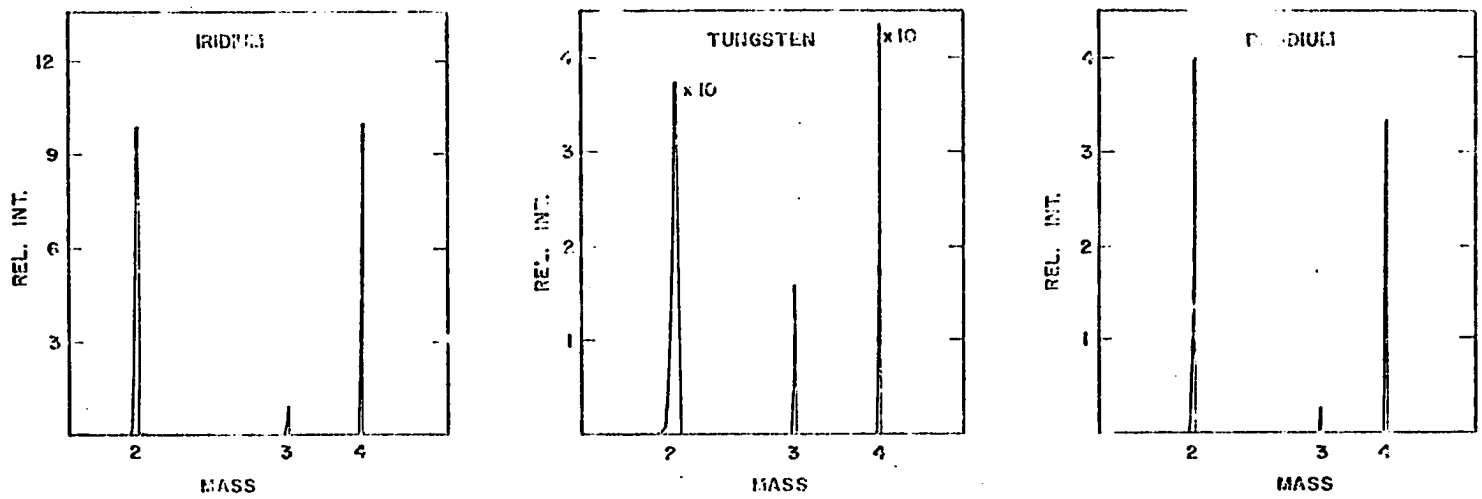

Figure 24. Equilibrium distribution of the hydrogen isotopes in the ambient

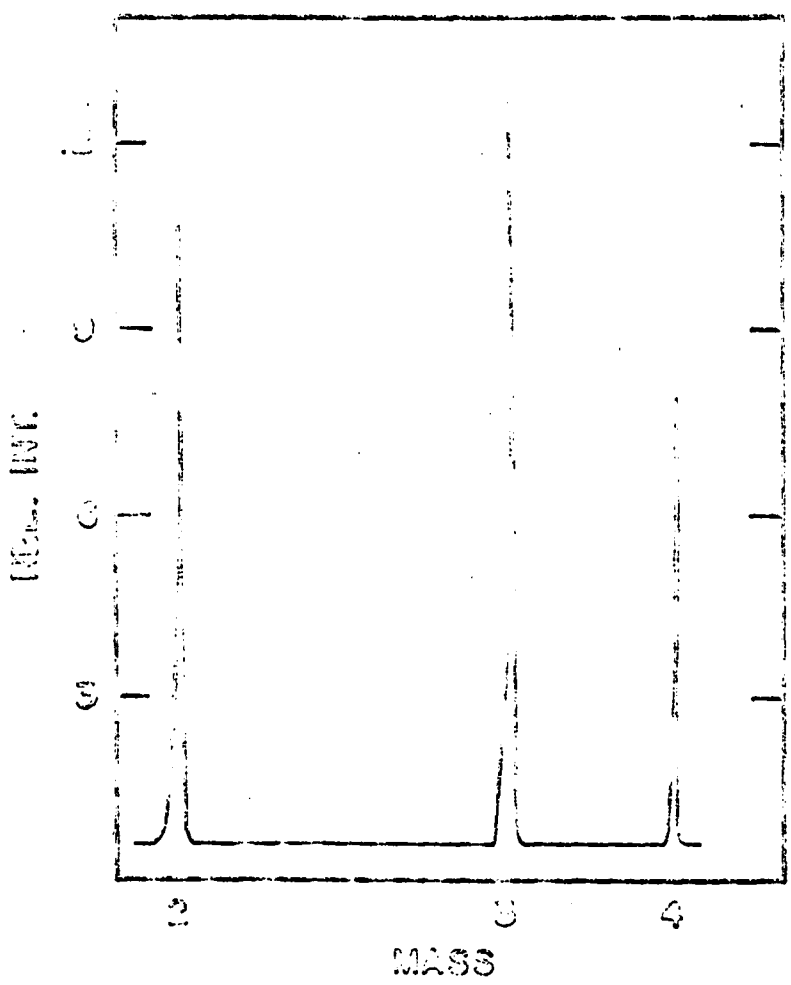

Figure 25. Effect of an evaporated rhodium film on the distribution of the hydrogen isotopes in the ambient

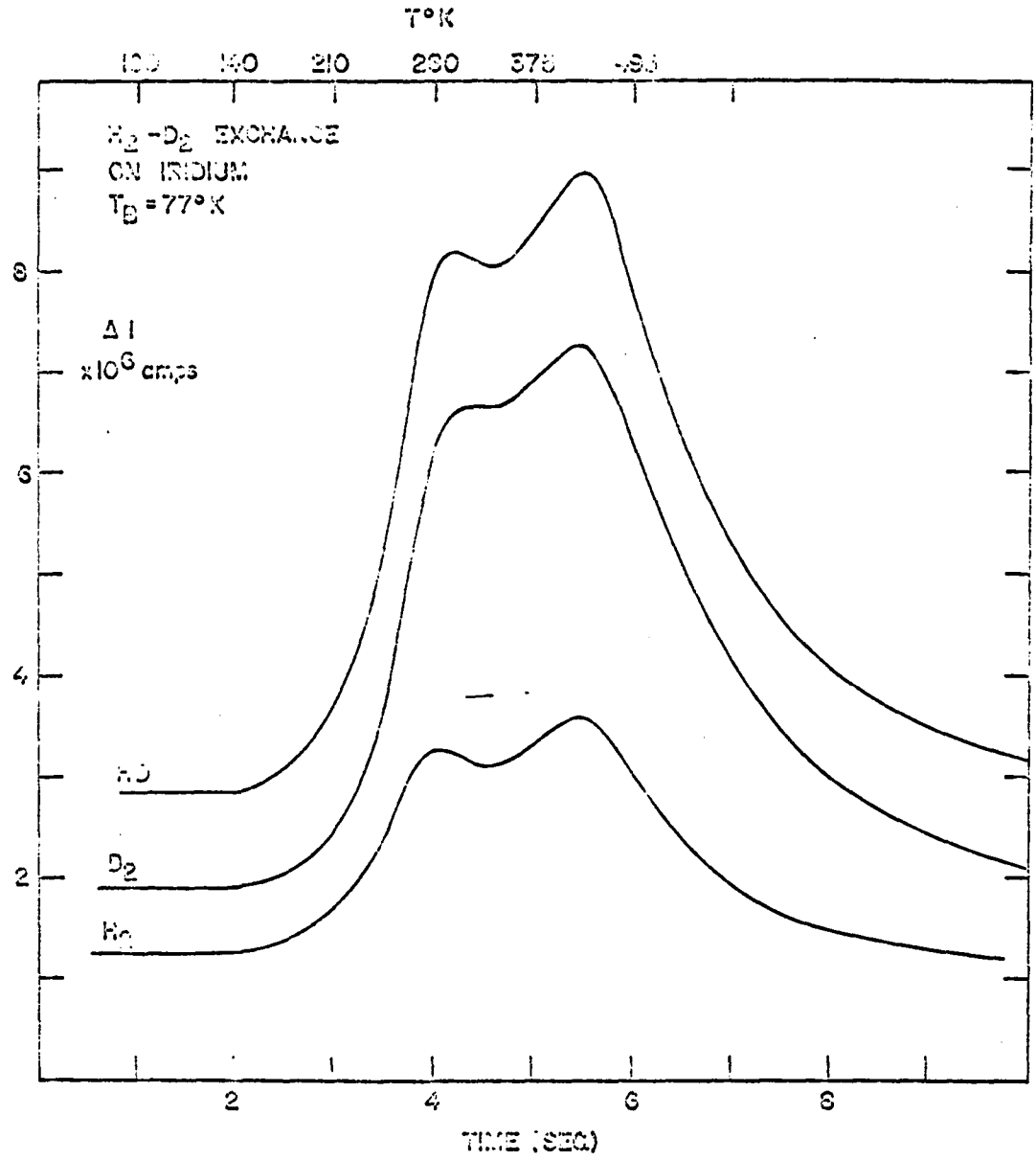

Figure 26. Desorption spectra of hydrogen isotopes from iridium dosed at 100°K with a mixture of H_2 and D_2

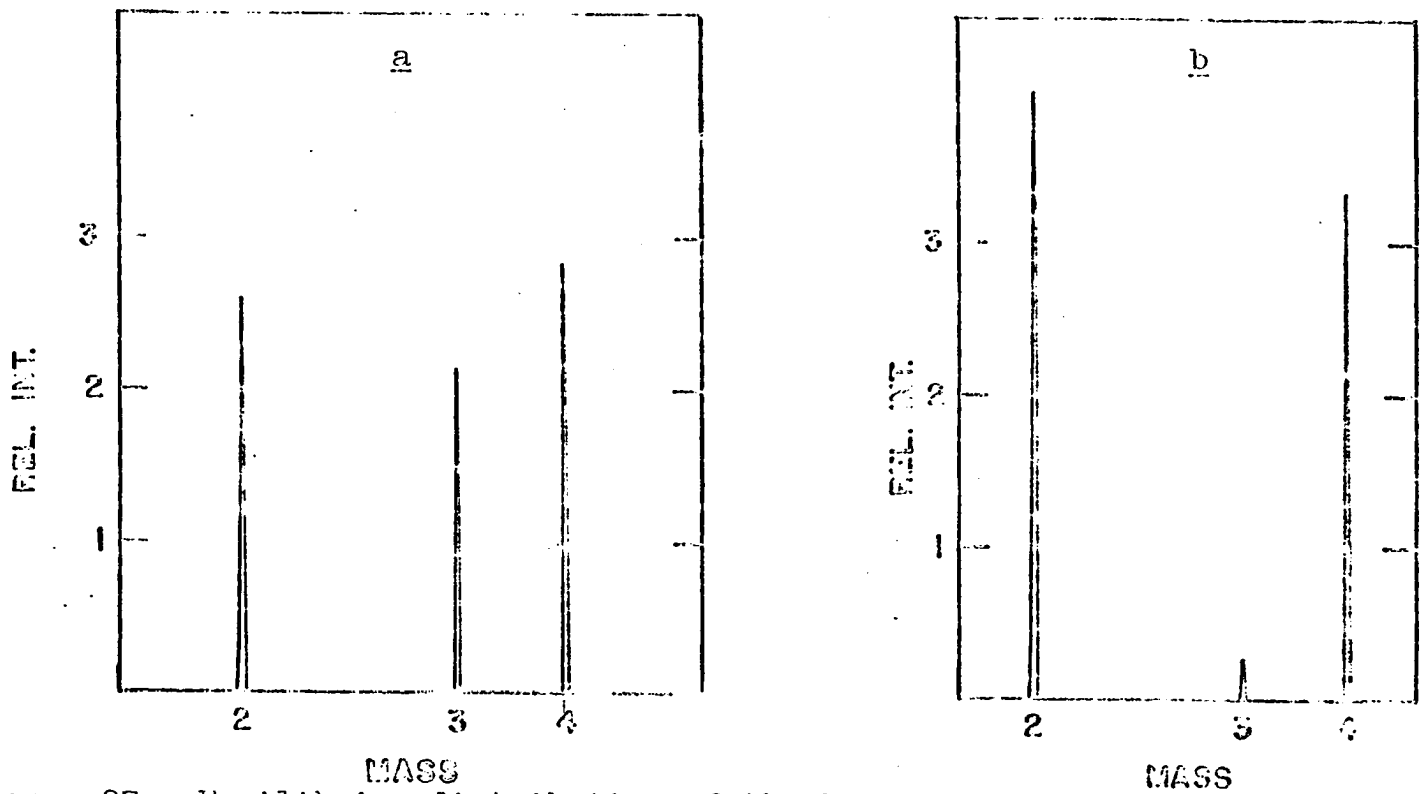

Figure 27. Equilibrium distribution of the hydrogen isotopes in the ambient with the rhodium filament at 300°K and 100°K

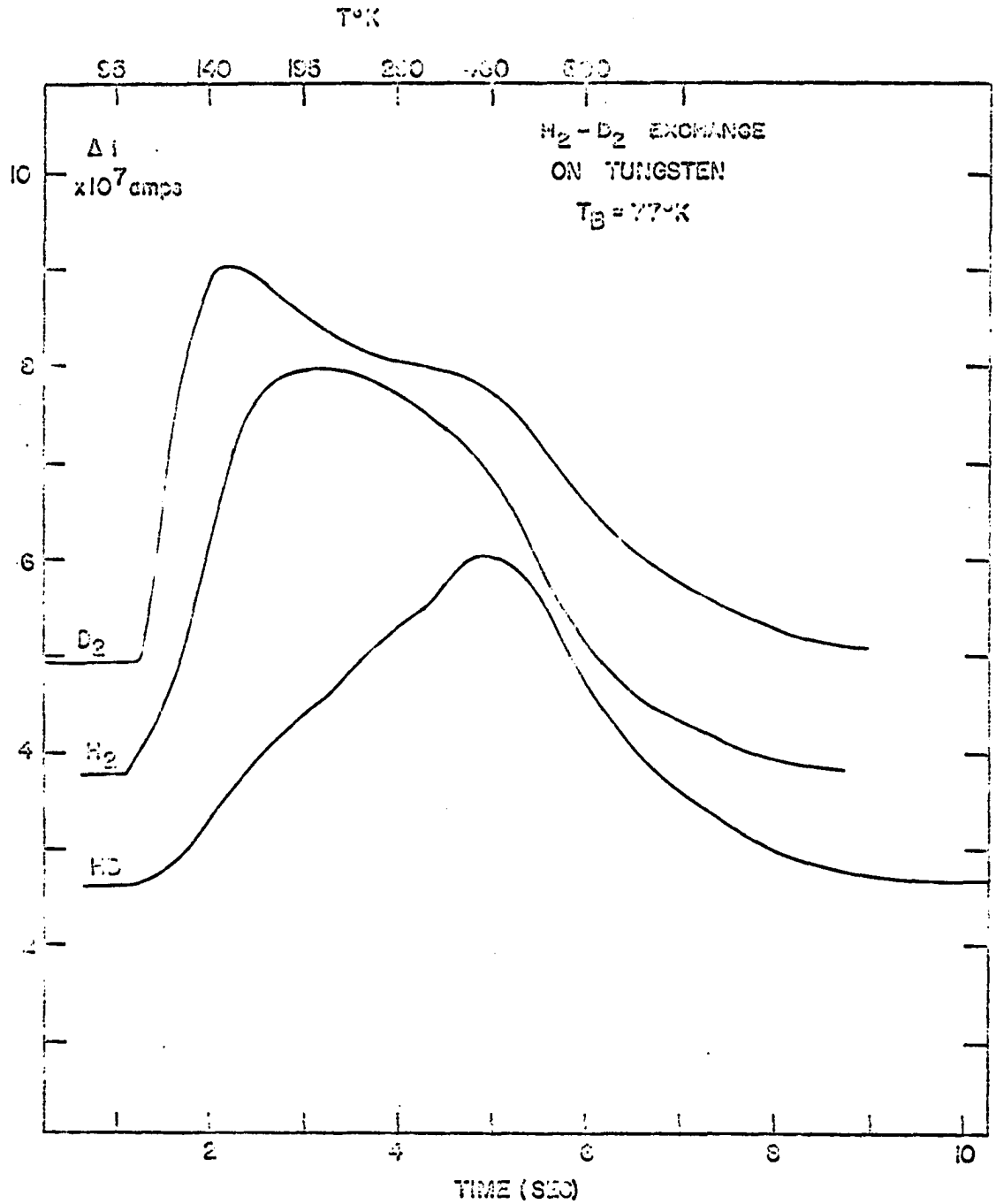

Figure 28. Desorption spectra of the hydrogen isotopes from tungsten dosed at 100°K with a mixture of H_2 and D_2

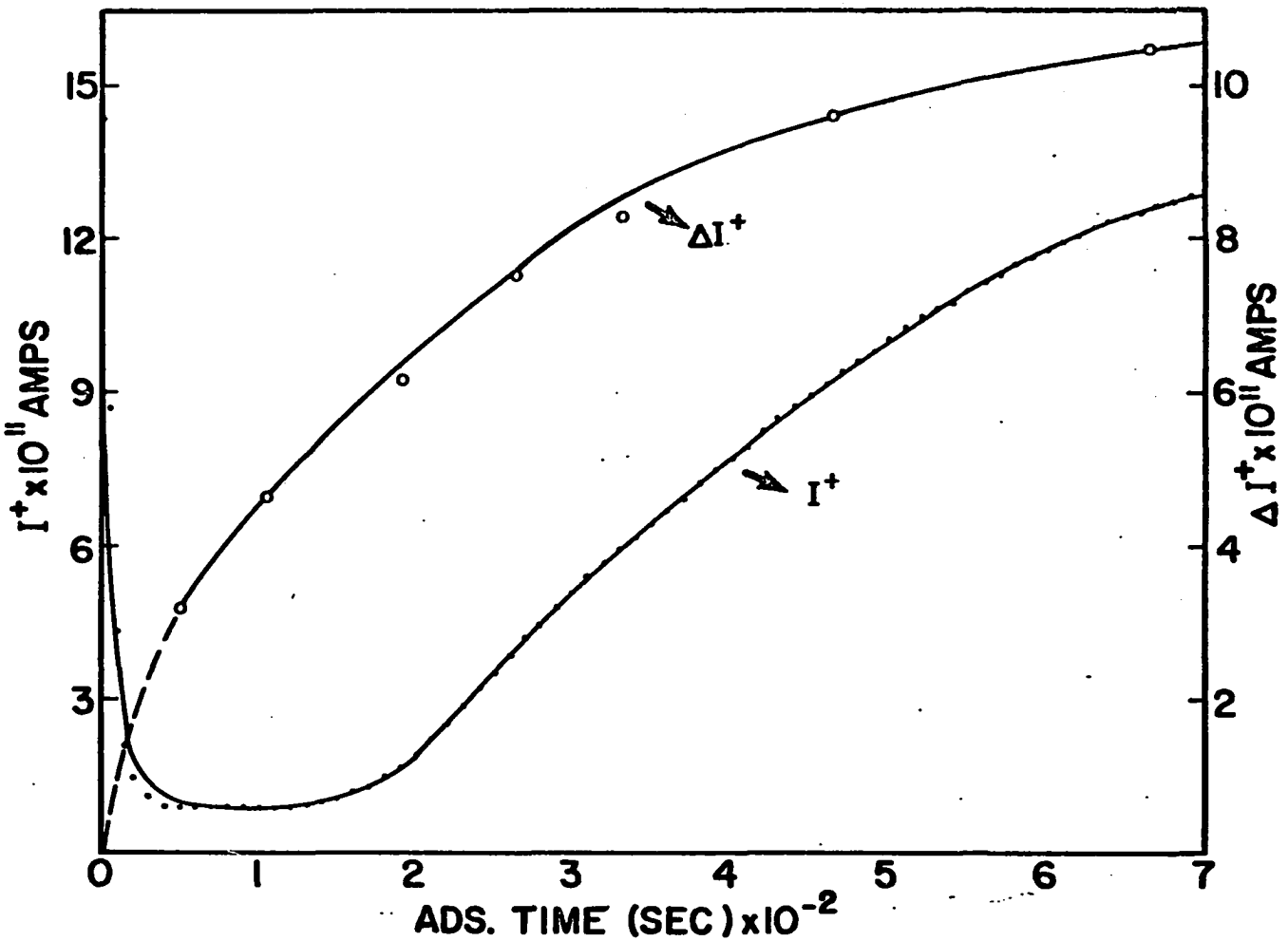

Figure 29. Variation of nitrogen sticking probability (s) with surface coverage, where $s = 0.22 \frac{1}{I} \frac{d\Delta I}{dt}$, ΔI is the change in ion current after indicated adsorption times

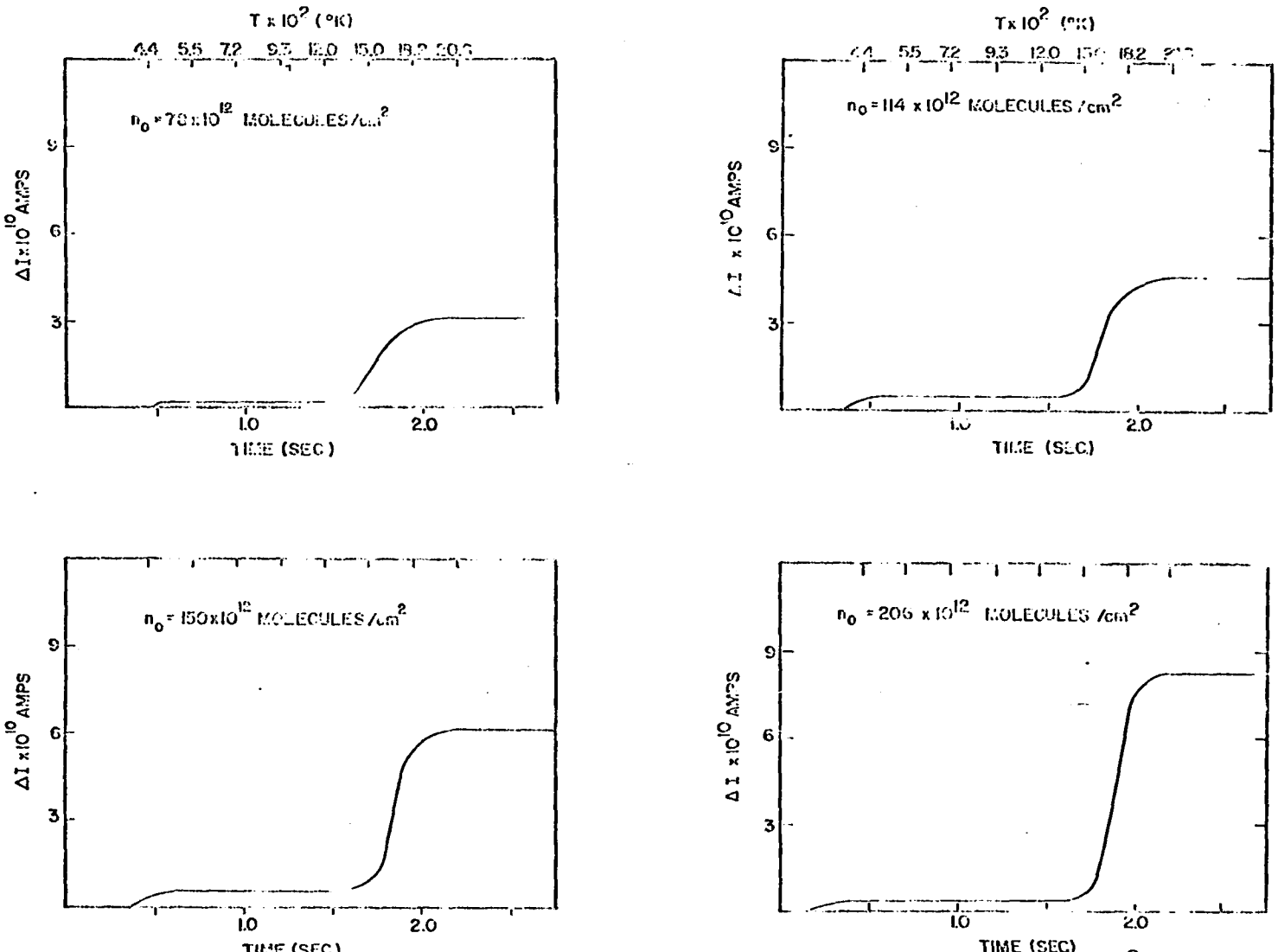

Figure 30. Flash desorption of nitrogen from tungsten dosed at 300°K

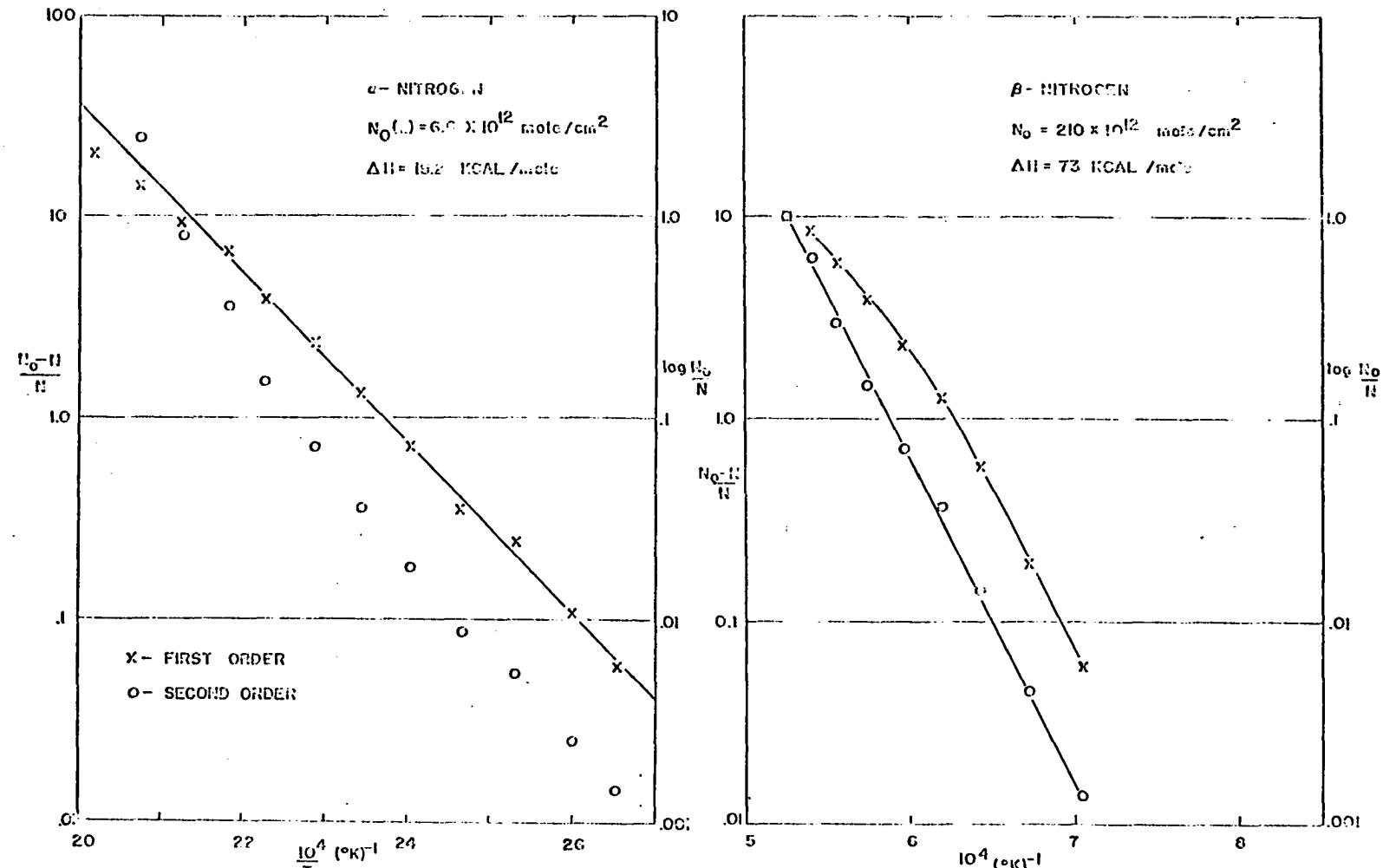

Figure 31. Kinetic analysis of the pressure-temperature data for α- and β-nitrogen

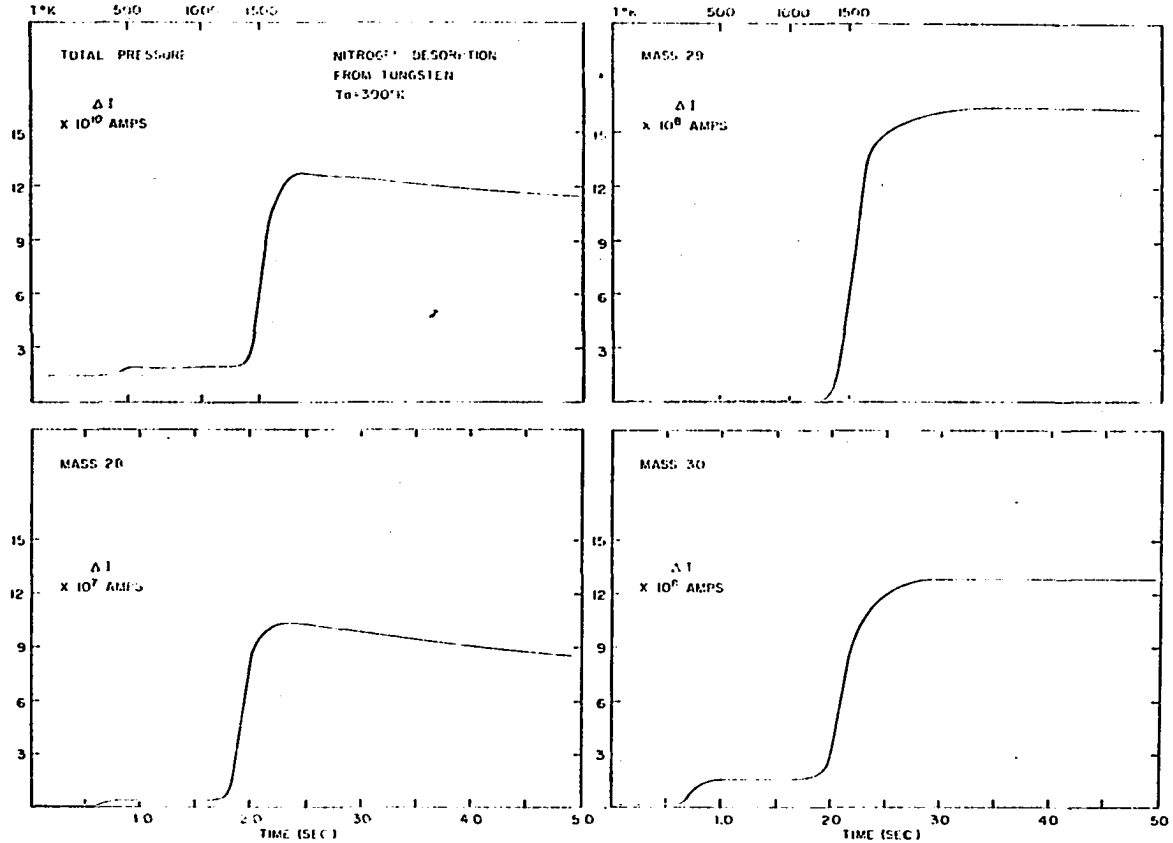

Figure 32. Flash desorption of nitrogen isotopes from tungsten dosed at 300°K with a mixture of $^{14}N_2$ and $^{15}N_2$

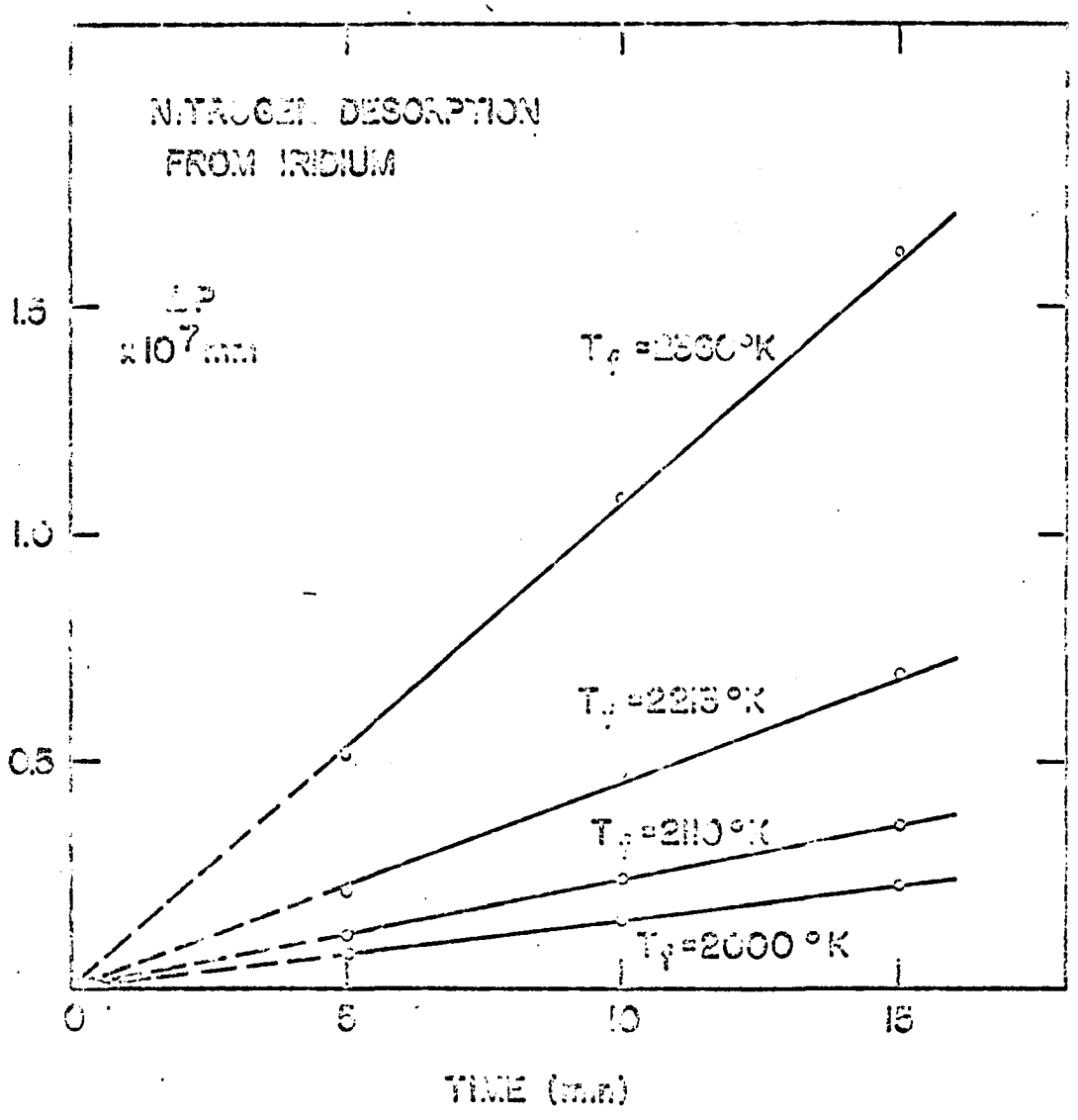

Figure 53. Desorption of nitrogen from iridium as a function of dosing time and temperature of the ion gauge filament

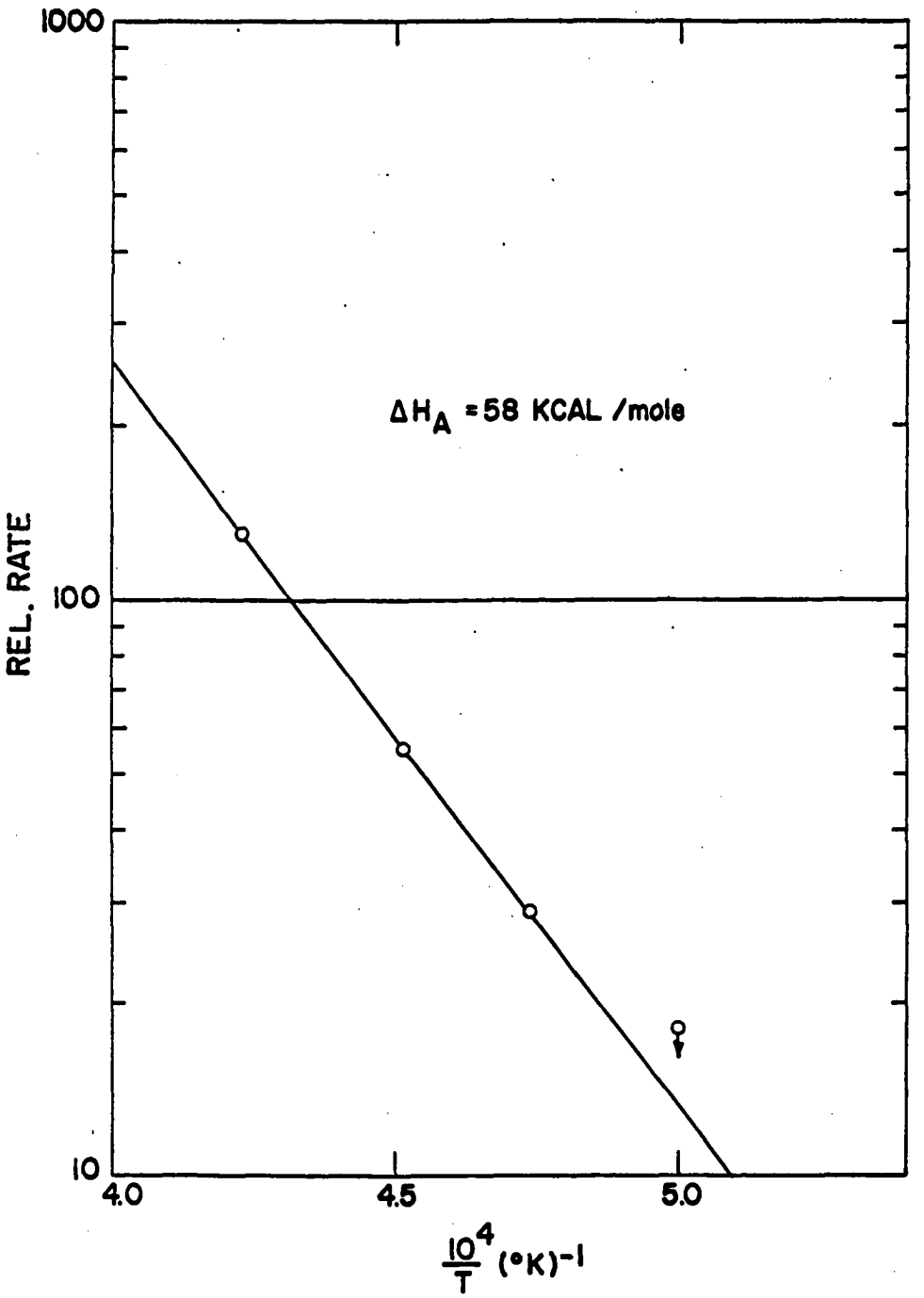

Figure 34. Dependence of rate of adsorption of activated nitrogen on iridium on the temperature of the activating source

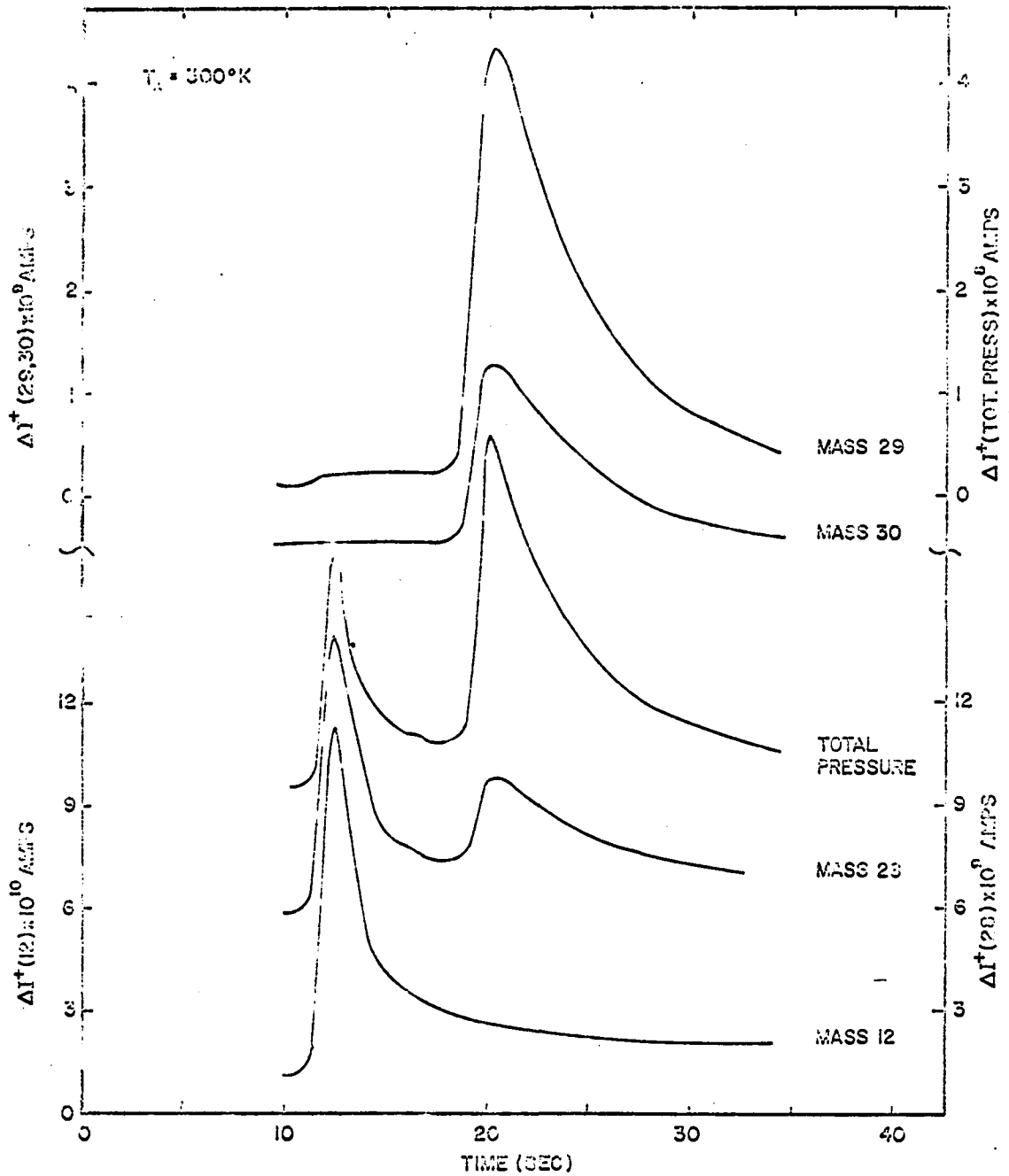

Figure 35. Desorption of nitrogen isotopes from rhodium dosed at 300°K with a mixture of $^{14}N_2$ and $^{15}N_2$

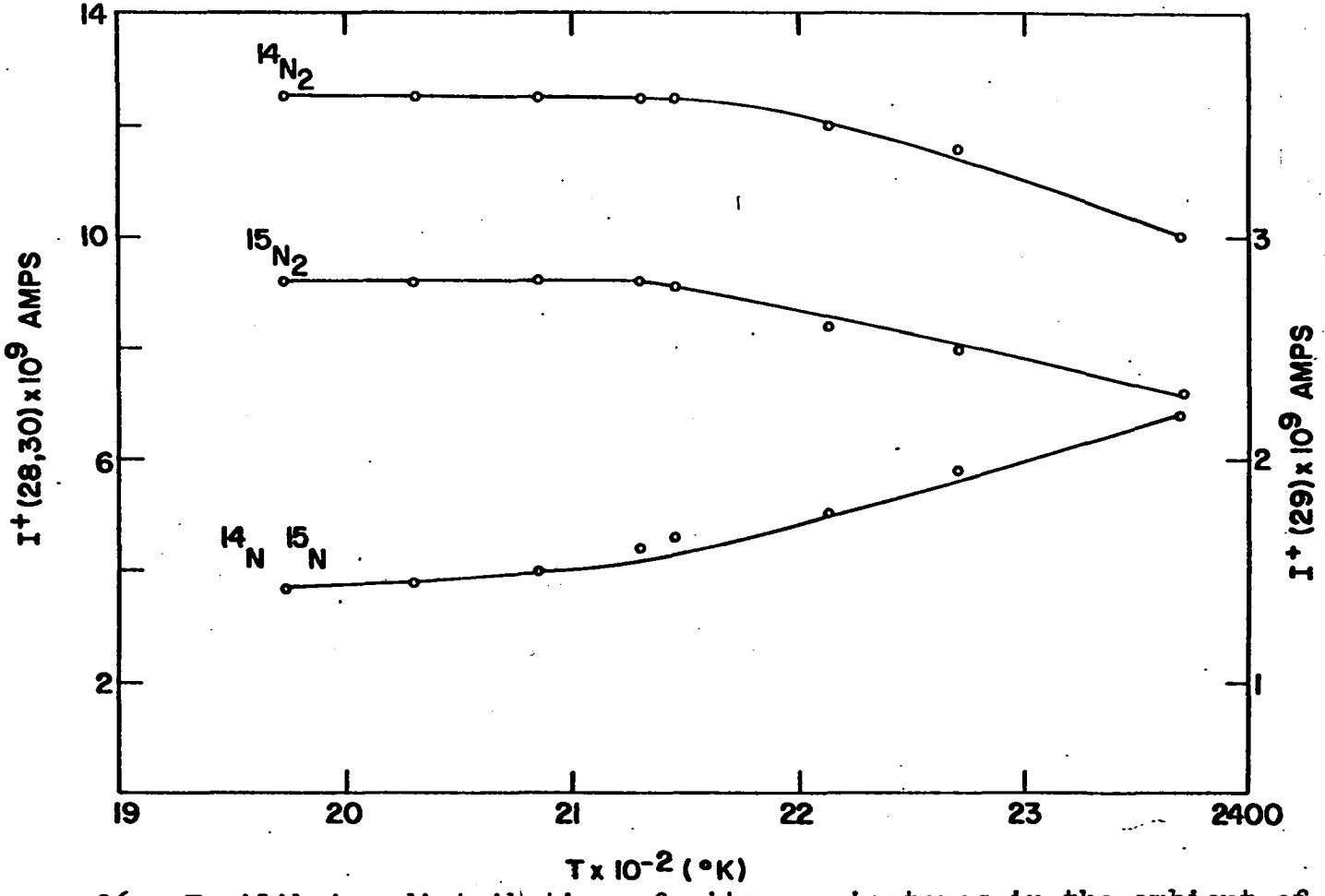

Figure 36. Equilibrium distribution of nitrogen isotopes in the ambient of a flow system as a function of the temperature of the ion gauge filament

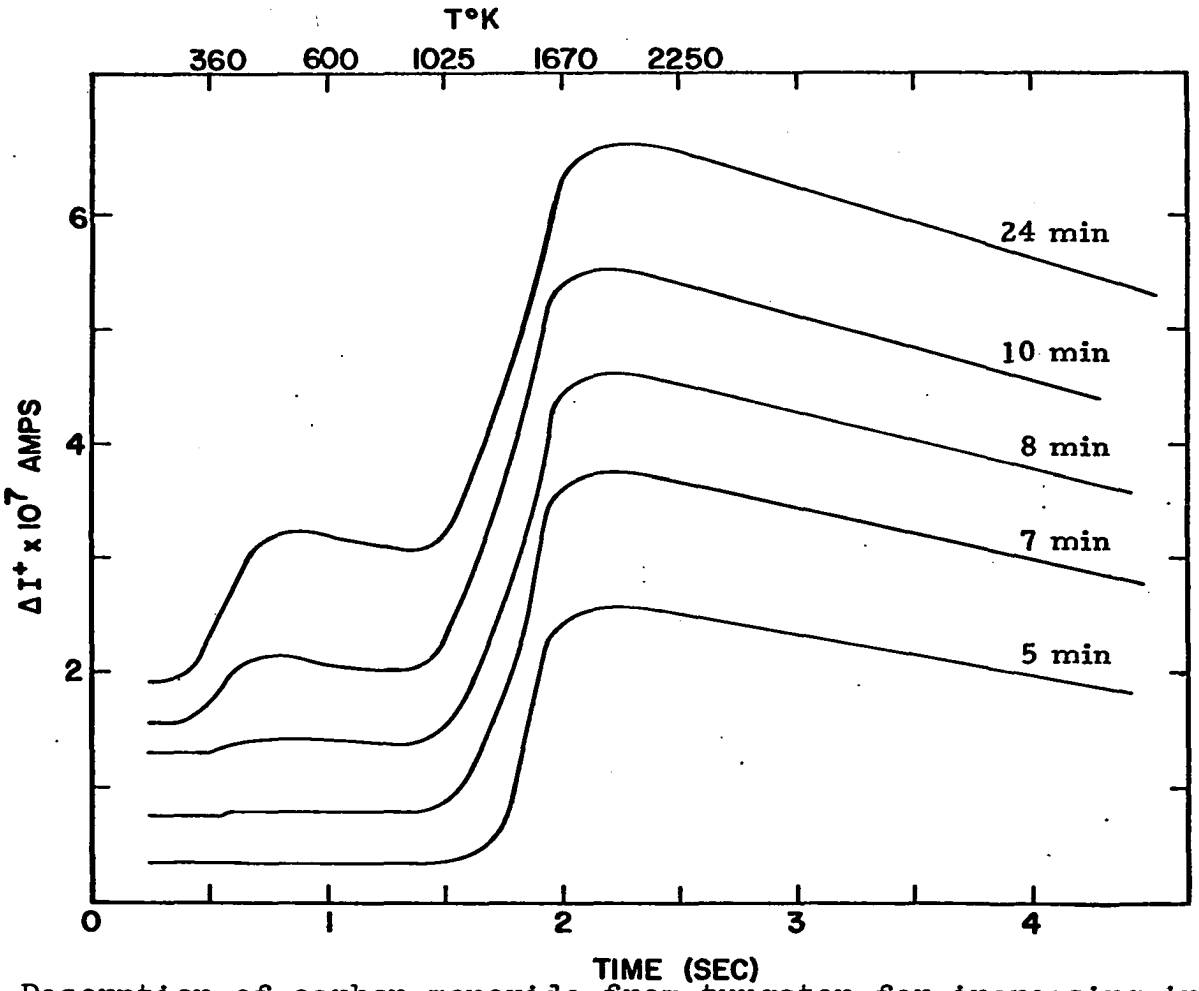

Figure 37. Desorption of carbon monoxide from tungsten for increasing initial doses at 300°K

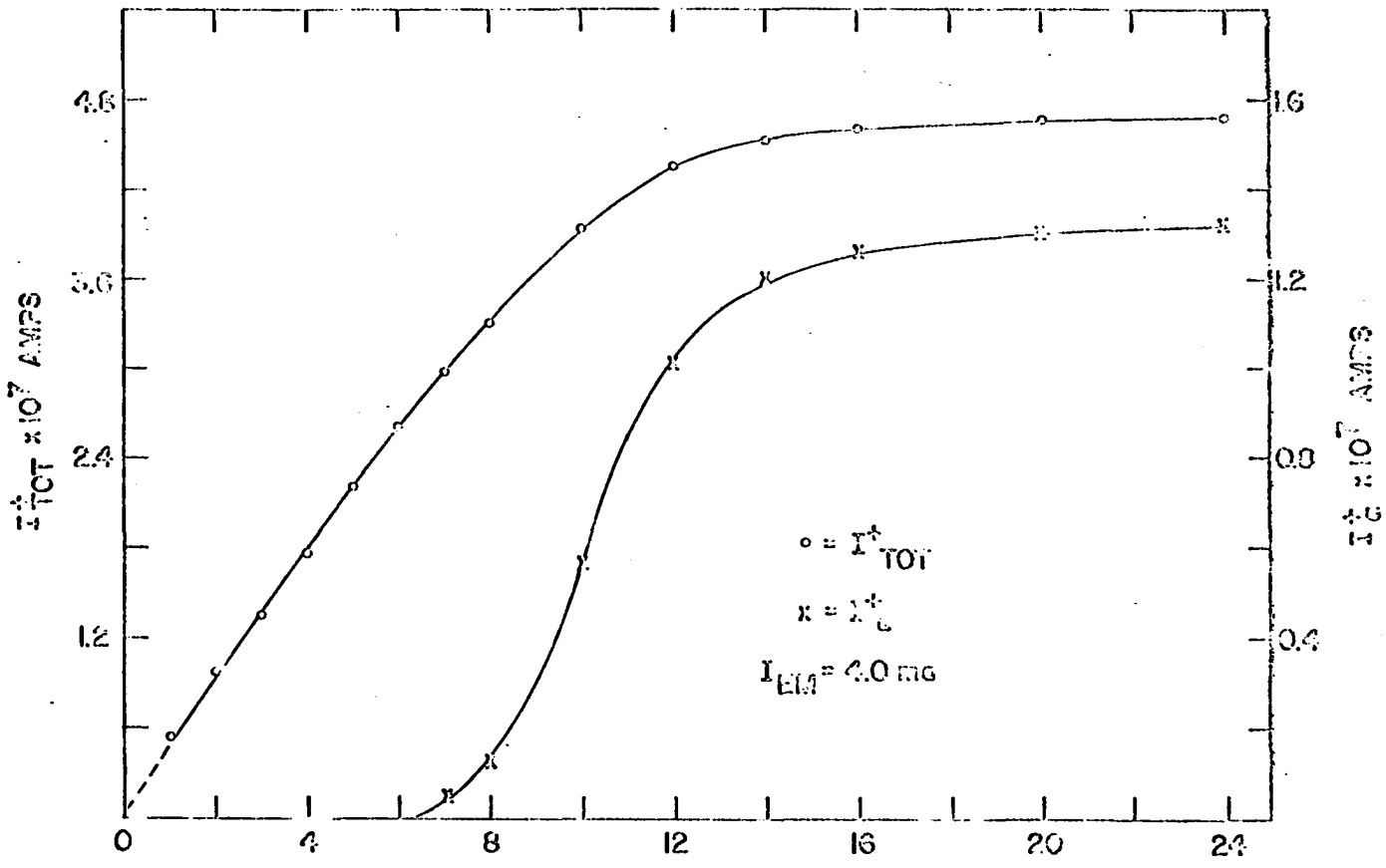

Figure 38. Dependence of α_{CO} on the amount of β_{CO} adsorbed

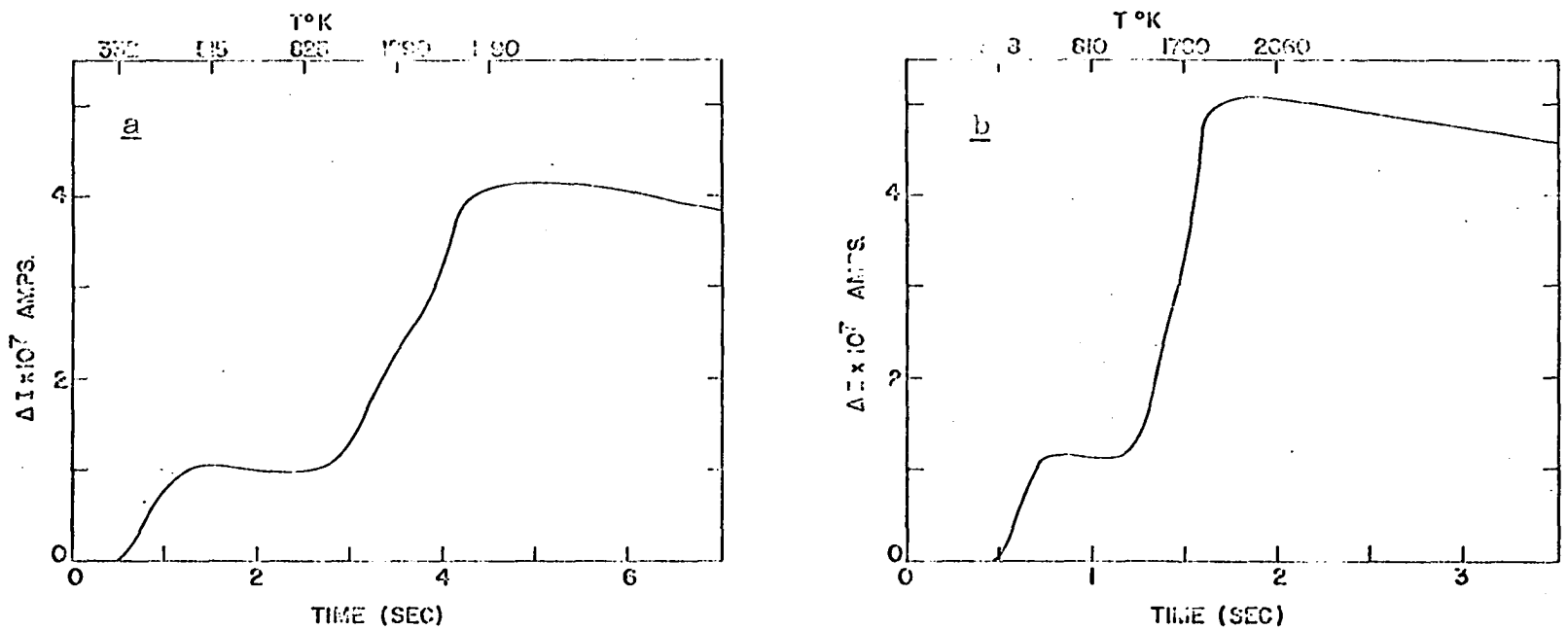

Figure 39. Desorption of carbon monoxide from tungsten. a. Heating rate 320°K/sec. b. Heating rate 1380°K/sec

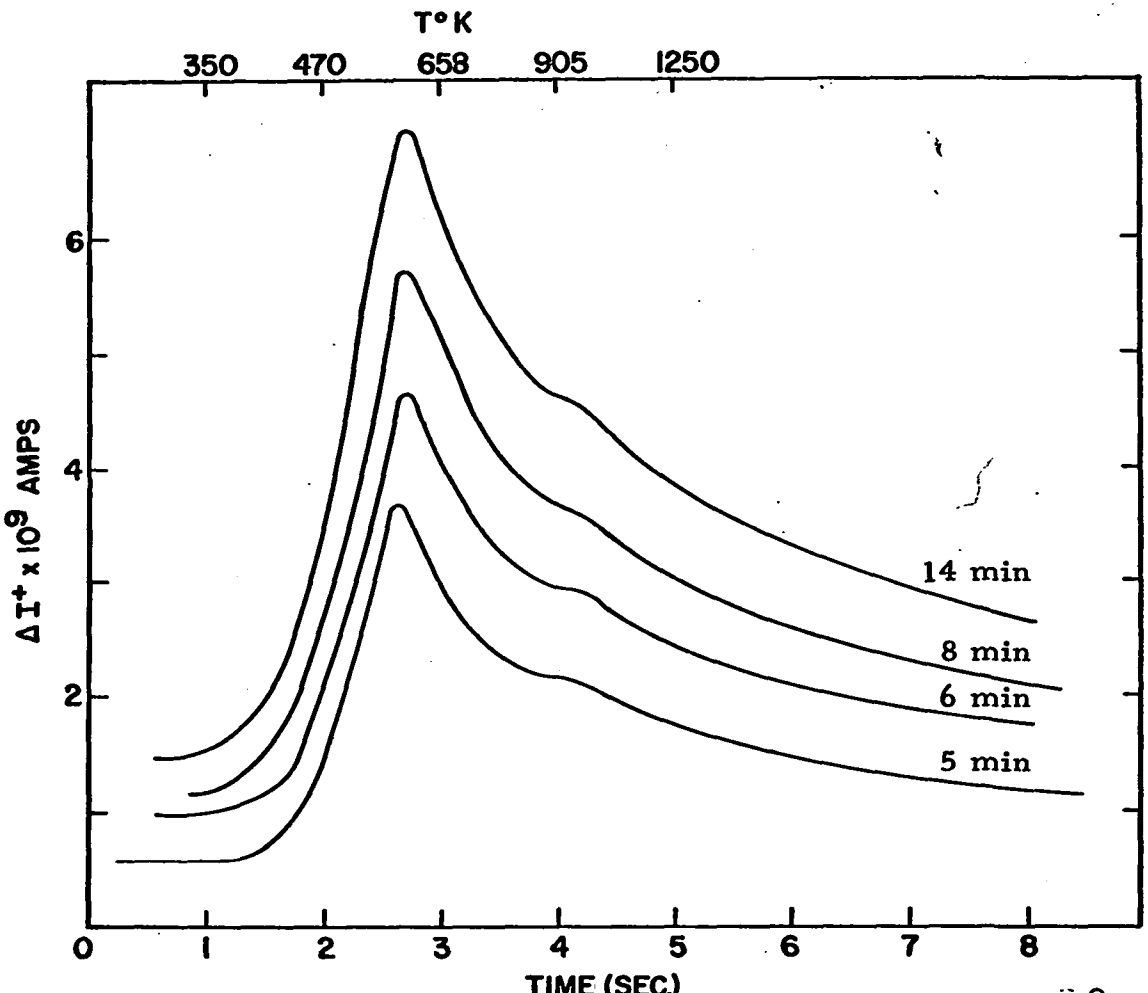

Figure 40. Desorption of carbon monoxide from rhodium dosed at 300°K

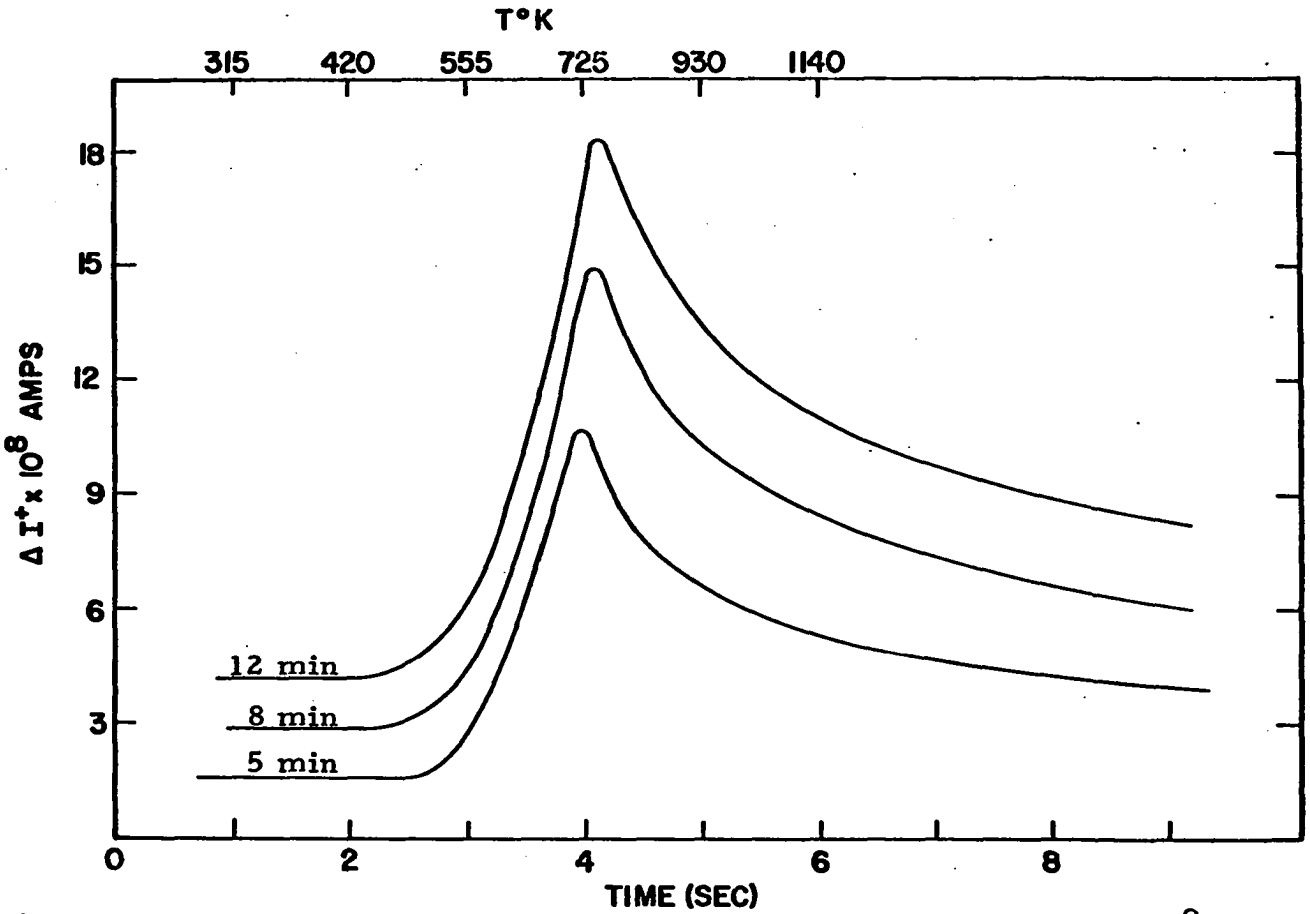

Figure 41. Desorption of carbon monoxide from iridium dosed at 300°K

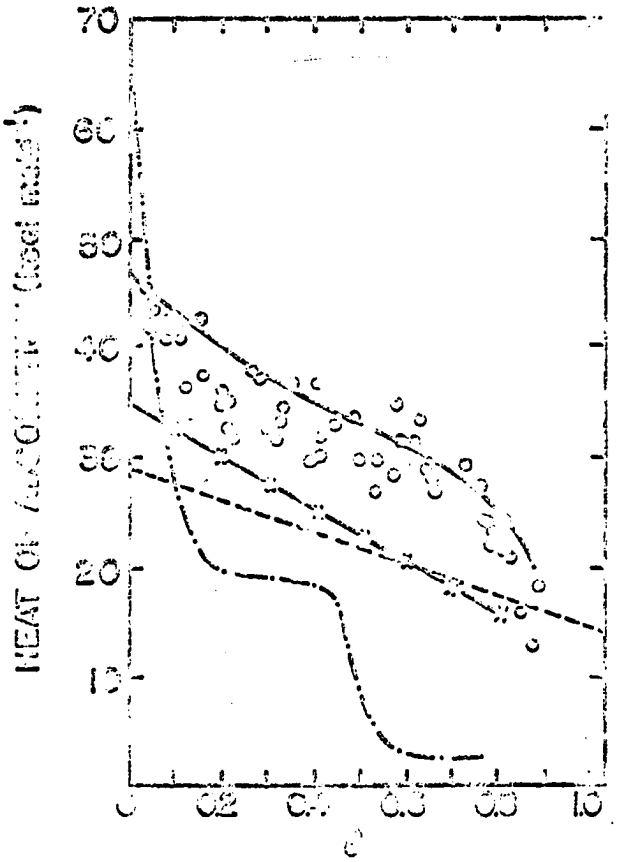

Figure 42. Variation of the heat of adsorption with surface coverage. ----- Hickmott (11), ——— Brennan and Hayes (58), o Beeck (66), —·—·—·— Gomer (55), ° Wabba and Kembal (77) —x—x—x present work

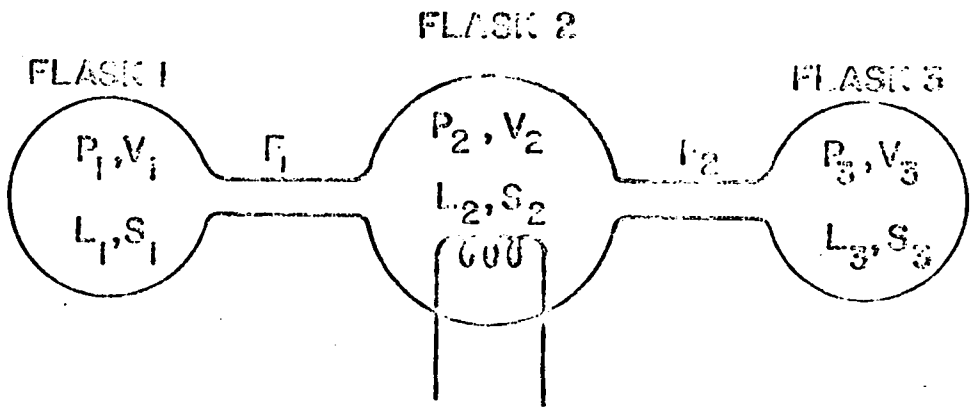

Figure 43. Schematic diagram of flash filament apparatus

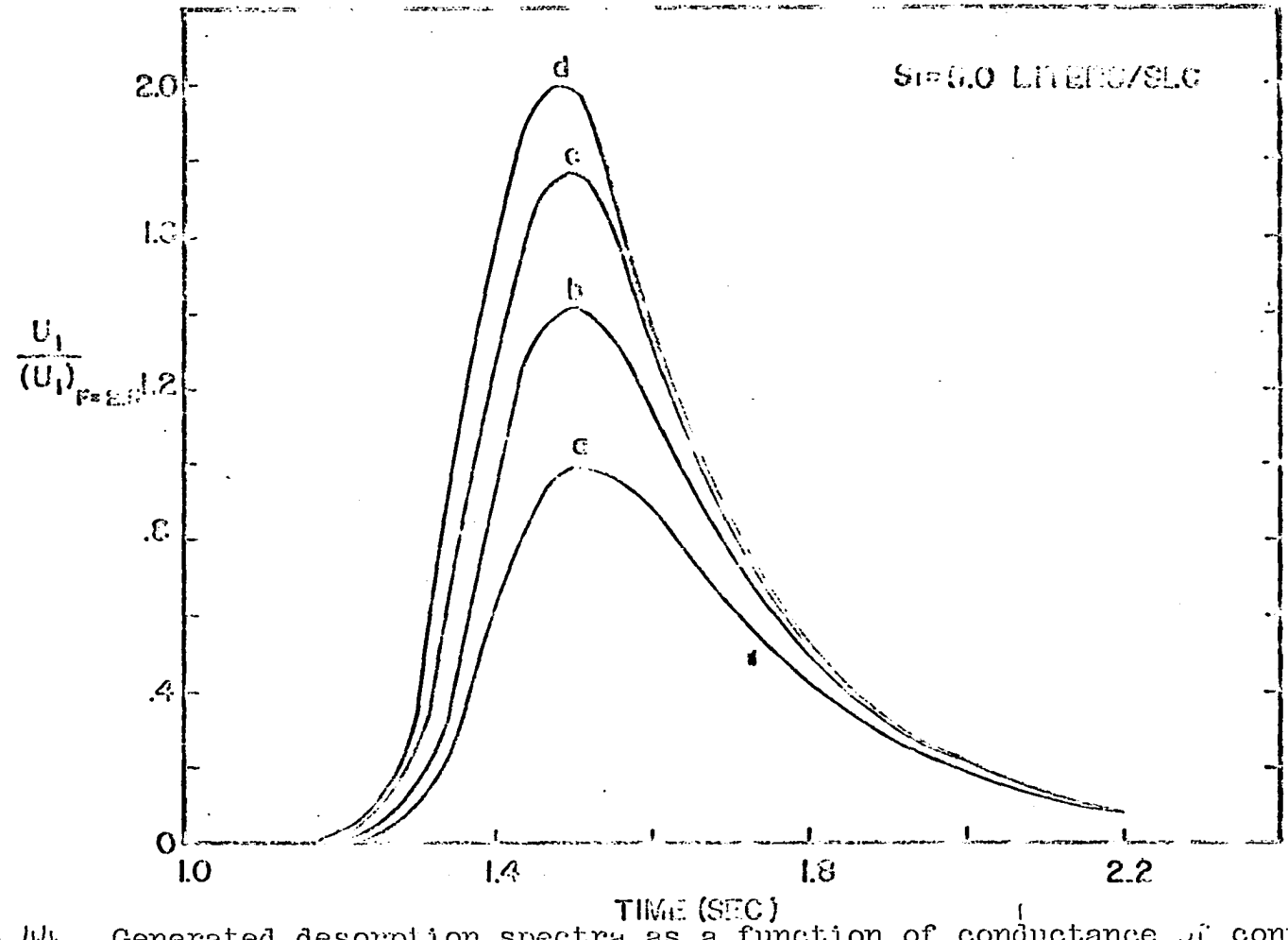

Figure 44. Generated desorption spectra as a function of conductance of connecting tubulation. a. F = 2.5 liters/sec, b. F = 5.0 liters/sec, c. F = 10 liters/sec, d. F = 20 liters/sec

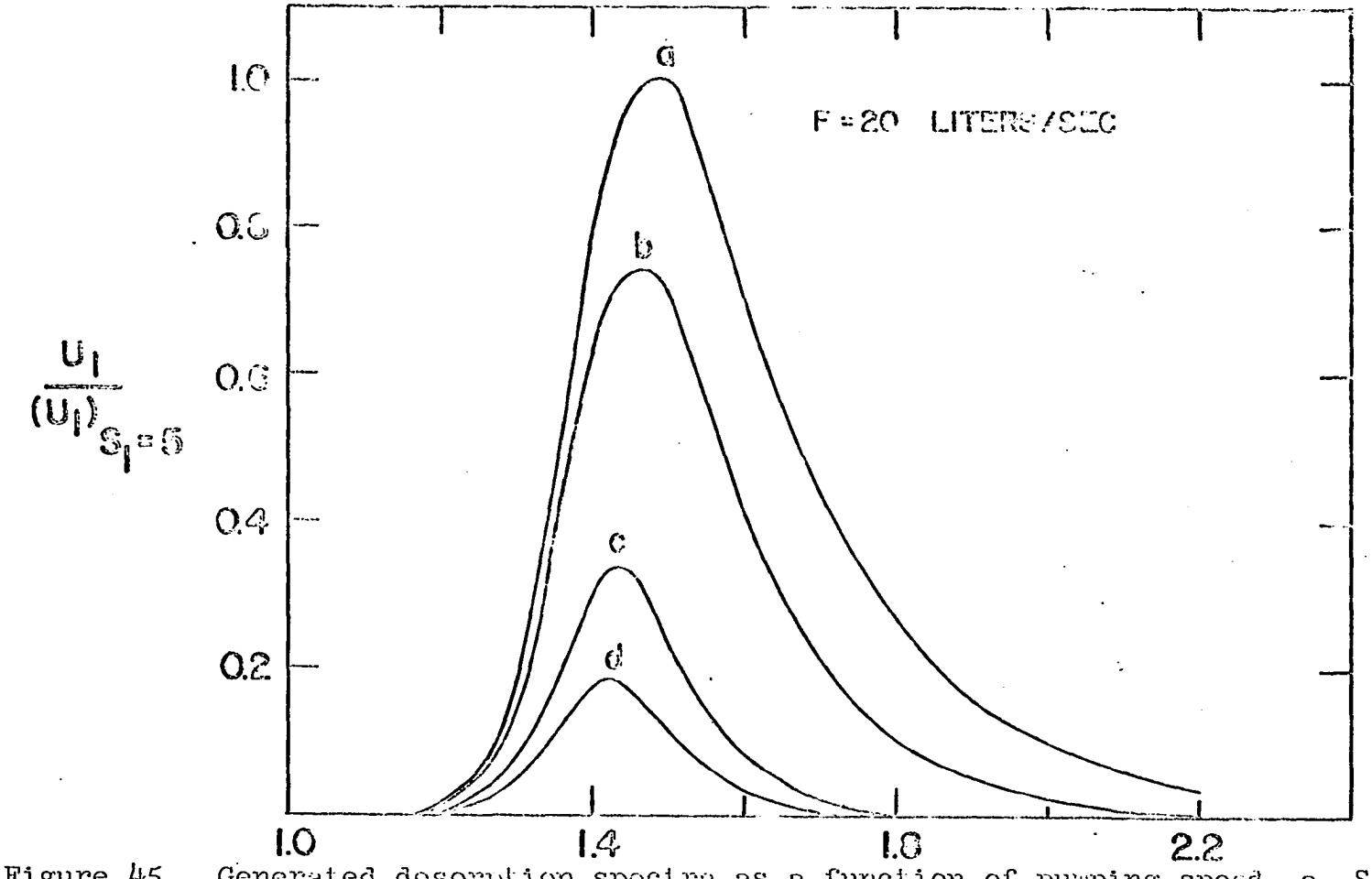

Figure 45. Generated desorption spectra as a function of pumping speed, a. S_1 = 5 liters/sec, b. S_1 = 10 liters/sec, c. S_1 = 40 liters/sec, d. S_1 = 80 liters/sec

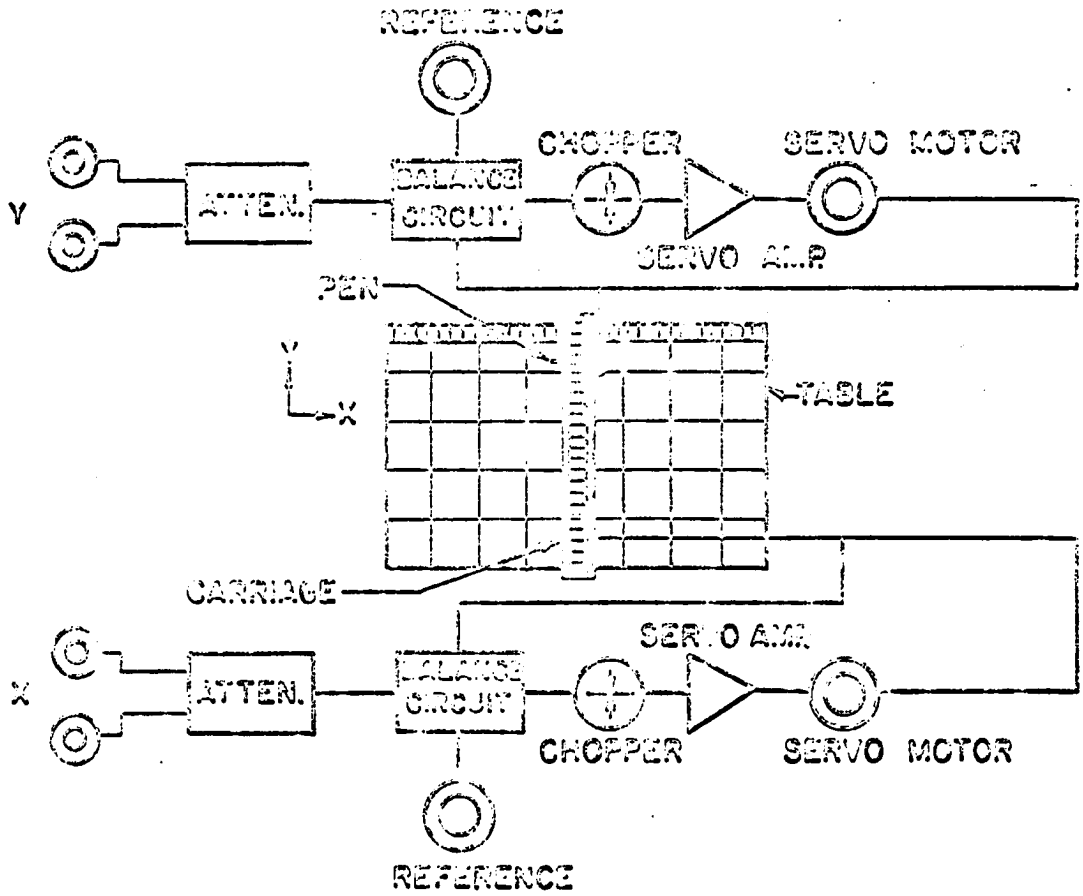

Figure 46. Block diagram of recording system

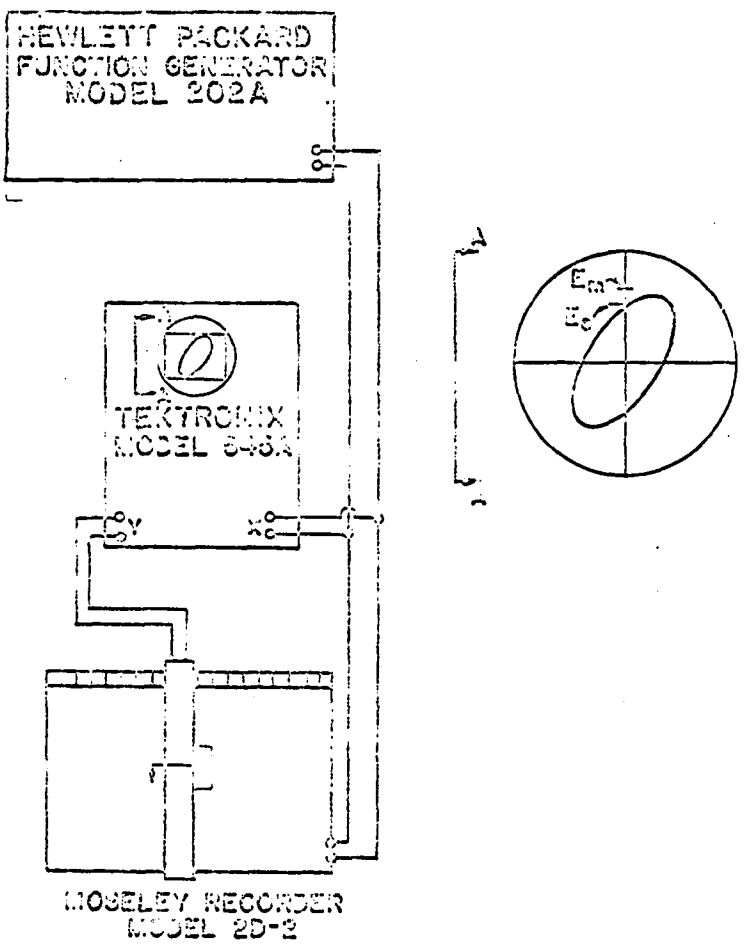

Figure 47. Schematic diagram for measuring the phase lag of the recorder

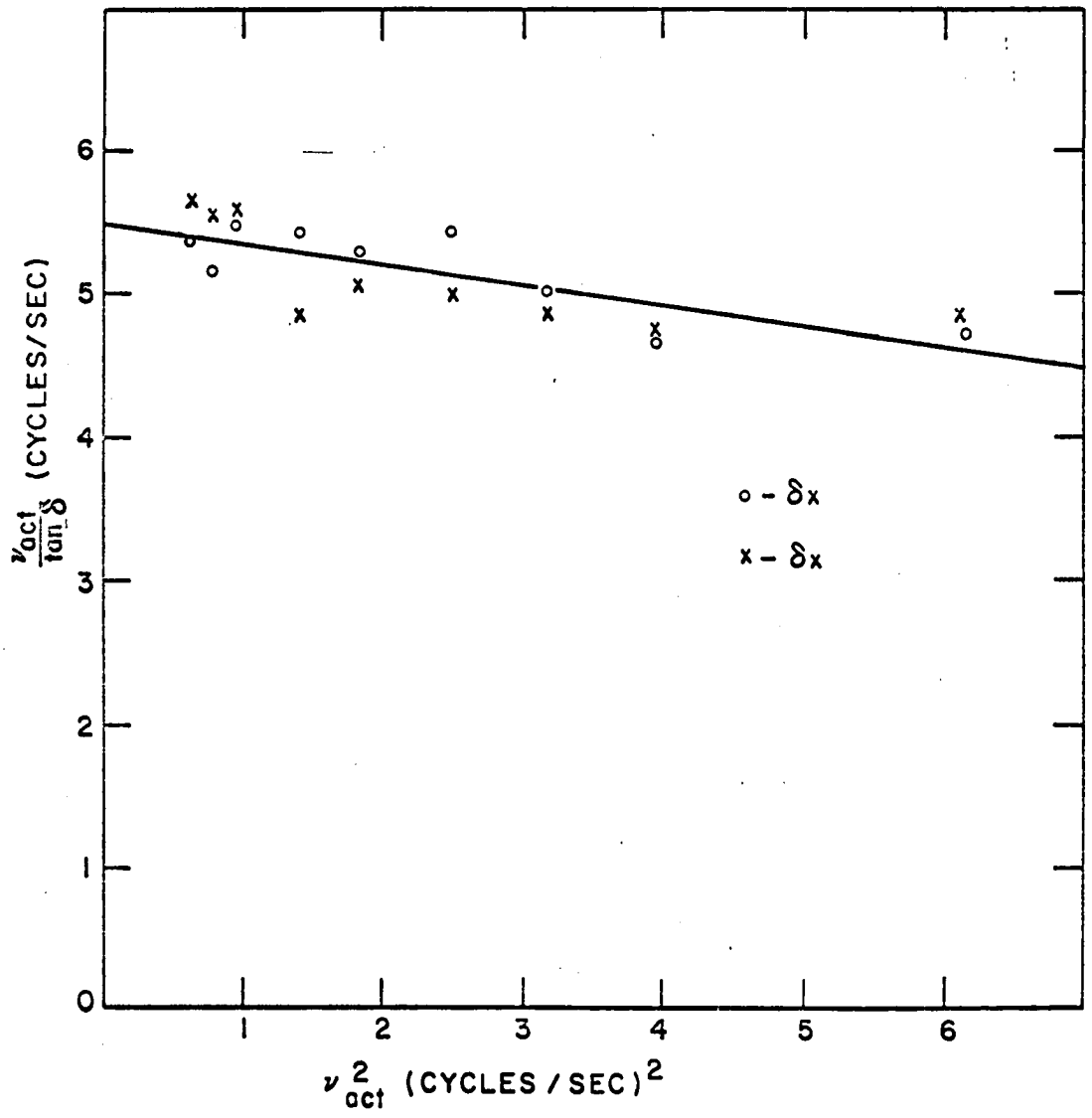

Figure 48. Recorder response as a function of frequency

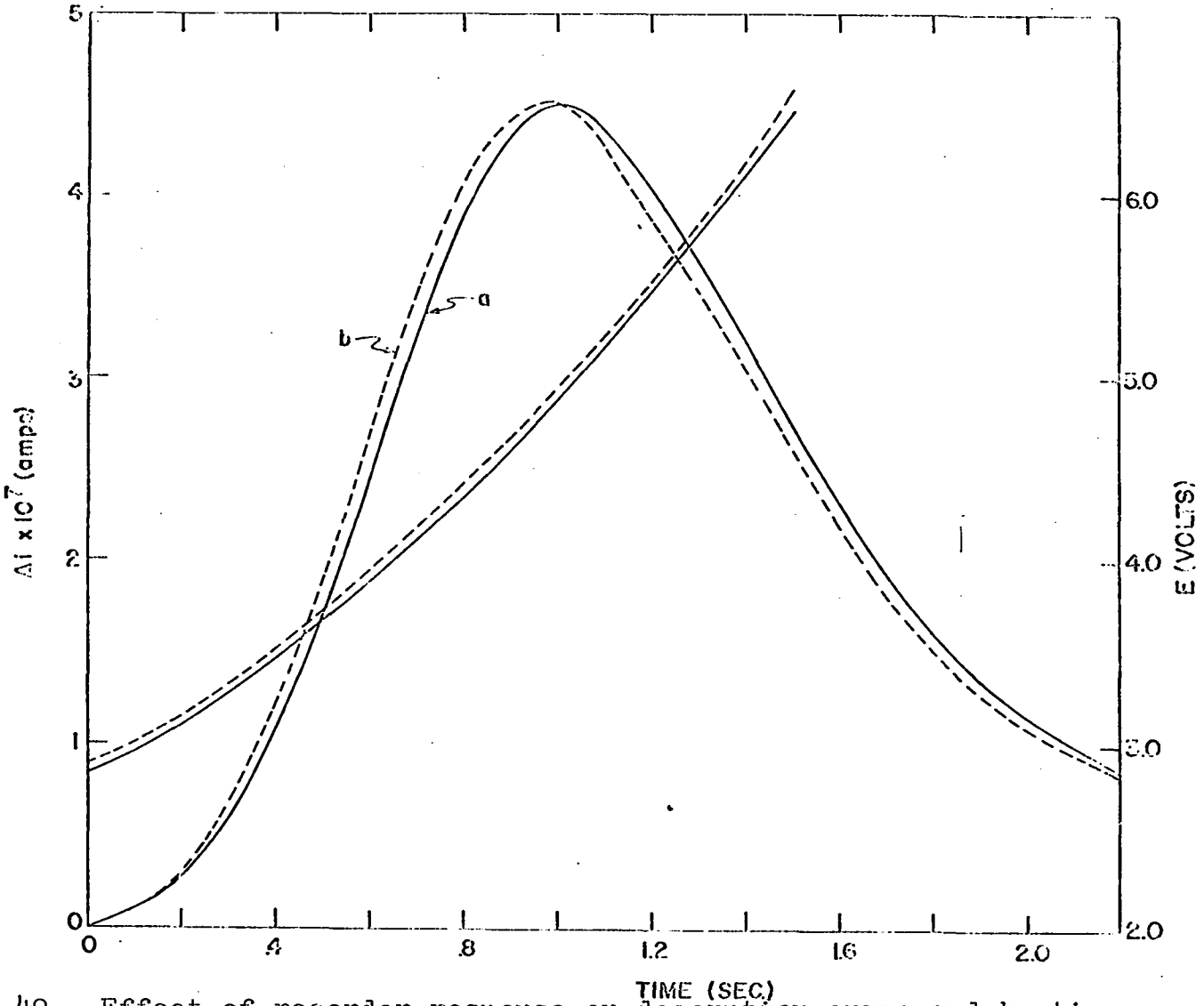

Figure 49. Effect of recorder response on desorption curve and heating curve

X. TABLES

Table 1. Effect of heating rate on pumping term S/V

Heating Current amps	Heating Rate deg/sec	S/V [a] $(sec)^{-1}$	S/V [b] $(sec)^{-1}$
0.8	215	0.89	0.31
0.9	292	0.98	0.32
1.0	380	1.09	0.32
1.1	445	1.18	0.30
1.2	525	1.26	0.29

[a] Nottingham ion gauge operating at 4 ma (2270°K).

[b] Nottingham ion gauge off.

Table 2. Distribution of hydrogen isotopes in the desorbed products from sample filaments dosed at 300°K with a mixture of hydrogen and deuterium

Sample	Adsorption Interval	Ambient Distribution	Product Distribution
Rhodium	4 min.	1.00:2.26:1.28 [a]	1.00:1.54:0.63 [a]
	—	1.00:1.16:1.12 [b]	1.00:1.31:0.64 [b]
	10 min.	1.00:2.23:1.25 [a]	1.00:1.48:0.55 [a]
		1.00:1.14:1.18 [b]	1.00:1.32:0.58 [b]
Iridium	3 min.	1.00:2.24:1.39 [a]	1.00:2.09:1.09 [a]
		1.00:0.83:1.19 [b]	1.00:1.77:1.08 [b]
	6 min.	1.00:2.32:1.60 [a]	1.00:2.08:1.15 [a]
		1.00:0.80:1.37 [b]	1.00:1.75:1.12 [b]
Tungsten	5 min.	1.00:0.60:0.09 [a]	1.00:0.68:0.12 [a]
		1.00:0.23:0.22 [b]	1.00:0.68:0.12 [b]
	10 min.	1.00:0.55:0.05 [a]	1.00:0.65:0.11 [a]
		1.00:0.10:0.24 [b]	1.00:0.61:0.12 [b]

[a] Statistical distribution.

[b] Observed distribution.

Table 3. Distribution of hydrogen isotopes in the desorbed products from an iridium filament dosed at 100°K with a mixture of hydrogen and deuterium

Adsorption Interval	Ambient Distribution	Product Distribution α-peak	β-peak
2 min.	1.00:2.09:1.09[a]		1.00:2.40:1.54[a]
	1.00:0.04:1.04[b]		1.00:1.91:1.44[b]
4 min.	1.00:2.16:1.16[a]	1.00:2.53:1.70[a]	1.00:2.44:1.59[a]
	1.00:0.03:1.08[b]	1.00:2.21:1.62[b]	1.00:2.12:1.52[b]
6 min.	1.00:2.12:1.12[a]	1.00:2.58:1.77[a]	1.00:2.53:1.71[a]
	1.00:0.03:1.06[b]	1.00:2.17:1.66[b]	1.00:2.14:1.62[b]
10 min.	1.00:2.14:1.25[a]	1.00:2.66:1.89[a]	1.00:2.64:1.86[a]
	1.00:0.04:1.07[b]	1.00:2.17:1.75[b]	1.00:2.20:1.73[b]

[a] Statistical distribution.

[b] Observed distribution.

Table 4. Distribution of hydrogen isotopes in the desorbed products from a rhodium filament dosed at 100°K with a mixture of hydrogen and deuterium

Adsorption Interval	Ambient Distribution	Product Distribution α-peak	Product Distribution β-peak
4 min.	1.00:1.70:0.73 [a]	1.00:2.52:1.69 [a]	1.00:2.33:1.45 [a]
	1.00:0.13:0.84 [b]	1.00:3.47:2.50 [b]	1.00:2.49:1.48 [b]
10 min.	1.00:1.63:0.67 [a]	1.00:3.06:2.49 [a]	1.00:2.33:1.45 [a]
	1.00:0.08:0.81 [b]	1.00:3.44:2.63 [b]	1.00:2.45:1.47 [b]
15 min.	1.00:1.66:0.69 [a]	1.00:3.16:2.66 [a]	1.00:2.39:1.53 [a]
	1.00:0.09:0.82 [b]	1.00:3.99:3.00 [b]	1.00:2.70:1.59 [b]

[a] Statistical distribution.

[b] Observed distribution.

Table 5. Effect of tube conductance and pumping speed on the relaxation parameters β_1, β_2 and β_3

	F (liters/sec)			
	2.5	5.0	10.0	20.0
S_1 = 5.0 liters/sec				
β_1	4.12	4.54	4.83	4.99
β_2	14.50	21.42	34.77	61.62
β_3	18.48	33.64	65.01	127.98
S_1 = 10 liters/sec				
β_1	4.51	5.47	6.43	7.15
β_2	16.74	28.54	42.56	69.08
β_3	25.85	35.59	65.62	128.37
S_1 = 20 liters/sec				
β_1	4.73	6.16	8.09	10.14
β_2	17.02	31.93	56.53	84.85
β_3	45.35	51.51	69.98	129.62
S_1 = 40 liters/sec				
β_1	4.84	6.57	9.38	13.30
β_2	17.10	32.37	62.35	112.44
β_3	85.16	90.66	102.87	138.86
S_1 = 80 liters/sec				
β_1	4.89	6.79	10.17	15.79
β_2	17.13	32.49	63.12	123.21
β_3	165.08	170.32	181.30	205.60

Table 6. Phase lag of the x-y recorder as a function of frequency

ν $\frac{\text{cycles}}{\text{sec}}$	ν_{act} $\frac{\text{cycles}}{\text{sec}}$	$\sin\delta_x$	δ_x deg	$\sin\delta_y$	δ_y deg	$\frac{\nu_{act}}{\tan\delta_x}$	$\frac{\nu_{act}}{\tan\delta_y}$
0.8	0.787	0.144	8.30	0.138	7.93	5.39	5.66
0.9	0.885	0.169	9.75	0.157	9.03	5.14	5.56
1.0	0.983	0.177	10.20	0.173	10.00	5.46	5.58
1.2	1.189	0.210	12.13	0.234	13.53	5.53	4.83
1.4	1.387	0.254	14.70	0.263	15.25	5.29	5.08
1.6	1.591	0.282	16.40	0.305	17.75	5.41	4.97
1.8	1.787	0.336	19.63	0.347	20.30	5.00	4.83
2.0	1.935	0.394	23.20	0.389	22.90	4.63	4.71
2.5	2.479	0.466	27.80	0.468	27.25	4.70	4.82

XI. BIBLIOGRAPHY

1. Apker, L. R. Industrial and Engineering Chemistry. 40: 846. 1948.

2. Becker, J. A. and Hartman, C. D. Journal of Physical Chemistry. 57:153. 1953.

3. Bayard, R. T. and Albert, D. Review of Scientific Instruments. 21:571. 1950.

4. Becker, J. A. Solid State Physics. 7:379. 1958.

5. Kisliuk, P. Journal of Physics and Chemistry of Solids. 3:95. 1957.

6. Kisliuk, P. Journal of Physics and Chemistry of Solids. 5:78. 1958.

7. Ehrlich, G. Journal of Physical Chemistry. 60:1388. 1956.

8. Ehrlich, G. Journal of Chemical Physics. 34:29. 1961.

9. Kisliuk, P. Journal of Chemical Physics. 30:174. 1959.

10. Hickmott, T. W. and Ehrlich, G. Journal of Physics and Chemistry of Solids. 5:47. 1958.

11. Hickmott, T. W. Journal of Chemical Physics. 32:810. 1960.

12. Hickmott, T. W. Journal of Applied Physics. 31:128. 1960.

13. Becker, J. A., Becker, E. J. and Brandes, R. G. Journal of Applied Physics. 32:411. 1961.

14. Eisinger, J. Journal of Chemical Physics. 29:1154. 1958.

15. Eisinger, J. Journal of Chemical Physics. 30:412. 1959.

16. Redhead, P. A. Transactions of the Faraday Society. 57: 641. 1961.

17. Ehrlich, G. Journal of Chemical Physics. 34:39. 1961.

18. Pasternak, R. A. and Weisendanger, H. U. D. Journal of Chemical Physics. 34:2062. 1961.

19. Moore, G. E. and Unterwald, F. C. Journal of Chemical Physics. 40:2626. 1964.

20. Arthur, J. R. A study of surface reactions by field emission microscopy. Unpublished Ph.D. thesis. Ames, Iowa, Library, Iowa State University of Science and Technology. 1961.

21. Arthur, J. R. and Hansen, R. S. Journal of Chemical Physics. 36:2062. 1962.

22. Harvey, J. C. Decomposition of methylacetylene on a rhodium filament. Unpublished M.S. thesis. Ames, Iowa, Library, Iowa State University of Science and Technology. 1964.

23. Weisendanger, H. U. D. Journal of Catalysis. 2:538. 1963.

24. Madey, T. E., Yates, J. T., Jr., and Stern, R. C. Journal of Chemical Physics. 42:1372. 1965.

25. Yates, J. T., Jr., and Madey, T. E. Journal of Chemical Physics. 43:1055. 1965.

26. Moore, G. E. and Unterwald, F. C. Bulletin of the American Physical Society. 10: 395. 1965.

27. Rigby, L. J. Canadian Journal of Physics. 43:532. 1965.

28. Rigby, L. J. Canadian Journal of Physics. 43:1020. 1965.

29. Ricca, F., Medana, R. and Saini, G. Transactions of Faraday Society. 61:1492. 1965.

30. Delchar, T. A. and Ehrlich, G. Journal of Chemical Physics. 42:2686. 1965.

31. Smith, A. W. and Aranoff, S. Journal of Physical Chemistry. 62:684. 1958.

32. Ehrlich, G. Journal of Applied Physics. 32:4. 1961.

33. Ehrlich, G. Advances in Catalysis. 14:255. 1963.

34. Redhead, P. A. Vacuum. 12:203. 1962.

35. Carter, G. Vacuum. 12:245. 1962.

36. Carter, G. Vacuum. 13:89. 1963.

37. Alpert, D. Journal of Applied Physics. 24:860. 1953.

38. Venema, A. Vacuum. 9:54. 1959.

39. Sommer, H., Thomas, H. A. and Hipple, J. A. Physics Review. 82:697. 1951.

40. Alpert, D. and Buritz, R. S. Journal of Applied Physics. 25:202. 1954.

41. Todd, B. J. Journal of Applied Physics. 26:1238. 1955.

42. Todd, B. J. Journal of Applied Physics. 27:1209. 1956.

43. Redhead, P. A. Canadian Journal of Physics. 37:1260. 1959.

44. Nottingham, W. B. Vacuum Symposium, Committee on Vacuum Techniques, Boston, Transactions 1954:76. 1954.

45. Redhead, P. A. Review of Scientific Instruments. 31: 343. 1960.

46. Torney, F. L. and Feakes, F. Review of Scientific Instruments. 34:1041. 1963.

47. Redhead, P. A. Canadian Journal of Physics. 40:1814. 1962.

48. Feakes, F. and Torney, F. L. National Vacuum Symposium, Transactions 10:257. 1963.

49. Dushman, S. Scientific foundations of vacuum technique. 2nd ed. New York, N.Y., John Wiley and Sons, Inc. 1962.

50. Davis, W. D. and Vanderslice, T. A. Transactions of the Seventh National Vacuum Symposium. 417. 1960. New York, N.Y., Pergamon Press. 1961.

51. Redhead, P. A., Hobson, J. P. and Kornelson, E. V. Advances in Electronics and Electron Physics. 17:

323. 1962.

52. Langmuir, I. Journal of the American Chemical Society. 34:1310. 1912.

53. Langmuir, I. Journal of the American Chemical Society. 37:417. 1915.

54. Oguri, T. Journal of the Physical Society of Japan. 18: 1280. 1963.

55. Gomer, R., Wortman, R. and Lundy, R. Journal of Chemical Physics. 26:1147. 1957.

56. Culver, R. V. and Tompkins, F. C. Advances in Catalysis. 11:67. 1959.

57. Pauling, L. The nature of the chemical bond. 3rd ed. Ithaca, N. Y., Cornell University Press, 1960.

58. Eley, D. D. Discussions of the Faraday Society. 8:34. 1950.

59. Johnson, R. P. Physical Review. 54:459. 1938.

60. Brennan, D. and Hayes, F. H. Transactions of the Faraday Society. 60:589. 1964.

61. Beeck, O. Advances in Catalysis. 2:151. 1950.

62. Wahba, M. and Kemball, C. Transactions of the Faraday Society. 49:1351. 1953.

63. Mignolet, J. C. P. Journal de Chimie et Physique. 54: 19. 1957.

64. Suhrmann, R., Wedler, G. and Gentsch, H. Zeitschrift fur Physikalische Chemie. Neue Folge, 17:350. 1958.

65. Sachtler, W. M. H. and Dorgelo, G. J. H. Zeitschrift fur Physikalische Chemie. Neue Folge, 25:69. 1960.

66. Gundry, P. M. and Tompkins, F. C. Transactions of the Faraday Society. 52:1609. 1956.

67. Pliskin, W. A. and Eischens, R. P. Zeitschrift fur Physikalische Chemie. Neue Folge, 24:11. 1960.

68. Toya, T. Journal of the Research Institute of Catalysis. 10:236. 1962.

69. Ehrlich, G. Journal of Chemical Physics. 35:1421. 1961.

70. Eischens, R. P. and Jacknow, J. Proceedings of the Third International Congress on Catalysis. 1:627. 1964.

71. Bond, G. C. Catalysis by metals. New York, N.Y., Academic Press. 1962.

72. Ehrlich, G. and Hudda, F. G. Journal of Chemical Physics. 35:1421. 1961.

73. Klein, R. Journal of Chemical Physics. 31:1306. 1959.

74. Ehrlich, G. Journal of Chemical Physics. 34:39. 1961.

75. Eischens, R. P. and Pliskin, W. A. Advances in Catalysis. 10:1. 1958.

76. Eischens, R. P., Francis, S. A. and Pliskin, W. A. Journal of Physical Chemistry. 60:194. 1956.

77. Hickmott, T. W. and Ehrlich, G. Journal of Chemical Physics. 24:1263. 1956.

78. Lanyon, M. A. H. and Trapnell, B. N. W. Proceedings of the Royal Society. A227:387. 1955.

79. Yang, A. C. and Garland, C. W. Journal of Physical Chemistry. 61:1504. 1957.

XII. ACKNOWLEDGEMENTS

The author wishes to express his gratitude to Dr. R. S. Hansen for his guidance and encouragement during the course of this research. The many illuminating discussions with him have added immensely to the author's scientific background and for this, the author is extremely grateful.

Special thanks are given to the men in the maintenance shop, especially Mr. Gary Wells and to the men in the glass shop whose prompt service contributed to the early development of this project.

The author wishes to thank Mr. Robert Frost for writing the computer programs that were used during the course of this research.

The author wishes to thank his wife, Lynne, for her encouragement during the course of this work.

The enjoyment provided by the author's two daughters made a major contribution to the continued progress of this work.

XIII. APPENDICES

A. Relaxation Phenomena Associated with Tube Conductances and Pumping Speeds

Consider the experimental arrangement of sources, pumps and detectors in a flash filament system shown in Figure 43. Let each of the flasks contain a leak and a pump, and in addition let flask 2, contain a desorbing filament. The only flask that actually contains a leak and a pump is flask 2; the other two flasks will act either as a pump or a source, depending on the state of outgassing, but for completeness, we will treat them as if leaks and sources exist in both. Maintaining a material balance in each flask, we obtain the following set of equations,

$$V_1 \frac{dP_1}{dt} = RTL_1 - S_1P_1 + F_1(P_2-P_1) \tag{48a}$$

$$V_2 \frac{dP_2}{dt} = RT\left(L_2 - A\frac{dn}{dt}\right) - S_2P_2 - F_1(P_2-P_3) \tag{48b}$$

$$V_3 \frac{dP_3}{dt} = RTL_3 - S_3P_3 + F_2(P_2-P_3) \tag{48c}$$

where V_i is the volume of the i^{th} flask, P_i is the pressure in torr in the i^{th} flask; L_i is the leak rate into the i^{th} flask, in molecules per second, S_i is the pumping speed of the pumps in the i^{th} flask and F_1 and F_2 are the conductances of the tubulation connecting flasks 1-2 and 2-3 respectively. F_1 and

F_2 can be made equal, but for completeness, assume that they are different. The i^{th} ($i = 1,2,3$) part of the system refers to the various components in Figure 43.

At steady state,

$$\frac{dn}{dt} = 0 \qquad \text{and} \qquad \frac{dP_1}{dt} = \frac{dP_2}{dt} = \frac{dP_3}{dt} = 0$$

Let P_1^o, P_2^o and P_3^o be the steady state pressure. Then Equation 48 reduce to,

$$RTL_1 - S_1P_1^o + F_1(P_2^o-P_1^o) = 0 \qquad (49a)$$

$$RTL_2 - S_2P_2^o - F_1(P_2^o-P_1^o) - F_2(P_2^o-P_3^o) = 0 \qquad (49b)$$

$$RTL_3 - S_3P_3^o + F_2(P_2^o-P_3^o) = 0 \qquad (49c)$$

Subtracting Equation 49 from the respective Equation 48, we obtain

$$V_1\frac{dP_1}{dt} = - S_1(P_1-P_1^o) + F_1\left\{(P_2-P_2^o) - (P_1-P_1^o)\right\} \qquad (50a)$$

$$V_2\frac{dP_2}{dt} = - ART\frac{dn}{dt} - S_2(P_2-P_2^o) - F_1\left\{(P_2-P_2^o) - (P_1-P_1^o)\right\} - F_2\left\{(P_2-P_2^o) - (P_3-P_3^o)\right\} \qquad (50b)$$

$$V_3\frac{dP_3}{dt} = - S_3(P_3-P_3^o) + F_2\left\{(P_2-P_2^o) - (P_3-P_3^o)\right\} \qquad (50c)$$

Let U_1, U_2 and U_3 equal $P_1-P_1^o$, $P_2-P_2^o$ and $P_3-P_3^o$ respectively,

then

$$\frac{dU_1}{dt} = \frac{dP_1}{dt}, \quad \frac{dU_2}{dt} = \frac{dP_2}{dt} \quad \text{and} \quad \frac{dU_3}{dt} = \frac{dP_3}{dt}$$

Substituting these values into Equation 50, yields

$$V_1\frac{dU_1}{dt} = - S_1U_1 + F_1\left[U_2-U_1\right]$$

$$V_2\frac{dU_2}{dt} = - ART\frac{dn}{dt} - S_2U_2 - F_1\left[U_2-U_1\right] - F_2\left[U_2-U_3\right] \quad (51b)$$

$$V_3\frac{dU_3}{dt} = - S_3U_3 + F_2\left[U_2-U_3\right] \quad (51c)$$

Let ν, μ_1, μ_2 and μ_3 be the Laplace transforms of n, U_1, U_2 and U_3 respectively; also, at t = 0, let $n = n_o$, $U_1 = U_1^o$, $U_2 = U_2^o$ and $U_3 = U_3^o$. Then on transforming Equation 51 and rearranging, we obtain

$$\mu_2\left[s + \frac{S_2+F_1+F_2}{V_2}\right] + \mu_1\left[-\frac{F_1}{V_2}\right] + \mu_3\left[-\frac{F_2}{V_2}\right] = -\frac{ART}{V_2}(s\nu - n_o) + U_2^o \quad (52a)$$

$$\mu_2\left[-\frac{F_1}{V_1}\right] + \mu_1\left[s + \frac{S_1+F_1}{V_1}\right] = U_1^o \quad (52b)$$

$$\mu_2\left[-\frac{F_2}{V_3}\right] + \mu_3\left[s + \frac{S_3+F_2}{V_3}\right] = U_3^o \quad (52c)$$

Let $\frac{S_1+F_1}{V_1} = \sigma_1$, $\frac{S_2+F_1+F_2}{V_2} = \sigma_2$, $\frac{S_3+F_2}{V_3} = \sigma_3$ and let $\frac{ART}{V_2} = \alpha$.

Then, by the method of determinants

$$\mu_1 = \frac{\begin{vmatrix} U_1^o & -F_1/V_1 & 0 \\ U_2^o - \alpha(s\nu - n_o) & s+\sigma_2 & -F_2/V_2 \\ U_3^o & -F_2/V_3 & s+\sigma_3 \end{vmatrix}}{\begin{vmatrix} s+\sigma_1 & -F_1/V_1 & 0 \\ -F_1/V_2 & s+\sigma_2 & -F_2/V_2 \\ 0 & -F_2/V_3 & s+\sigma_3 \end{vmatrix}} \qquad (53)$$

Equation 53 can be evaluated to give,

$$\mu_1 = \frac{\dfrac{(F_2)^2U_1^o}{V_2V_3} - \dfrac{F_1F_2U_3^o}{V_1V_2} - (s+\sigma_2)(s+\sigma_3)U_1^o}{\dfrac{(F_2)^2(s+\sigma_1)}{V_2V_3} + \dfrac{(F_1)^2(s+\sigma_3)}{V_1V_2} - (s+\sigma_1)(s+\sigma_2)(s+\sigma_3)}$$

$$\frac{- \dfrac{(s+\sigma_3)F_1}{V_1}\left[U_2^o - \alpha(s\nu - n_o)\right]}{\dfrac{(F_2)^2(s+\sigma_1)}{V_2V_3} + \dfrac{(F_1)^2(s+\sigma_3)}{V_1V_2} - (s+\sigma_1)(s+\sigma_2)(s+\sigma_3)} \qquad (54)$$

$$\mu_1 = \frac{\dfrac{(s+\sigma_3)F_1}{V_1}\left[U_2^o - \alpha(s\nu - n_o)\right] + U_1^o(s+\sigma_2)(s+\sigma_3)}{(s+\beta_1)(s+\beta_2)(s+\beta_3)}$$

$$+ \frac{\dfrac{F_1F_2U_3^o}{V_1V_2} - \dfrac{(F_2)^2U_1^o}{V_2V_3}}{(s+\beta_1)(s+\beta_2)(s+\beta_3)} \qquad (54a)$$

where, β_1, β_2 and β_3 are defined by

$$(s+\beta_1)(s+\beta_2)(s+\beta_3) = (s+\sigma_1)(s+\sigma_2)(s+\sigma_3)$$

$$- \frac{(F_2)^2(s+\sigma_1)}{V_2V_3} - \frac{(F_1)^2(s+\sigma_3)}{V_1V_2} \qquad (55)$$

Hence,

$$\mu_1 = \frac{\frac{F_1(s+\sigma_3)}{V_1}(n_o+s\nu)}{(s+\beta_1)(s+\beta_2)(s+\beta_3)} +$$

$$\frac{\frac{(s+\sigma_3)F_1}{V_1}U_2^o + U_1^o(s+\sigma_2)(s+\sigma_3) + \frac{F_1F_2}{V_1V_2}U_3^o - \frac{(F_2)^2}{V_2V_3}U_1^o}{(s+\beta_1)(s+\beta_2)(s+\beta_3)} \qquad (56)$$

In a characteristic flash desorption experiment, $U_1^o = U_2^o = U_3^o = 0$, then Equation 56 reduces to

$$\mu_1 = \frac{\alpha F_1}{V_1}\left[\frac{(\sigma_3-\beta_1)(n_o+\beta_1\nu)}{(\beta_2-\beta_1)(\beta_3-\beta_1)(s+\beta_1)} + \right.$$

$$\left. \frac{(\sigma_3-\beta_2)(n_o+\beta_2\nu)}{(\beta_1-\beta_2)(\beta_3-\beta_2)(s+\beta_2)} + \frac{(\sigma_3-\beta_3)(N_o+\beta_3\nu)}{(\beta_1-\beta_3)(\beta_2-\beta_3)(s+\beta_3)}\right] \qquad (57)$$

The inverse transform of $\frac{n_o+\beta_i\nu}{(s+\beta_i)}$ is obtained from the convolution integral.

That is

$$L^{-1}\ \frac{(N_o+\beta_i\nu)}{(s+\beta_i)} = n_o e^{-\beta_i t} + \beta_i \int_o^t n(\tau) e^{-\beta_i(t-\tau)}\, d\tau \qquad (58a)$$

$$= e^{-\beta_i t}\left[n_o + \beta_i \int_o^t n(\tau) e^{\beta_i \tau}\, d\tau \right] \qquad (58b)$$

But the right hand side of Equation 58b can be simplified further. That is

$$e^{-\beta_i t}\left[n_o + \beta_i \int_o^t n(\tau) e^{\beta_i \tau}\, d\tau \right.$$

$$= e^{-\beta_i t}\left[n_o + \int_o^t n\, de^{\beta_i \tau} \right] \qquad (59a)$$

$$= e^{-\beta_i t}\left[n_o + n e^{\beta_i t} - n_o - \int_{n_o}^{n} e^{\beta_i \tau}\, dn \right] \qquad (59b)$$

$$= n + e^{-\beta_i t} \int_{n_o}^{n} e^{\beta_i \tau}\, dn \qquad (59c)$$

Treating the remaining terms in Equation 57 similarly, we find that Equation 57 becomes

$$U_1 = \frac{ART\ F_1}{V_1 V_2 (\beta_3-\beta_1)(\beta_3-\beta_2)(\beta_2-\beta_1)}$$

$$\left[(\sigma_3-\beta_1)(\beta_3-\beta_2)\left\{ n + e^{-\beta_1 t} \int_n^{n_o} e^{\beta_1 \tau}\, dn \right\}\right.$$

$$- (\sigma_3-\beta_2)(\beta_3-\beta_1)\left\{ n + e^{-\beta_2 t} \int_n^{n_o} e^{\beta_2 \tau}\, dn \right\}$$

$$+ (\sigma_3-\beta_3)(\beta_2-\beta_1)\left\{ n + e^{-\beta_3 t} \int_n^{n_o} e^{\beta_3 \tau}\, dn \right\} \qquad (60)$$

The coefficients of n in Equation 60 cancel, and there remains only

$$U_1 = \frac{ART\ F_1}{V_1V_2(\beta_3-\beta_1)(\beta_3-\beta_2)(\beta_2-\beta_1)}$$
$$\Big[(\sigma_3-\beta_1)(\beta_3-\beta_2)\ e^{-\beta_1 t}\int_n^{n_o} e^{\beta_1\tau}\,dn$$
$$-(\sigma_3-\beta_2)(\beta_3-\beta_1)\ e^{-\beta_2 t}\int_n^{n_o} e^{\beta_2\tau}\,dn$$
$$+(\sigma_3-\beta_3)(\beta_2-\beta_1)\ e^{-\beta_2 t}\int_n^{n_o} e^{\beta_3\tau}\,dn\ \Big] \qquad (61)$$

The relaxation parameters, β_1, β_2 and β_3 are related to the pumping speed and the conductances by Equation 55, which on expansion becomes

$$f(s) = (s+\beta_1)(s+\beta_2)(s+\beta_3) = s^3 + (\sigma_1+\sigma_2+\sigma_3)s^2$$
$$+\Big(\sigma_1\sigma_2+\sigma_1\sigma_3+\sigma_2\sigma_3 - \frac{(F_2)^2}{V_2V_3} - \frac{(F_1)^2}{V_1V_2}\Big)s$$
$$+\Big(\sigma_1\sigma_2\sigma_3 - \frac{(F_2)^2\sigma_1}{V_2V_3} - \frac{(F_1)^2\sigma_3}{V_1V_2}\Big) \qquad (55a)$$

The values of β_1, β_2 and β_3 for various values of F and S_1 are shown in Table 6. For small values of S_1, the relaxation parameter β_1 reflects the pumping speed and not the conductance, whereas for large values of S_1, β_1 reflects the conductance and not the pumping.

Recall that in Equation 61, $U_1 = P_1-P_1^o$, there U_1 is the

pressure increase measured in a flask separated from a flask by tubulation of conductance F and containing a desorbing filament. Hence, from Equation 61, it is possible to observe the effect of pumping speed and conductance on U_1, once a rate process is assumed.

Consider a second-order reaction

$$-\frac{dn}{dt} = \nu n^2 \, e^{\alpha t} \tag{62}$$

where,

$$\alpha = -\frac{\Delta Hb}{R} > 0$$

Integrating and rearranging we obtain

$$n = \frac{n_o}{1 + n_o \frac{\nu}{\alpha} (e^{\alpha t} - 1)} \tag{63}$$

Now

$$\int_n^{n_o} e^{\beta_1 \tau} \, dn = \int_o^t \nu \, n^2 \, e^{\alpha \tau} \, e^{\beta_1 \tau} \, d\tau \tag{64}$$

$$= \nu n_o^2 \int_o^t \frac{e^{(\alpha+\beta_1)\tau}}{\left[1+n_o\frac{\nu}{\alpha}(e^{\alpha\tau}-1)\right]^2} \, d\tau \tag{64a}$$

Substituting these integrals into Equation 61, we obtain

$$\frac{U_1}{ART} = \frac{\nu n_o^2 F_1}{V_1 V_2 (\beta_3-\beta_1)(\beta_3-\beta_2)(\beta_2-\beta_1)}$$

$$\left\{(\sigma_3-\beta_1)(\beta_3-\beta_2)e^{-\beta_1 t} \int_o^t \frac{e^{(\alpha+\beta_1)\tau}}{Y^2} \, d\tau \right.$$

$$- (\sigma_3-\beta_2)(\beta_3-\beta_1)\, e^{-\beta_2 t} \int_o^t \frac{e^{(\alpha+\beta_2)\tau}}{Y^2}\, d\tau$$

$$+ (\sigma_3-\beta_3)(\beta_2-\beta_1)\, e^{-\beta_3 t} \int_o^t \frac{e^{(\alpha+\beta_3)\tau}}{Y^2}\, d\tau \Big\} \quad (65)$$

where $Y = \left[1 + n_o \frac{\nu}{\alpha} (e^{\alpha\tau} - 1)\right]$

$\frac{U_1}{ART}$ can best be determined by programming a computer to evaluate the right hand side of Equation 65. There are several parameters that can be varied, namely n_o, ν, F and S but for the purpose of the present work only F and S will be considered. The results are summarized in Figures 44 and 45. It is evident from Figure 44, that the conductance of the connecting tubulation has a pronounced effect on the desorption spectrum and hence, on any parameters obtained from the desorption curve. Similar results are obtained for larger values of S_1 with a further reduction in peak height by a factor of four for S_1 = 80 liters per second. Since the conductance of a cylindrical tube is proportional to a^3/ℓ (49), where a and ℓ are the radius and length respectively, then by the proper choice of a and ℓ, the effect of conductance on desorption spectra can be minimized. In the present apparatus a = 1.6 cm and ℓ = 10 cm which corresponds to a conductance of 40 liters per second for air.

B. Response Characteristics of a Linear Recording System

The response characteristics of a linear recording system can be completely specified by the relative magnitude and phase input and output of sine wave test signals. Since the amplitude and phase vary with frequency and their dependence on frequency is easily observable, then it is theoretically possible to predict exactly how any complex wave would be distorted. The dependence of phase shift on frequency will generate a transfer function, and this function operating on the actual recorded function will generate the true signal, or driving function.

It is possible to state the requirements for the theoretically ideal recording system. These are: first, constant amplitude response for all frequencies from zero to infinity, and second, a phase shift which is zero for all frequencies. No physically realizable system can meet these requirements and the problem then becomes one of trying to correlate departure from ideal with the distortion which will result in a particular recording.

Consider the sequence of operations in the recording instrument by which an input signal is transformed into a permanent recorded trace. The input signal, after passing through the attenuator and input filter (Figure 46), is applied to the balance circuit where it is cancelled by an

internally supplied opposing voltage. Under these conditions, there is no signal output from the balance circuit and the servo system is at rest. When the input signal changes to a new value it is no longer cancelled in the balance circuit and the unbalance voltage or error signal, is applied to the chopper where it is converted to a 60 cycle form. The ac output of the chopper is amplified and applied to the control winding of a two phase servo motor. The motor is mechanically coupled to the balance circuit potentiometer and thus changes the balance voltage until it again cancels the new value of the input signal. If the input signal is changing at rates within the limitations of the recorder, then this rebalancing action is continuous. Hence, the position of the balance circuit potentiometer and of the pen and carriage, to which they are coupled, are always directly proportional to the amplitudes at the respective input terminals.

There will be an inertia, some friction and a spring constant associated with the mechanical motion of the pen and its moving parts. There will also be a net inductance, resistance and capacitance associated with the electrical conversion of the input signal to the mechanical motion of the pen. Let J represent the moment of inertia of the pen and its associated moving parts and the net inductance of the circuit; F, the coefficient of friction associated with the

moving parts and the net resistance; and k, the spring constant and the net capacitance. Then the differential equation of motion[1] relating the recorded signal, R(t) to the true input signal, S(t) is,

$$JR''(t) + FR'(t) + kR(t) = S(t) \qquad (66)$$

Of the three parameters J, F and k, we can assume one set, when a scale factor is set; the other two parameters are related to the instrumental damping properties. Hence without any loss of generality, we set ks = S, jk = J, fk = F, then Equation (66) reduces to,

$$jR''(t) + fR'(t) + R(t) = s(t) \qquad (67)$$

If R(t) and the parameters j and f are known, then S(t) can be calculated. The determination of j and f remains an experimental problem.

It appears that Equation (67) is somewhat too simple to adequately represent the observed dependence of the response on the signal. We have assumed that the parameters j and f are not functions of R(t), whereas in reality they do depend on R(t) as illustrated by the distortion of the sinusoidal test signal at high frequencies (~2.0 cycles per second). Consider, for example, the parameter J in Equation 66. It can be represented as follows,

---

[1]Pearson, Eric B., Technology of Instrumentation, London, England, The English Universities Press Ltd., 1957.

$$J \equiv J(R) = J(0) + J'(0)R + \frac{1}{2}J''(0)R^2 \qquad (68)$$

It is evident from Equation 68 that $J = J(0)$ if R is small. Hence, it is possible to adjust R so that the distortion of the input test signal is small over the frequency range of interest, that is 0.5 cps to 2.5 cps. Therefore, if the parameters j and f are determined from known signals and responses similar to those of physical interest, and the results used to correct the observed responses, then the correction should be reasonably accurate.

Consider the input signal to be a sine wave. It is sufficiently similar to signals of physical interest and it is simple to treat mathematically. That is, let $s = \sin\omega t$; then $R(0) = R'(0) = 0$. Then on transforming Equation 67, we obtain

$$(js^2 + fs + 1)\, r(t) = \frac{\omega}{s^2+\omega^2} \qquad (69)$$

where r is the Laplace transform of R(t), i.e. $r = \int_0^\infty Re^{-st}dt$. Then

$$r = \frac{\omega}{j(s^2+\omega^2)(s+\alpha_1)(s+\alpha_2)} \qquad (70)$$

where

$$\alpha_{\frac{1}{2}} = \frac{f}{j}\left[1 \pm \left(1 - \frac{4j}{f^2}\right)^{1/2}\right] \qquad (71)$$

$$\alpha_2 = \frac{f}{2j}\left[1-\left(1-\frac{4j}{f^2}\right)^{1/2}\right] \tag{71a}$$

Hence,

$$r = \frac{\omega}{j}\left[\frac{1}{(s+i\omega)(s-i\omega)(s+\alpha_1)(s+\alpha_2)}\right] \tag{72}$$

Using the method of partial fractions, Equation 72 decomposes to:

$$r = \frac{\omega}{j}\left[\frac{1}{(\alpha_2-\alpha_1)}\left\{\frac{1}{(s+\alpha_1)(\alpha_1^2+\omega^2)} - \frac{1}{(s+\alpha_2)(\alpha_2^2+\omega^2)}\right\}\right.$$

$$\left. + \frac{\dfrac{(\alpha_1\alpha_2-\omega^2)}{(s^2+\omega^2)} - \dfrac{(\alpha_1+\alpha_2)s}{(s^2+\omega^2)}}{(\alpha_1^2+\omega^2)(\alpha_2^2+\omega^2)}\right] \tag{73}$$

Taking the inverse transform of Equation 73, we obtain the following,

$$R = \frac{\omega}{j(\alpha_2-\alpha_1)}\left[\frac{e^{-\alpha_1 t}}{(\alpha_1^2+\omega^2)} - \frac{e^{-\alpha_2 t}}{(\alpha_2^2+\omega^2)}\right]$$

$$+ \frac{(\alpha_1\alpha_2-\omega^2)\sin\omega t-(\alpha_1+\alpha_2)\omega\cos\omega t}{j(\alpha_1^2+\omega^2)(\alpha_2^2+\omega^2)} \tag{74}$$

As t becomes large, the terms with $e^{-\alpha_1 t}$, $e^{-\alpha_2 t}$ vanish and there remains the periodic function,

$$R_{per} = \frac{(\alpha_1\alpha_2-\omega^2)\sin\omega t - (\alpha_1+\alpha_2)\omega\cos\omega t}{j(\alpha_1^2+\omega^2)(\alpha_2^2+\omega^2)} \tag{75}$$

$$= A\sin(\omega t - \delta) \tag{76}$$

where,

$$A = \frac{\left[(\alpha_1\alpha_2-\omega^2)^2 + \omega^2(\alpha_1+\alpha_2)^2\right]^{1/2}}{j(\alpha_1^2+\omega^2)(\alpha_2^2+\omega^2)} \tag{77}$$

$$A = \frac{1}{j\left[\alpha_1^2\alpha_2^2+\omega^2(\alpha_1^2+\alpha_2^2)+\omega^4\right]^{1/2}} \tag{78}$$

$$\text{Also, } \tan\delta = \frac{(\alpha_1+\alpha_2)\,\omega}{(\alpha_1\alpha_2-\omega^2)} \tag{79}$$

From Equation 71 and 71a, we obtain the following relations,

$$\alpha_1 + \alpha_2 = \frac{f}{j} \tag{80}$$

$$\alpha_1\alpha_2 = \frac{1}{j} \tag{81}$$

$$\alpha_1^2+\alpha_2^2 = \frac{f^2}{j^2} - \frac{2}{j} \tag{82}$$

Substituting these values in Equations 78 and 79, we get

$$A = \left[1 +\omega^2(f^2 - 2j)+\omega^4 j^2\right]^{-1/2} \tag{78a}$$

and

$$\tan\delta = \frac{\omega f}{1 - j\omega^2} \tag{79a}$$

Equation 78a can be rearranged as follows:

$$\frac{A^{-2}-1}{\omega^2} = (f^2-2j)+j^2\omega^2 \tag{78b}$$

Hence, a plot of $(A^{-2} - 1)/\omega^2$ versus ω^2 should give a straight with a slope, j^2, and an intercept $(f^2 - 2j)$.

Also, Equation 79a can be rearranged to give

$$\frac{\omega}{\tan\delta} = \frac{1}{f} - \frac{j}{f}\omega^2 \qquad (79b)$$

from which it can be seen that a plot of $\omega/\tan\delta$ versus ω^2 should be linear with a slope, $-j/f$, and an intercept, $1/f$.

Either of the Equations 78b and 79b can be used to determine the parameters f and j. Equation 78b involves measuring the amplitude attenuation as a function of frequency and Equation 79b, the phase lag as a function of frequency. The latter method is more sensitive than the former method in the frequency range below 1.5 cycles per second, which is the range of physical significance in flash desorption experiments. Also, in the former method, if the amplitude of the input signal is chosen to give full scale deflection at low frequencies, then at higher frequencies, one not only observes an attenuation but also a distortion of the sinusoidal test signal, since the parameters relating the response to the input signal are functions of the response.

Measurement of the Phase Lag

The simplest way to determine the phase lag is to measure the eccentricity of a Lissajous pattern. A Lissajous pattern

is the figure created on an oscilloscope screen when sine-wave potentials are applied to both the horizontal and vertical deflecting plates. If the frequencies of these two component potentials are the same but they differ in phase, the resulting pattern is a measure of the phase difference between the two waves.

To see that this is so, suppose that the potential across the horizontal deflecting plates of the scope is

$$e_x = E_1 \sin(\omega t + \theta_1) \tag{83}$$

and that across the vertical plates is

$$e_y = E_2 \sin(\omega t + \theta_2) \tag{84}$$

Then

$$\frac{e_x}{E_1} = \sin \omega t \cos \theta_1 + \cos \omega t \sin \theta_1 \tag{83a}$$

and

$$\frac{e_y}{E_2} = \sin \omega t \cos \theta_2 + \cos \omega t \sin \theta_2 \tag{84a}$$

To eliminate the time factor we proceed as follows: multiply Equation 83a by $\cos \theta_2$ and Equation 84a by $\cos \theta_1$, subtract to obtain

$$\frac{e_x}{E_1} \cos \theta_2 - \frac{e_y}{E_2} \cos \theta_1 = \cos \omega t(\sin \theta_1 \cos \theta_2 - \cos \theta_1 \sin \theta_2) \tag{85}$$

Multiplying Equation 83a by sin θ_2 and Equation 84a by sin θ_1 and subtracting, there results

$$\frac{e_x}{E_1} \sin \theta_2 - \frac{e_y}{E_2} \sin \theta_1 = \sin \omega t(\cos \theta_1 \sin \theta_2 - \sin \theta_1 \cos \theta_2) \tag{86}$$

Squaring Equation 85 and 86 and adding, gives

$$\frac{e_x^2}{E_1^2} + \frac{e_y^2}{E_2^2} - \frac{2e_x e_y}{E_1 E_2} \cos(\theta_1 - \theta_2) = \sin^2(\theta_1 - \theta_2) \tag{87}$$

This is an equation of an ellipse, the orientation of which depends upon the phase difference.

The experimental procedure necessary for measuring the phase difference between the two potentials is quite direct and consists of measuring the two distances E_o and E_m in Figure 47. The distance E_o is evidently the value of e_g when e_x is zero. This requires that

$$E_o = E_2 \sin (\theta_1 - \theta_2) \tag{88}$$

Likewise, the value E_m is the maximum value of e_y and from Equation 84a is given by $E_2 = E_m$. Substituting this value into Equation 88, yields

$$\sin \delta = \frac{E_o}{E_m} \tag{89}$$

where $\delta = \theta_1 - \theta_2$.

The experimental arrangement used to measure the phase lag of the recorder is shown in Figure 47. It consists of

applying simultaneously a sinusoidal test signal to the input terminals of the recorder and to the horizontal deflection plates of the oscilloscope. The signal that appears at the slidewire of the recorder is applied to the vertical deflection plates of the oscilloscope. The existence of a phase difference between the two signals is indicated by the appearance of an ellipse on the oscilloscope and the eccentricity of the ellipse is equal to the sine of the phase lag. The results of the measurements are summarized in Table 6 and Figure 48.

Substituting $2\pi\nu$ for ω in Equation 79b yields,

$$\frac{\nu}{\tan\delta} = \frac{1}{2\pi f} - \frac{j}{f} 2\pi\nu^2 \qquad (90)$$

Now, substituting in Equation 90, the value of the intercept and the slope determined from Figure 48, we obtain the values 3.1×10^{-2} and 5.85×10^{-4} for the parameters f and j respectively.

The problem that remains is to apply these correction parameters to a sample desorption spectrum. This is best accomplished by fitting the spectrum with an analytical expression. The desorption spectrum was divided into three intervals and an equation was obtained for each interval. The three equations are:

$$0 < t \leq 0.85, \quad I = 2.466 + 8y - 20y^3, \quad y = t - 0.602 \qquad (91a)$$

$$0.85 \leq t \leq 1.15, \quad I = 4.50 - 15y^2, \quad y = t - 1.002 \qquad (91b)$$

$$1.50 \leq t \leq 1.85, \quad I = 41.1 \exp\left[-1.833y\right], \quad y = t \qquad (91c)$$

Since the heating schedule is recorded simultaneously with the desorption spectrum, it must also be corrected. The analytical expression used to represent the heating schedule is expressed in terms of a voltage drop across the filament and this is directly proportional to the temperature for a set current. That is

$$0 \leq t \leq 1.5, \quad E = 2.85 + 1.27t + 0.74t^2 \qquad (92)$$

and this is related to the temperature of the sample filament by the following relation,

$$T^{\circ}K = \frac{154.7E}{I} + 6 \qquad (93)$$

The result of applying the correction parameters, f and j, to the desorption spectrum and the heating schedule is shown in Figure 49.

Analyzing the corrected spectrum by the method described previously, we obtain the value of 9.60 for the slope of the plot of $\ln(n_o-n)/n$ vs T^{-1}, compared to the value of 9.66 for the uncorrected spectrum. This agreement is due to partial cancellation of corrections in the desorption spectrum and in the heating schedule. It is clear from the equation for ΔH, that the correction of the heating schedule and of the desorption spectrum have opposite effects on the value of ΔH.

Therefore, we can conclude that the response time of the recorder may have a serious effect on the driving signal, if

the rate of change of the true signal approaches the response time of the recorder.

C. Kinetic Analysis of Pressure-Temperature Data, Fortran Program

```
     START     ACCNTA0087      @VJM@      MAXTIME   4MIN                  PUGO
               FLAG   MAP,GO                                              PUGO
 FLAG FORT,MAIN,COMPILE,LIST
C
C         FORTRAN PROGRAM FOR PROCESSING
C              FLASH FILAMENT DATA
C         WITH OR WITHOUT PUMPING CORRECTION
C
C
C         T  =TIME(SEC),CURVE A
C         DI =ION CURRENT (SCALE DIV),CURVE A
C         DK =POT DROP ACROSS FILAMENT (SCALE DIV),CURVE C
C         A  =ND-N
C         E  =VOLTS CORRESPONDING TO DK
C         BI =ION CURRENT (SCALE DIV),CURVE B
C         TB =TIME(SEC),CURVE B
C         CU =HEATING CURRENT (AMPS)
C
      DIMENSION T(100),DI(100),DK(100),DELI(100),A(100),E(100),B(100),T1
     1(100),TT(100),Z(10),ACD(8),BCD(8),CC(100),DC(100),TY(100),BI(100),
     2TB(100),BLUG(100)
      READ 26,NY,PO,PI,CU
C         NY =NUMBER OF CURVES TO BE PROCESSED
C         TEMP OF FILAMENT GIVEN BY PO*E/CU-PI
   26 FORMAT(I5,3F10.0)
      READ 1 ,(BCD(I),I=1,8),P1,P                                          SIMU
C
C         A.  LABLES FOR PLOTS. COL 1-10 10000/T,
C         11-25 LOG((NO-N)/.),26-40 LOG(LOG(NO/N)),
C         41 P1, 42 P, PLOT SYMBOLS 1ST AND 2ND ORDER
C
C         ANALYSIS OF 1ST AND 2ND ORDER DATA PLOTTED USING
C         IBM 1627 MODEL I DIGITAL INCREMENTAL PLOTTER
C
   14 FORMAT(8A5,2A1)                                                      SIMU
      NTP=10                                                               SIMU
      CALL LABEL(NTP)                                                      SIMU
      DO 25 J=1,NY
      READ 1,M,L,XA,VO,RO,(Z(I),I=1,8)
C
C         M  =NUMBER OF POINTS IN CURVE A
C         L  =NUMBER OF POINTS IN CURVE B
C         L  =0, IF PUMPING TERM (S/V) IS ZERO
C         XA =SCALE FACTOR (AMPS/DIV)
C         VO =SCALE FACTOR (VOLTS/DIV)
C         RO =SCALE FACTOR (MOLECULES/AMP)
C         Z  =TITLE
C
    1 FORMAT(I3,I2,3E10.4,8A5)
    2 READ 3,TI,TII
C
C         TI =INITIAL TIME CURVE A
C         TII=INITIAL TIME CURVE B (0,IF L=0)
C
      READ 3,(DI(I),I=1,M)
      READ 3,(DK(I),I=1,M)
    3 FORMAT(8F10.0)
```

Fortran Program 1. Kinetic Analysis of Pressure-Temperature Data

```
      PRINT 11,(Z(I),I=1,8)
   11 FORMAT(1H1,//20X8A5///)
      T(1)=TI
      DO 15 I=2,M
   15 T(I)=T(I-1)+0.05
C          GENERATE TIME INTERVALS FOR CURVE A
      IF(L)29,25,29
   26 DO 4 I=1,M
      DELI(I)=DI(I)*XA
      A(I)=DELI(I)*RO
    4 E(I)=DK(I)*VO
      GO TO 27
   29 TB(1)=TII
      DO 16 I=2,L
   16 TB(I)=TB(I-1)+0.10
C          GENERATE TIME INTERVALS FOR CURVE B
      READ 3,(BI(I),I=1,L)
      PRINT 33
   33 FORMAT(21X4HTIME,7X2HDI,9X9HS/V*DI*DT,5X10HSUM(COL.3),6X8HDI + SUM
     1///)
      SUM1=0
      SUM2=0
      SUM3=0
      SUM4=0
C          DETERMINE PUMPING CORRECTION AND
C               CORRECT CURVE A
      DO 17 I=1,L
      BLOG(I)=ALOG10F(BI(I)*XA)
      SUM1=SUM1+BLOG(I)
      SUM2=SUM2+TB(I)
      SUM3=SUM3+TB(I)*TB(I)
   17 SUM4=SUM4+BLOG(I)*TB(I)
      AA=L
      SLOPE=((SUM1*SUM2-AA*SUM4)/(AA*SUM3-SUM2*SUM2))*2.303
      SLOP=SLOPE*0.05
      DEL=0
      DO 18 I=1,M
      DEL=DI(I)*XA
      DE=DEL*SLOP
      DEL=DEE+DE
      DELI(I)=DEL+DEE
      A(I)=DELI(I)*RO
      E(I)=DK(I)*VO
      PRINT 20,T(I),DEL,DE,DEE,DELI(I)
   18 CONTINUE
   20 FORMAT(20XF5.2,4E15.4)
      PRINT 19,SLOPE
   19 FORMAT(//40X4HS/V=,E15.4///)
   27 IP=1
C          DETERMINE NO
C
      DO 21 I=2,M
      IF(A(I)-A(I-1))22,21,21
   22 IF(IP-1)21,24,21
   24 IP=3
      AO=A(I-1)
      N=I-2
   21 CONTINUE
```

Fortran Program 1 (continued)

```
      PRINT 10
   10 FORMAT(14X4HTIME,4X6HDELTAI,9X4HNO-N,4X9H(NO-N)/NO,5X8H(NO-N)/N,4X4
     1HNO/N,3X7HLOG NO/N,1X7H10000/T,2X4HTEMP,3X5HE/OLTS,4X5HDN/DT,5X9HD(
     2I/T)/DT///)
      NX=N
C          CALCULATE AND PRINT
      DO 5 I=1,N
      B(I)=AO-A(I)
      C=A(I)/B(I)
      D=AO/B(I)
      G=LOGXF(D)
      CC(I)=LOGXF(C)                                                    SIMO
      DC(I)=LOGXF(G)                                                    SIMO
      BBB=A(I)/AO
      T1(I)=PO*E(I)/CO-PI
      TT(I)=1.0/T1(I)
      TX=10000.0*TT(I)
      TY(I)=TX
      IF(I-1)6,7,6
C          EVALUATE DERIVATIVES DN/DT AND D(1/T)/DT
    6 X=(B(I)-B(I-1))/0.05
      Y=(TT(I)-TT(I-1))/0.05
    7 PRINT 8,T(I),DELI(I),A(I),BBB,C,D,G,TX,T1(I),E(I),X,Y
    8 FORMAT(F5.2,4E12.4,5F8.3,2E12.4)
    5 CONTINUE
      XMIN=0                                                            SIMO
      YMIN=0                                                            SIMO
      ZMIN=0                                                            SIMO
      DX=0                                                              SIMO
      DY=0                                                              SIMO
      DZ=0                                                              SIMO
      DO 30 I=1,6                                                       SIMO
   30 ACD(I)=Z(I)                                                       SIMO
      CALL SCALE (CC,NX,9.,YMIN,DY,1)                                   SIMO
      CALL SCALE (DC,NX,9.,ZMIN,DZ,1)                                   SIMO
      CALL SCALE (TY,NX,9.,XMIN,DX,1)                                   SIMO
      CALL AXIS (0,0,BCD(3),15,9.,90.,YMIN,DY,NTP)                      SIMO
      CALL AXIS (0,0,BCD(1),-10,9.,0,XMIN,DX,NTP)                       SIMO
      CALL AXIS (9.,0,BCD(6),-15,9.,90.,ZMIN,DZ,NTP)                    SIMO
      XX=5.5                                                            SIMO
      XY=5.5                                                            SIMO
      YY=8.3                                                            SIMO
      YX=8.0                                                            SIMO
      CALL SMBL4(XX,YY,.2,ACD(1),0,15,NTP)                              SIMO
      CALL SMBL4(XY,YX,.2,ACD(4),0,15,NTP)                              SIMO
      DO 48 I=1,N                                                       SIMO
      CALL SMBL4(TY(I),CC(I),.10,P1,0,1,NTP)                            SIMO
      TY(I)=TY(I)-0.1                                                   SIMO
   48 CALL SMBL4(TY(I),DC(I),.10,P,0,1,NTP)                             SIMO
      CALL PLOT(15.,0,-3,NTP)                                           SIMO
   25 CONTINUE
      STOP 00
      END
```

Fortran Program 1 (continued)

D. Variation of the Activation Energy of Desorption with Surface Coverage; Fortran Program

```
     START     ALCNTA0087      @VJM@      MAXTIME   2MIN                  PCGO
               FLAG   MAP,GO                                              PCGO
 FLAG FORT,MAIN,COMPILE,LIST
C
C         FORTRAN PROGRAM FOR DETERMINING VARIATION OF
C           ACTIVATION ENERGY WITH SURFACE COVERAGE
C
C         DELTA H DETERMINED FROM LOW SURFACE COVERAGE DATA
C         VARIATION OF ACTIVATION ENERGY (ALPHA) DETERMINED
C              FOR SUBSEQUENT SURFACE COVERAGES
C
C
C              A  =(NO-N)/NO EXP.
C              T  =1000/TEMP (DEG K)
C              A1 =(NO-N)/N  EXP.
C              AN =(NO-N)/NO CALC.
C              V2 =SECOND-ORDER FREQUENCY FACTOR
C
      DIMENSION A(50),T(50),A1(50),TT(50),V2(50),AN(50),V(12),C(50),V3(5
     10)
      READ 1,N,DH,DFH,ALPHA,DAL,DFA
C
C              N  =NO. OF CURVES TO BE PROCESSED
C              DH =INITIAL INCREMENT OF DELTA H
C              DFH=FINAL INCREMENT OF DELTA H
C              ALPHA=INITIAL ESTIMATE OF ALPHA
C              DAL=INITIAL INCREMENT OF ALPHA
C              DFA=FINAL INCREMENT OF ALPHA
C
    1 FORMAT(I6,2E12.4,3F10.0)
      READ 50,(C(I),I=1,3)
   50 FORMAT(3E12.4)
      READ 51,J1,J2,J3,NN
C
C         SECOND-ORDER FREQUENCY FACTOR  MAY BE TREATED
C              SIMULTANEOUSLY IN THREE WAYS
C
C           CASE I      V2 = C(1)*V
C           CASE II     V2 = C(2)*T
C           CASE III    V2 = C(3)*SQRT(T)
C
C              NN =NO. OF FREQ. FACTORS READ IN
C                 =0, IF CASE I IS OMITTED
C
C         SET J1,J2,J3 AS FOLLOWS FOR VARIOUS
C         COMBINATIONS OF CASES I,II, AND III
C            1)FOR I,II,III          1,3,1
C            2)FOR I,II              1,2,1
C            3)FOR I,III             1,3,2
C            4)FOR I ALONE           1,1,1
C            5)FOR II ALONE          2,2,1
C            6)FOR III ALONE         3,3,1
C
   51 FORMAT(4I5)
      IF(J1-2)41,53,53
   41 READ 43,(V(J),J=1,NN)
   43 FORMAT(6E12.4)
```

Fortran Program 2. Variation of the Activation Energy of Desorption

```
   53 DO 100 I=1,N
      READ 2,N1,A0
    2 FORMAT(I5,E12.4)
      READ 3,(A(J),J=1,N1)
      READ 3,(T(J),J=1,N1)
      IF(I-1)71,70,71
   70 READ 3,(A1(J),J=1,N1)
C
C          REQUIRED ONLY FOR FIRST CURVE OF SET
C
    3 FORMAT(8F10.0)
   71 DO 150 JJ=J1,J2,J3
      IF(JJ-2)72,73,73
   72 DO 101 II=1,NN
   73 TT(1)=T(1)/1000.0
      IF(JJ-2)54,55,56
   54 V2(1)=C(JJ)*V(II)
      GO TO 57
   55 V2(1)=C(JJ)/TT(1)
      GO TO 57
   56 V2(1)=C(JJ)*SQRTF(1.0/TT(1))
   57 DO 4 J=2,N1
      TT(J)=(T(J)+T(J-1))/2000.0
      IF(JJ-2)58,59,60
   58 V2(J)=V2(1)
      GO TO 4
   59 V2(J)=C(JJ)/TT(J)
      GO TO 4
   60 V2(J)=C(JJ)*SQRTF(1.0/TT(J))
    4 CONTINUE
      IF(I-1)44,42,44
C
C          MINIMIZE LOW SURF. COV. CURVE TO DETERMINE
C          DELTA H USING LOG((NO-N)/N) VS 1/TEMP
C
   42 X=0.0
      Y=0.0
      Z=0.0
      W=0.0
      DO 7 K=1,N1
      TX=T(K)/1000.0
      XX=LOGF(A1(K))
      X=X+XX*TX
      Y=Y+XX
      Z=Z+TX
    7 W=W+TX*TX
      U=N1
      DELHO=(Y*Z-U*X)/(U*W-Z*Z)
      LYO=1
      LXO=1
      SUM1=0.0
      DELH=DELHO
      P1=0.0
    8 SUM=0.0
    9 DELN=0.0
      AX=A0
```

Fortran Program 2 (continued)

```
      DO 10 J=1,N1
      AA=-DELH*TT(J)
      CALL EX(AA,P1)
      DELN=DELN+V2(J)*AX*AX*P1*0.05
      AX=AO-DELN
      IF(AX)61,63,63
   61 PRINT 62,V2(JJ),TT(J)
   62 FORMAT(1H1,///20X27HEITHER V2 OR TEMP TOO LARGE,5X4HV2 =,E10.4,5X8
     1H1/TEMP =,F10.3///)
      J3=2
      GO TO 99
   63 IF(LYO-1)11,12,11
   12 A2=LOGF(DELN/AX)-LOGF(A1(J))
      SUM=SUM+A2*A2
      GO TO 10
   11 AN(J)=DELN/AO
   10 CONTINUE
      IF(LYO-1)14,13,14
   13 IF(LXO-1)16,15,16
   15 LXC=3
   17 SUM1=SUM
      DELH=DELH+CH
      GO TO 8
   16 IF(SUM-SUM1)17,18,18
   18 IF(ABSF(CH)-CFH)19,20,20
   20 CH=-CH/2.0
      GO TO 17
   19 LYC=3
      GO TO 9
   14 CC=N1-1
      STDEV=SQRTF(SUM/CC)
      DEH=DELH*1.987/1000.0
      DEHO=DELHO*1.987/1000.0
      PRINT 21,AO,DEHO,DEH,STDEV
   21 FORMAT(1H1,10X4HNO =,E12.4,5X1CHDELTA HO =,F7.3,5H KCAL,5X9HDELTA
     1H =,F7.3,5H KCAL,10X8HST DEV =,E12.4///)
C
C          DELTA HO  INITIAL VALUE
C          DELTA H   MINIMIZED VALUE
C
   79 GO TO (80,81,82),JJ
   80 PRINT 83
      GO TO 89
   81 PRINT 84
      GO TO 89
   82 PRINT 85
   83 FORMAT(//50X13HV2 IS A CONST//)
   84 FORMAT(//50X12HV2 IS A F(T)//)
   85 FORMAT(//50X18HV2 IS A F(SQRT(T))//)
   89 PRINT 22
   22 FORMAT(36X6H100O/T,8X15H((NO-N)/NO) EXP,4X16H((NO-N)/NO) CALC.15X2
     1HV2//)
      DO 24 J=1,N1
   24 PRINT 23,T(J),A1(J),AN(J),V2(J)
   23 FORMAT(30XF15.3,3F20.4,E20.4)
      GO TO 99
```

Fortran Program 2 (continued)

```
   44 CA=DAO
      DO 25 J=1,N1
      AA=-DELH*TT(J)
      CALL EX(AA,P1)
   25 V3(J)=V2(J)*P1
      LXO=1
      LYC=1
      SUM1=0.0
   26 SUM=0.0
   27 DELN=0.0
      AX=AC
      DO 30 J=1,N1
      AA=ALPHA*AX*TT(J)/1.987E12
      CALL EX(AA,P1)
      DELN=DELN+V3(J)*AX*AX*P1*0.05
      AX=AC-DELN
      IF(LYO-1)29,28,29
   28 A2=(DELN/AO)-A(J)
      SUM=SUM+A2*A2
      GO TO 30
   29 AN(J)=DELN/AO
   30 CONTINUE
      IF(LYO-1)32,31,32
   31 IF(LXO-1)34,33,34
   33 LXC=3
   35 SUM1=SUM
      ALPHA=ALPHA+CA
      GO TO 26
   34 IF(SUM-SUM1)35,36,36
   36 IF(ABSF(CA)-DFA)37,38,38
   38 CA=-CA/2.0
      GO TO 35
   37 LYC=3
      GO TO 27
   32 CC=N1-1
      STDEV=SQRTF(SUM/CC)
      PRINT 39,AO,DEH,ALPHA,STDEV
   39 FORMAT(1H1,10X4HNO =,E12.4,5X9HDELTA H =,F7.3,5H KCAL,5X7HALPHA =,
     1F7.3,5X8HST DEV =,E12.4///)
      GO TO 79
   99 IF(JJ-2)101,150,150
  101 CONTINUE
  150 CONTINUE
  100 CONTINUE
      STOP 00
      END
 FLAG FORT,1601                                                    1601
C
C          SUBROUTINE TO EVALUATE EXPONENTIALS
C
      SUBROUTINE EX(R,S)
      IF(ABSF(R)-110.0)1,1,3
    1 S=EXPF(R)
      GO TO 4
    3 S=0.
    4 RETURN
      END
```

Fortran Program 2 (continued)